Deep–Sea Research I 180 (2022) 103681

Contents lists available at ScienceDirect

Deep-Sea Research Part I

journal homepage: www.elsevier.com/locate/dsri

Sedimentary processes in the Discovery Gap (Central–NE Atlantic): An example of a deep marine gateway

T. Glazkova [a,*], F.J. Hernández-Molina [a], E. Dorokhova [b,c], A. Mena [d], C. Roque [e,f], F. J. Rodríguez-Tovar [g], V. Krechik [b,c], L. Kuleshova [b], E. Llave [h]

[a] Dept. Earth Sciences, Royal Holloway Univ. London, Egham, Surrey TW20 0EX, United Kingdom
[b] Shirshov Institute of Oceanology, Russian Academy of Sciences, Moscow, 117218, Russia
[c] Immanuel Kant Baltic Federal University, Kaliningrad, 236016, Russia
[d] Departamento de Xeociencias Mariñas e Ordenacion do Territorio, Universidad de Vigo, Vigo, 36310, Spain
[e] EMEPC – Estrutura de Missão para a Extensão da Plataforma Continental, 2770-047, Paço de Arcos, Portugal
[f] IDL – Instituto Dom Luiz, University of Lisbon, Campo Grande, 1749-016, Lisbon, Portugal
[g] Departamento de Estratigrafía y Paleontología, Universidad de Granada, 18002, Granada, Spain
[h] Instituto Geológico y Minero de España, 28003, Madrid, Spain

ARTICLE INFO

Keywords:
Deep-water sedimentation
Bottom currents
Paleocirculation
Antarctic bottom water
Contourites
Deep marine gateways
Discovery gap
Central–NE Atlantic

ABSTRACT

Paleoceanographic studies of abyssal bottom currents are often complicated by low current speeds and sedimentation rates, resulting in sediment condensation or erosion. However, increased rates of erosion and deposition may occur where bottom current velocities change as they pass through deep marine gaps and gateways. Despite this, the depositional processes in these gateways and their paleoceanographic implications remain poorly understood. Based on new sedimentological, hydrological and geophysical (high resolution seismic and bathymetry) data from Discovery Gap (Azores–Gibraltar Fracture Zone) collected during the 43rd cruise of the R/V *Akademik Nikolaj Strakhov* in 2019, the key sedimentary processes occurring in the Late Quaternary have been determined. Two depressions with depths exceeding 5300 m in the centre and south of Discovery Gap have been identified, the latter filled with contouritic deposits. These depressions are separated by a roughly N–S trending central sill at 4860 m and a sediment filled terrace at 4720 m water depth. Elongated NE–SW trending highs and sills, are present in the north and south of the study area. Their importance in controlling the flow of water through Discovery Gap is determined by the presence of erosion at the base of these highs with adjacent sheeted or mounded contourite drifts. Pelagic, hemipelagic, reworked pelagic/hemipelagic and fine-grained contourite sedimentary facies have been identified. The sedimentary facies associations point to remarkable variability in the Antarctic Bottom Water (AABW), linked to glacial–interglacial changes, and its intermittent influence in Discovery Gap during the Quaternary. During glacial intervals (MIS 6, 4 and 2) and at their terminations there was enhanced bottom current activity coeval with higher terrigenous content, and increased carbonate dissolution. The results of this study improve our understanding of sedimentary processes in abyssal environments and highlight the value of the sedimentary record in deep marine gateways for interpreting the interaction of bottom water with abyssal morphology. Future work in other modern deep gaps is essential to shed more light on how deep gaps form and to fully reconstruct deep-water paleocirculation within oceanic basins.

1. Introduction

Deep marine gaps, gateways and channels can foster the exchange of deep water, sediment and biota between adjacent abyssal plains (Heezen et al., 1959; Hernández-Molina et al., 2008, 2011). Where oceanic basins lie at different depths, overflow through these gateways can occur (Legg et al., 2009). Intensification of near-bottom water flow through these constrictions (Dickson et al., 1985) amplifies erosional processes, while a decrease in current velocity leads to sediment deposition (Hollister et al., 1974; Whitmarsh, 1970). Sediment accumulations in these gateways may, therefore, hold near-continuous records of the paleocirculation of deep water (Knutz, 2008; Hernández-Molina et al.,

* Corresponding author.
E-mail address: Tatiana.Glazkova.2016@live.rhul.ac.uk (T. Glazkova).

https://doi.org/10.1016/j.dsr.2021.103681
Received 30 June 2021; Received in revised form 20 November 2021; Accepted 22 November 2021
Available online 29 November 2021

2011).

Deep marine gateways are often linked to fracture zones and/or topographic expressions of volcanic activity. The former cut through mid-ocean ridges and connect different ocean basins; for example, the Charlie Gibbs and Vema Fracture Zones across the Mid-Atlantic Ridge (e.g., Morozov et al., 2010; Bashirova et al., 2017). The latter connect abyssal plains separated by seamounts, rises and plateaus related to hotspot or volcanic arc activity through deep marine passages such as the Vema and Hunter Channels in the Rio Grande Rise (Johnson, 1984; Zenk et al., 1999) or the Samoan Passage in the Manihiki Plateau (Hollister et al., 1974). Our understanding of inter-ocean and intra-basin deep ocean circulation has benefited greatly from the study of deep passages (Morozov et al., 2010).

The propagation of Antarctic Bottom Water (AABW) through the Atlantic Ocean has been of great interest since the water mass was identified by Georg Wüst (1936). The AABW has to use deep passages to reach all the basins in the Atlantic, as very little direct flow from the Southern Ocean makes it through the Walvis Passage, in the Walvis Ridge, directly into the eastern Atlantic (Connary and Ewing, 1974; Warren and Speer, 1991). Consequently, very little AABW reaches the NE Atlantic (McCartney, 1992), and the transport of AABW from the Central to the NE Atlantic is not well understood. Invigoration of sluggish abyssal plain currents through deep marine gateways could be a key element in this exchange of deep water, and sediment deposits can provide information about this exchange in the past.

In this study, a multi-scale integrated approach —including hydrological, bathymetric, acoustic data, and a detailed sediment core analysis— was used to study Discovery Gap (Central–NE Atlantic, Fig. 1), a prime example of a deep marine gateway, so as to: 1) establish the flow and paleo-flow of the AABW and determine which factors control its exchange in the Central–NE Atlantic; and 2) elucidate the sedimentary processes involved and present a sedimentary model and its Quaternary evolution.

2. Geological setting

The Central and NE Atlantic are separated by the Azores–Gibraltar Fracture Zone (AGFZ), which forms the westernmost part of the African (Nubia)–Eurasian (Iberia) plate boundary (Fig. 1) running from the Azores Triple Junction to the Strait of Gibraltar (e.g., Udías et al., 1976; Miranda et al., 2018). The AGFZ is subdivided into three segments characterized by different morphology, seismic activity and kinematics (Buforn et al., 1988; Jiménez-Munt et al., 2001) with slow slip rates varying from 4.0 $mmyr^{-1}$ to 18.0 $mmyr^{-1}$ (Argus et al., 1989; Bezzeghoud et al., 2014). The central segment, orientated WNW–ESE to E–W between 14° 30' W and 24° 30' W, corresponds to the dextral strike-slip Gloria transform fault (Laughton et al., 1972; Laughton and Whitmarsh, 1974; Batista et al., 2017; Omira et al., 2019) (Fig. 1). While the western part of the Gloria Fault is seismically quiet, the eastern part has been the source of high magnitude earthquakes, such as the 1931 (Mw 7.1), 1941 (Mw 8.4) and 1983 October (Mw 6.4) events (e.g., Bezzeghoud et al., 2014), clustered near Discovery Gap.

Although the age of the underlying crust is unknown, Discovery Gap is located on the African plate within the Cretaceous Magnetic Quiet Zone, westwards of the M0 magnetic anomaly (120.6–121.2 Ma) (e.g., Bird et al., 2007; Vissers and Meijer, 2012a). Therefore, it is presumed to have formed in the Cretaceous and shortly thereafter. A complex geodynamic evolution of the AfricaEurasia plate boundary followed through to the Late Miocene involving several episodes of plate boundary jumping and rearrangement of the African, Eurasian and Iberian plates (Srivastava et al., 1990; Miranda et al., 2018). The present-day location and tectonic configuration of the AGFZ was finally established around 2.45 Ma (Luis et al., 1994).

The area surrounding Discovery Gap has been affected since the Late Cretaceous by alkaline magmatism related to mantle plume activity (e.g., Geldmacher et al., 2005) which is responsible for the edification of the Madeira–Tore Rise (MTR). This NNE–SSW first-order, tectono-magmatic structure developed along the M0 magnetic anomaly and presents an age progression from north to south ranging from the late Early Cretaceous (~100 Ma) to the late Miocene (~12 Ma) (Merle et al., 2006, 2009, 2018). Of the seamounts created by this activity, three are near Discovery Gap: the Gago Coutinho (~92 Ma), Josephine (~12 Ma) and Jo Sister (~86–89 Ma) (Merle et al., 2006). Josephine Seamount is the most prominent and shallowest feature in the study area with a summit reaching 190 m water depth.

Seamounts surrounding abyssal plains are often the source of turbidites that fill the distal abyssal plains but many of the largest turbidites that reach the Madeira abyssal plain originate from the Canary and Madeira Islands and the Moroccan margin (e.g., Weaver and Rothwell, 1987; Weaver et al., 1992; Lebreiro et al., 1998; Stevenson et al., 2013). This sediment may then be reworked and distributed across the plain by weak bottom currents or form sediment drifts. At the southern end of the MTR, Madeira Drift is a relic sedimentary drift (Fig. 1) possibly created by —previously— vigorous AABW flow in the Central Atlantic (Embley et al., 1978; Roque et al., 2015, 2017). If this is the case, Discovery Gap is in an ideal position relative to the east-intensified bottom current to record changes in its flow (Saunders, 1987).

3. Oceanographic setting

The study area is located in a rather dynamic zone of the north-eastern part of the sub-tropical gyre. To the north the surface Azores Current (AzC) flows eastward, while in the eastern part along the Iberian Peninsula the Portugal Current (PC) is directed southward (Machín et al., 2006). At the same time, Discovery Gap is also influenced by the Mediterranean waters that, flowing out through the Strait of Gibraltar, move predominantly westward (Mosquera Giménez et al., 2019). This combination of dynamic factors leads to a diversity of water masses in the surface and intermediate layers of the study area.

Below the surface and thermocline waters there is the Eastern North Atlantic Central Water (ENACW), which is formed in the vicinity of the study site during the winter convection. A distinctive feature of this water is the salinity minimum, which confines it from below (Prieto et al., 2013). In contrast, the core of the Mediterranean Overflow Water (MOW), the warmest and the most saline intermediate water mass in the northeast Atlantic, is characterized by a distinct salinity maximum (Harvey and Arhan, 1988; van Aken, 2000a). The formation of this water occurs in the Gulf of Cadiz due to the mixing of Mediterranean Water from the Strait of Gibraltar with Atlantic waters at the same isopycnic level (Mosquera Giménez et al., 2019). The MOW interacts isopycnically with the Antarctic Intermediate Water (AAIW) and the Subarctic Intermediate Water (SAIW). AAIW generally does not spread north beyond 32 °N (van Aken, 2000a). However, seasonal variability of the water mass means that traces are able to reach the study area, entrained by the eddies in the MOW (Roque et al., 2019). During glacial periods and glacial–interglacial transitions, incursions of AAIW reached up to 60°N (Rickaby and Elderfield, 2005; Thornalley et al., 2011), affecting depths between 550 and 1100 m (Dubois-Dauphin et al., 2016). SAIW flows southwards along the Iberian margin and is thought to compete with the AAIW at intermediate depths (400–900 m), dominating when the AAIW is weaker but not extending out into the open Atlantic (Roque et al., 2019).

North Atlantic Deep Water (NADW) occupies the majority of the water column between 1400 and about 4000 m water depth (Fig. 1). It is composed of Labrador Sea Water (LSW) and dense Arctic overflow water combined with Lower Deep Water (LDW) —a mixed water with an Antarctic component (van Aken, 2000b). Below 4000 m, the deepest water mass is the Antarctic Bottom Water (AABW); following the classic definition given by Wüst (1936), this water mass would have a potential temperature of $\theta < 2$ °C. It is also recognised by tracers such as low salinity and oxygen content, and high silicate content (McCartney, 1992). The AABW mainly forms in the Weddell Sea (Orsi et al., 1999),

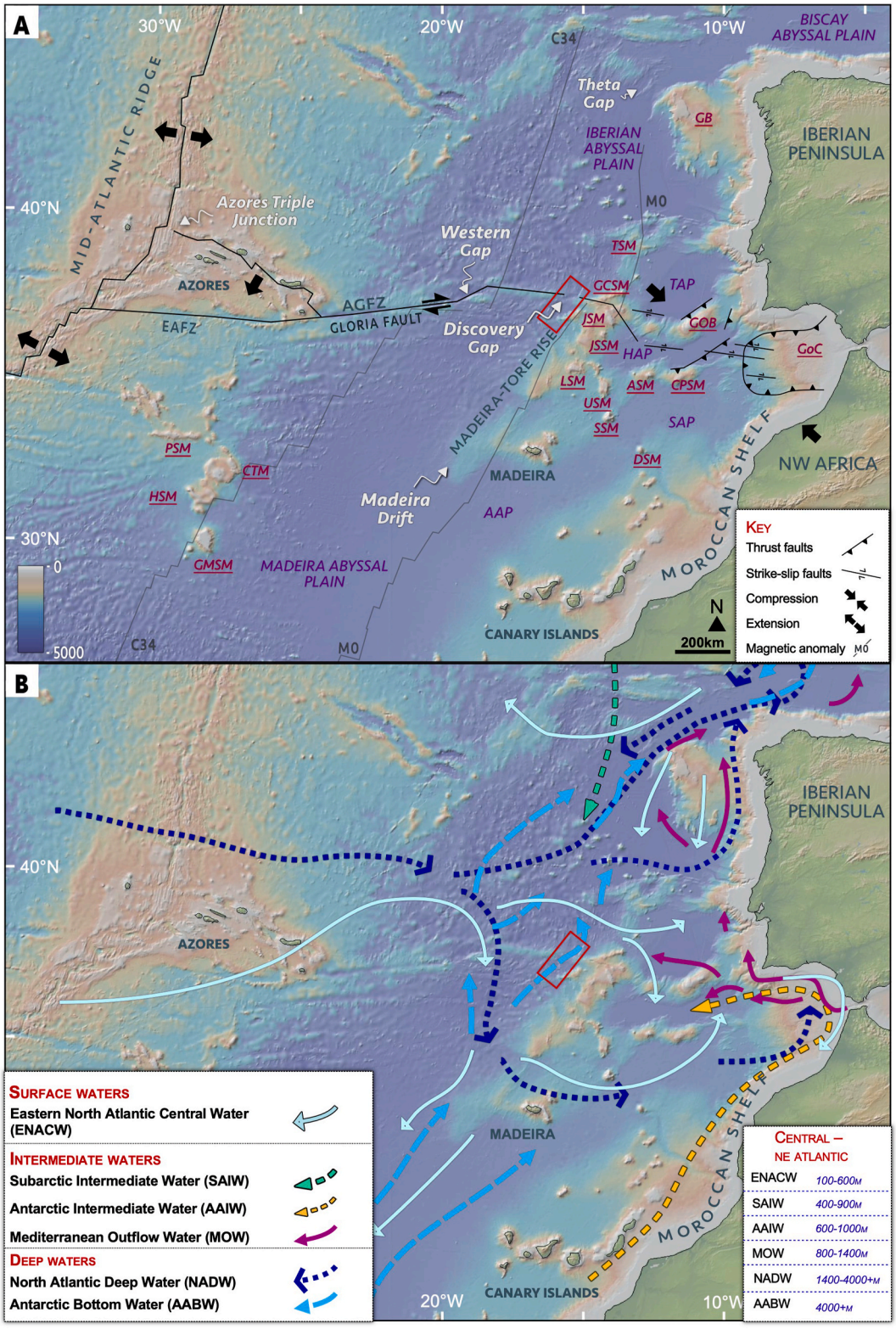

Fig. 1. A regional overview of the study area and the corresponding key water currents. Deep and surface water adapted from Hernández-Molina et al. (2011) and intermediate water from adapted from Roque et al. (2019). Magnetic anomalies M0 and C34 from Müller et al. (1997). Tectonics based on Gutscher et al. (2012) and Hensen et al. (2019). Abbreviations: AAP – Agadir Abyssal Plain; ABR – Azores—Biscay Rise; AGFZ – Azores–Gibraltar Fracture Zone; ASM – Ampere Seamount; BAP – Biscay Abyssal Plain; CPSM – Coral Patch Seamount; CTM – Cruiser Tablemount; DSM – Dacia Seamount; EAFZ – East Azores Fracture Zone; GCSM – Gago Coutinho Seamount; GB – Galicia Bank; GMSM – Great Meteor Seamount; GOB – Gorringe Bank; GoC – Gulf of Cadiz; HAP – Horseshoe Abyssal Plain; HSM – Hydrea Seamount; JSM – Josephine Seamount; JSSM – Jo Sister Seamount; LSM – Lion Seamount; PSM – Plato Seamount; SAP – Seine Abyssal Plain; SSM – Seine Seamount; TAP – Tagus Abyssal Plain; TSM – Tore Seamount; USM – Unicorn Seamount. The base map comes from Ryan et al. (2009).

however, the passage of AABW northwards from the Southern Ocean over sills, ridges and abyssal basins, leads to mixing with overlying waters. Since AABW temperature and salinity are increased by this passage, a range of other criteria have been used to identify the modified-AABW's upper boundary in the eastern Atlantic: $\theta = 2.08 \pm 0.15$ °C (Broecker et al., 1976), $\theta = 2.05$ °C (Saunders, 1987), $\theta = 2$ °C (McCartney et al., 1991), potential density $\sigma_4 = 45.87$ kgm^{-3} (Morozov et al., 2010), and neutral density $\gamma^n \geq 28.11$ kgm^{-3} (de Lavergne et al., 2016). This modified-AABW flows through Discovery Gap with a northward flux of water cooler than $\theta = 2.05$ °C of 0.21 ± 0.04 Sv (1 Sv $= 1 \times 10^6$ m^{3}s^{-1}) (Saunders, 1987). But large, random variations in the flow and recirculation within the gap led Tarakanov et al. (2013) to record a net flux of 0.28 Sv below $\theta = 2.015$ °C to the southwest, where the measured flow to the NE was ~0.1 Sv. A decrease in the temperature was recorded from 1982 (2.011 °C) to 2011 (2.002 °C) (Tarakanov et al., 2013), which may be an indirect indicator of changes in the intensity of near-bottom flow in the gap.

4. Dataset and methods

To characterise the sedimentary processes and ascertain the degree of paleoceanographic change in AABW flow through Discovery Gap, hydrological, multibeam bathymetric, acoustic and sedimentary data were used (Fig. 2). The data were collected during the 43rd cruise of the R/V *Akademik Nikolaj Strakhov* (ANS43) in September–October 2019 (Dorokhova et al., 2021). We supplemented this dataset with previously collected high-resolution acoustic lines and seafloor photos.

4.1. Dataset

4.1.1. Hydrological data

We determined the present distribution of water masses using CTD data collected at five stations in the gap (ANS43001/2/4/5/6) (Dorokhova et al., 2021). To establish the N–S change through the gap, one station (ANS43006) was placed in the deepest part of the gap in the southern depression. Another station (ANS43004) was positioned outside the exit of the gap in the north (Fig. 2). Measurements of temperature (SBE-3), conductivity (SBE-4C), and pressure (strain gauge) at the stations were carried out using the SBE 19plus V2 SeaCAT probe (Sea-Bird Electronics, USA) in profiling mode with a frequency of 4 Hz. The device lowering speed was about 1 ms^{-1}. Potential temperature, salinity, and depth were derived from temperature, conductivity and pressure. The potential density relative to 4000 dbar surface and neutral density calculations were performed using the Ocean Data View software (Schlitzer, 2002). Additionally, we used information from the public World Ocean Database (WOD18) (Boyer et al., 2018) and the CLIVAR and Carbon Hydrographic Data Office (CCHDO) database (https://cchdo.ucsd.edu/). Data were extracted for three regions: the Madeira abyssal plain (23 CTD stations in an area with the upper left corner coordinates 37.0° N, 17.6° W and lower right corner coordinates of 35.9° N, 16.0° W), Discovery Gap (18 CTD stations in an area with coordinates of upper left corner 37.8° N, 16.3° W and lower right corner 37.0° N, 15.2° W) and the Iberia abyssal plain (13 CTD stations in the area with coordinates of upper left corner 39.1° N, 17.5° W and lower right corner 37.8° N, 14.0° W). All stations were checked for duplicates using the built-in Ocean Data View software tools. Potential density limits defining ENACW and MOW were determined following Prieto et al. (2013). The potential density value at the upper boundary of the modified AABW was taken from Morozov et al. (2010). We also used the

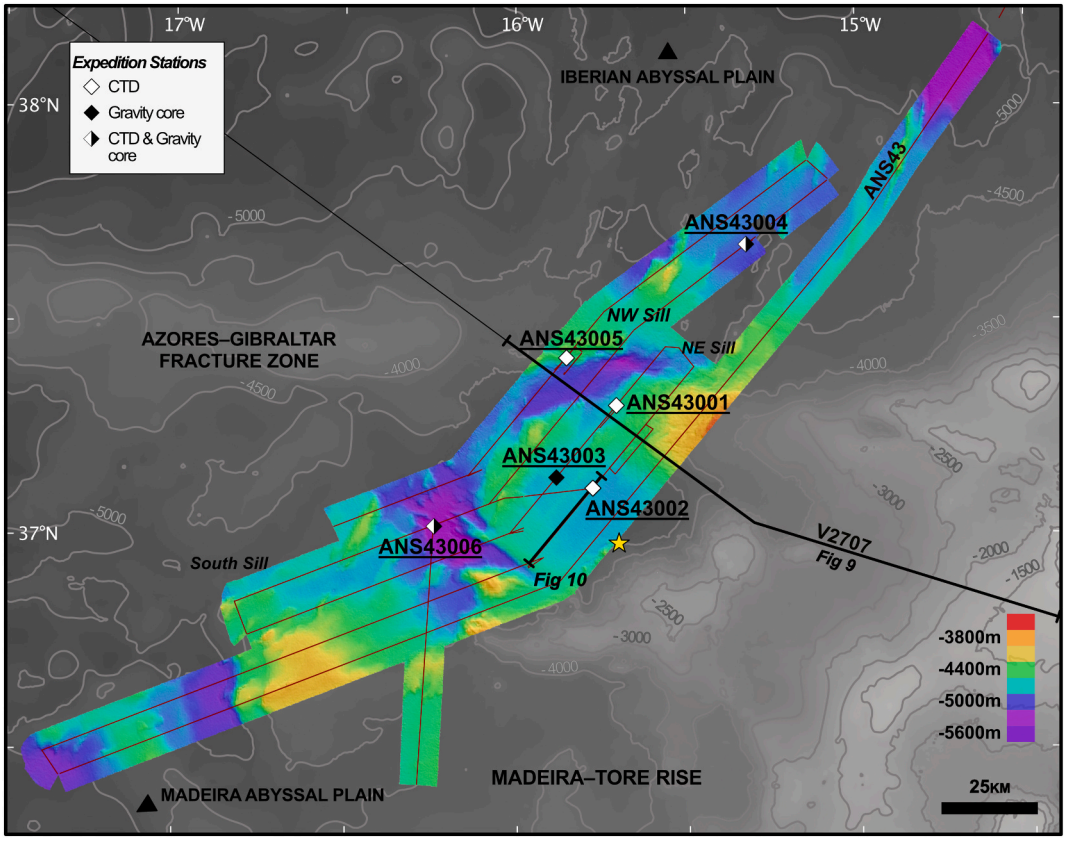

Fig. 2. An overview of the data collected in 2019 and the position of V2707. Hydrological data was collected at stations ANS43001, 43002, 43004, 43005 and 43006. Sediment cores were collected at ANS43003, 43004 and 43006. The yellow star marks the location of seafloor photos. (For interpretation of the references to colour in this figure legend, the reader is referred to the Web version of this article.)

results published in Saunders (1987) and Tarakanov et al. (2013).

4.1.2. Bathymetric and high-resolution seismic data

Large scale erosional, depositional and mixed erosional/depositional features were identified using a Reason SeaBat 7150 to collect bathymetric data. The equipment was recalibrated twice during the expedition to account for the large changes in bathymetry. Details regarding the processing of this dataset are provided by Dudkov and Dorokhova (2020). The resulting dataset has a 50 m resolution. A publicly available GEBCO 2019 base map was also used (GEBCO, 2019).

The subsurface sequence of sedimentary deposits was studied using ultra-high resolution seismic reflection profiles, which were acquired simultaneously with bathymetric data by means of an EdgeTech 3300 Chirp profiler with an emitted pulse of 2–8 kHz. The data were recorded using the EdgeTech Discover Sub-Bottom 3.52 software. One additional line was used to supplement the collected data and increase coverage: line V2707 (Fig. 2) collected with a sub-bottom profiler onboard the R/V *Vema*.

4.1.3. Seafloor photos

The resolution of the bathymetric and acoustic data is too limited to allow us to assess present seafloor features in detail. Fortunately, four seafloor photos from the study area were collected from a single station during R/V *Vema* 30 (Fig. 2) and stored at the NOAA National Centre for Environmental Information (url: https://www.ngdc.noaa.gov/mgg/curator/data/vema/vm30/seabed_photos/) and were available through the GeoMapApp database (www.geomapapp.org).

Provided coordinates (36.983 °N and 15.717 °W) and depths (2395 m) do not correlate well with the bathymetry, but general locations suffice in this case. Roughly 3.5 by 2 m of seafloor is covered by each image, oriented with reference to the photographed compass. The oriented bedforms then served to evaluate the relative bottom current velocities using the bedform matrix from Stow et al. (2009).

4.1.4. Sedimentological dataset

A detailed study of small-scale sedimentary deposits was possible with four gravity cores collected from three sites in Discovery Gap (Fig. 2) using a 6 m by 12.7 cm, 1100 kg gravity corer. The corer was lined with a hard-plastic tube, 11 cm in diameter, to preserve sediment integrity. Upon retrieval, the cores were cut into 95 cm sections, tightly packaged in plastic and securely placed in the vessel's cold storage at 4 °C for the remainder of the voyage. The parameters of the collected cores are provided in Table 1.

4.2. Methodology

4.2.1. Large- and medium-scale characterisation of features

Analysis of the bathymetric and acoustic data entailed: classification of morpho-sedimentary features, mapping the distribution of echo-types in the gap, identification of seismic units and correlation of discontinuities. Echo-types were mapped using the classification of Damuth and Hayes (1977) and Damuth (1978, 1980), adjusted to better describe the range of echo-types observed in the study area (Fig. 3).

Seismic unit characterisation followed the basic procedure of Mitchum et al. (1977) and Catuneanu et al. (2009) and included a description of boundaries, reflection terminations, internal configuration of reflections and the overall shape of the seismic unit. For unit thickness estimations, the difference in the speed of sound between water and sediment was taken to be 1500 ms^{-1}. The extent to which seismic units could be identified in the V2707 profile was limited by image quality, so units are identified only from the ANS43 data.

Table 1
Parameters of the collected cores from ANS43. Coordinates come from the acoustic pinger used during core retrieval. Note that the two cores from ANS43006 were collected 10 m apart.

Core	Coordinates	Depth (m)	Length (cm)
ANS43003	37°08.229'N 15°53.073'W	4687	302
ANS43004	37°40.775'N 15°19.681'W	4875	195
ANS43006_A (Kaliningrad)	37°01.591'N 16°14.437'W	5225	395
ANS43006_B (Vigo)	37°01.585'N 16°14.437'W	5225	391

4.2.2. Small-scale characterisation of features and deposits: sedimentary facies

A detailed sedimentological analysis of the cores was carried out which included visual logging, CT scanning, XRF and MS analysis, grain size, thin-section, and ichnological analysis to characterise sedimentary facies and the facies relationships.

4.2.3. Visual logging

Visual logging was done to a 1 mm scale. Boundaries between units, sedimentary structures and grain size changes were identified in relation to changes in colour, which were determined using a Munsell™ soil colour chart.

4.2.4. Grain size analysis

Changes in grain size can reveal fine-scale alterations in depositional processes. We sampled at 1 cm intervals and used grain size data from every 2 cm from cores ANS43003, ANS43004, and ANS43006_B. Both bulk and $CaCO_3$-removed grain sizes were measured with a Mastersizer 2000 at the University of Bordeaux, EPOC Laboratory, France. The laser diffraction method of particle analysis was deemed suitable for the range of grain sizes measured (0.02–2000 μm) over the large number of samples. Although there has been some criticism regarding the use of laser diffraction methods for the analysis of muddy sediments due to particle shape effects (McCave and Hall, 2006), recently it has been acknowledged that laser sizers can successfully be used for the investigation of near-bottom current effects (McCave and Andrews, 2019).

The geometric mean, skewness, kurtosis, and sorting were then calculated using the Gradistats software (Blott and Pye, 2001) following the method of Folk and Ward (1957). These parameters were used to discern subtle changes associated with winnowing and reworking of fine-grained sediments by bottom currents (Brackenridge et al., 2018; de Castro et al., 2020, 2021).

Increases in the part of the fine fraction that can be sorted by currents, sortable silt (10–63 μm), can be used to aid in the identification of changes in bottom current activity (McCave and Hall, 2006; McCave et al., 2017). As the sedimentary processes in Discovery Gap have not been studied previously, and the degree of bottom current influence on deposition was unknown, we tested the viability of the sortable-silt method using the procedure outlined by McCave and Andrews (2019). The geometric mean $\overline{S}\overline{S}$ of the 10–63 μm fraction was calculated using Gradistats software (Folk and Ward, 1957; Blott and Pye, 2001). The SS method was deemed suitable if the slope of $\overline{S}\overline{S}$–SS% exceeded 0.07 and the correlation between $\overline{S}\overline{S}$ and SS% was greater than 0.5. Several such intervals were identified in the core (Fig. S1 *in supplementary material*), hence it was possible to draw conclusions about bottom current velocity from $\overline{S}\overline{S}$ for these units.

4.2.5. CT scanning

The sedimentary structures, density distribution and bioturbation within the cores can be viewed by means of X-ray Computed Tomographic (CT) imaging without disturbing the sediment (Mena et al., 2015). A HITACHI ECLOS 16 Multislice CT scanner at the Veterinary Teaching Hospital Rof Codina in Lugo (Galicia, Spain) was used. We followed the protocol for data acquisition presented by Mena et al. (2015) using the MRIcron software to visualise the data (Rorden and Brett, 2000).

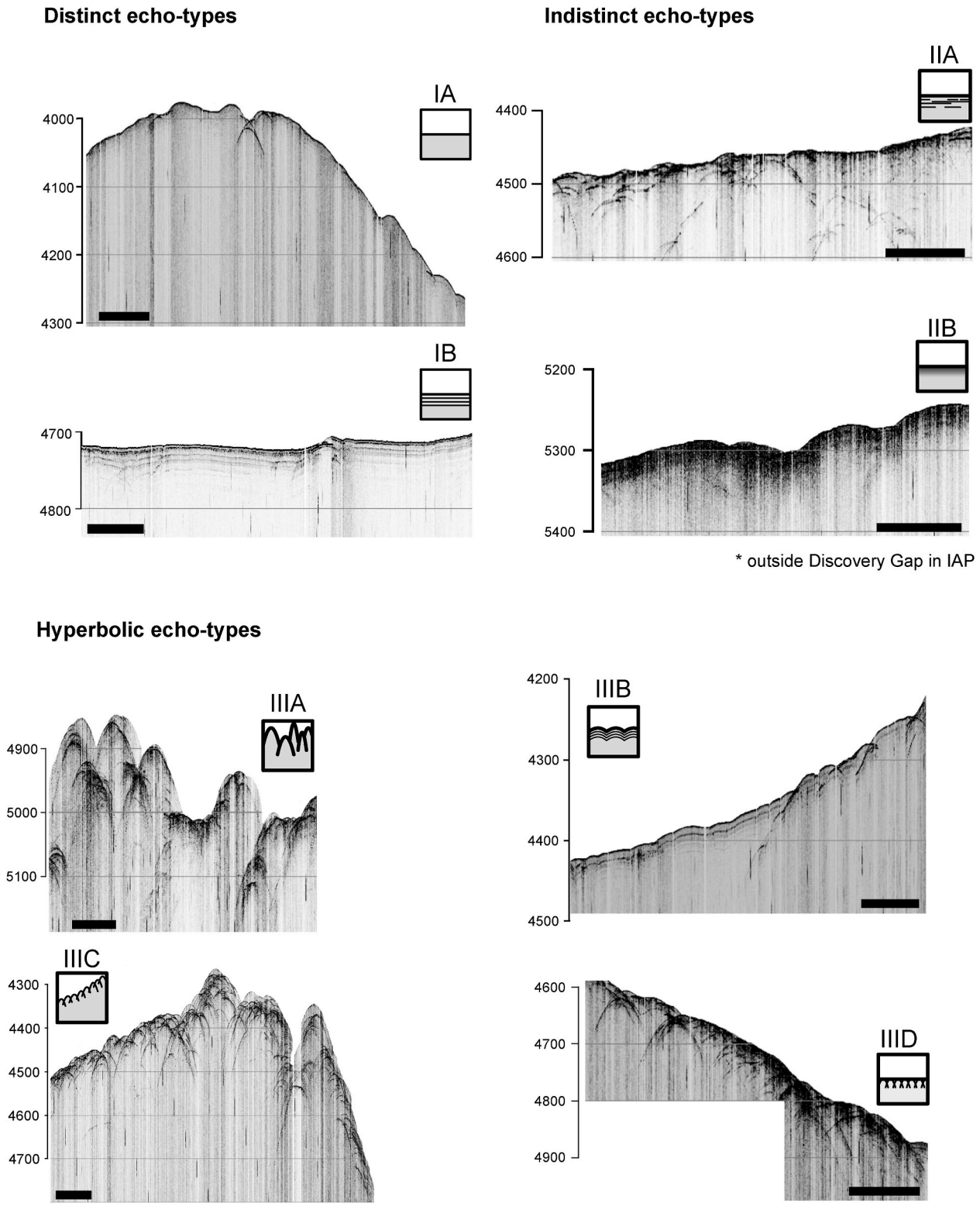

Fig. 3. The echo-types identified in Discovery Gap used to classify the large-scale features in the gap. Based on Damuth and Hayes (1977) and Damuth (1978, 1980). Distinct echo-types: IA — Continuous reflection with no sub-bottoms; IB — Extensive continuous reflection with parallel continuous sub-bottom reflections. Indistinct echo-types: IIA — sub-bottom reflections present but often discontinuous and difficult to follow; IIB — "Mushy" profile with no sub-bottom reflections observed. Hyperbolic echo-types: IIIA — Singular, large, irregular hyperbolic echoes with vertices with widely ranging heights above the seafloor, no sub-bottoms; IIIB — Regular hyperbolas with conformable sub-bottoms; IIIC — Regular, repeating hyperbolic echoes with vertices tangent to the seafloor, though vertex height can vary; IIID — Regular, repeating hyperbolic echoes with vertices tangent to the seafloor or a sub-bottom reflector. The horizontal scale is 2 km in all figures. Depths are given in metres.

4.2.6. X-ray fluorescence and magnetic susceptibility

Downcore changes in elemental composition were conducted using X-ray fluorescence (XRF). This non-destructive method has been previously used to determine interglacial–glacial cyclicity, aeolian input, sediment provenance and hiatuses in deposition, as well as helping in core correlation and facies analysis (Rothwell and Croudace, 2015). XRF is considered a semi-qualitative method, as factors such as textural and porosity changes, horizontal compositional changes, and water content affect the recorded elemental composition (Rothwell and Rack, 2006).

We used an ITRAX XRF at the CACTI from the University of Vigo (Spain) with a Mo X-ray tube and PACS-2 reference sediment for trace metals. Parameters of the ITRAX were set at 30 kV voltage with a current of 55 mA and a step size of 1 cm taking 20 s. For core ANS43006_A, we used a portable Olympus Vanta–C with an Ag anode and Si drift detector (power 4 W and a step size of 1 cm taking 6 min) at the Atlantic Branch of the Shirshov Institute of Oceanology, Russian Academy of Sciences (Kaliningrad). This proved advantageous, since ANS43006_B had separated 16 cm in the centre during collection, and it was possible to correlate the two cores.

Element counts from the major elements that had the best signal-noise ratio (i.e., Si, K, Fe, Ti, Ca, Rb, Zr, Sr) were standardised against their mean and standard deviation. Natural logs of element ratios were plotted so that a better comparison could be drawn between cores and XRF scanners, which can give different raw element counts (Weltje and Tjallingii, 2008).

Magnetic susceptibility (MS) measurements were also carried out, as the presence of many terrestrial Fe- and Ti-bearing minerals is closely correlated with magnetic susceptibility peaks (Rothwell and Croudace, 2015). Direct contact with the core surface is needed for this, typically through a thin mylar film across the surface of the cores. The concentration downcore could then be extracted to aid in core correlation.

4.2.7. Thin sections

Microfacies can be used to differentiate deposits and the extent of bottom current influence (de Castro et al., 2020, 2021; de Weger et al., 2020; Hüneke et al., 2021). Sixteen 30 mm by 8 mm thin sections were prepared at the Department of Earth Sciences, Royal Holloway, University of London, UK. Thin sections were taken from areas of the core that were determined to be most representative of the sediment units in the core. Microfacies were described by texture, presence of mineral grains, dissolution and infill of foraminifera tests (Flügel, 2004).

4.2.8. Ichnological analysis

Rate of sedimentation and bottom water energy are two depositional conditions determining habitability of the benthic habitat for the macrobenthic trace maker community, especially in seafloors affected by bottom currents (Rodríguez-Tovar and Hernández-Molina, 2018; Rodríguez-Tovar et al., 2019a,b; ; Miguez-Salas and Rodríguez-Tovar, 2019, 2021; Miguez-Salas et al., 2020, 2021). Changes in bottom conditions can affect the types of communities present, abundance and diversity of trace fossil assemblages, the size and shape of burrows, and taphonomy of trace fossils. A detailed ichnological analysis was conducted on high-resolution images that were digitally enhanced to increase the visibility of biogenic structures following previously defined procedure (Dorador and Rodríguez-Tovar, 2014, 2015, 2018; Dorador et al., 2014a,b, 2019). Ichnological features such as ichnodiversity, orientation, shape, size, distribution of burrows, infilling material and the degree of bioturbation were recorded.

4.2.9. Stable isotopes and age model

Stable oxygen ($\delta^{18}O_{Cw}$) and carbon ($\delta^{13}C_{Cw}$) isotopes were measured on carbonate tests of the epibenthic foraminiferal species *Cibicidoides wuellerstorfi* from core ANS43006_A. Four to eight specimens of *C. wuellerstorfi* in the >250 μm size fraction were picked out per sample at 10 cm intervals for analysis at the Leibniz Laboratory for Radiometric Dating and Stable Isotope Research (Kiel, Germany) using a Thermo Finnigan MAT 253 mass spectrometer system. Values of stable isotope data were calibrated relative to the Vienna Pee Dee Belemnite (VPDB) scale and expressed as $\delta^{18}O_{Cw}$ and $\delta^{13}C_{Cw}$ (‰ vs. VPDB). The analytical precision was better than ±0.08‰ for $\delta^{18}O_{Cw}$ and better than ±0.05‰ for $\delta^{13}C_{Cw}$.

An age model of core ANS43006_A was constructed by comparing our $\delta^{18}O_{Cw}$ record to the stacked LR04 global $\delta^{18}O$ benthic isotope curve by Lisiecki and Raymo (2005) and supported by $\delta^{13}C_{Cw}$, $CaCO_3$, and MS data. The chronology of other cores ANS43006_B, ANS43003, and ANS43004 is based on the visual correlation of In(Ca/Fe) and MS curves with ANS43006_A data.

Nomenclature

Even slow-moving bottom currents can displace sediment, so we use the term contourites to denote sediments deposited or substantially reworked by the persistent action of bottom currents (Rebesco and Camerlenghi, 2008; Faugères and Mulder, 2011; Rebesco et al., 2014). Sediments that are affected but not *fully* modified were considered as reworked sediments.

When the velocity of the currents decreases, vertical sedimentation takes place. These deposits can be hemipelagic when they contain >25% terrestrial material, or pelagic when there is <25% terrestrial content (Stow and Tabrez, 1998).

5. Results

5.1. Physiographic domains in the study area

According to the sea-floor gradient, the study area can be subdivided into three main domains: topographic highs, abyssal plains and the deep gateway. The easternmost part of the central segment of the AGFZ defines the northwest limit of Discovery Gap creating a WNW–ESE elongated and asymmetrical relief about 3500 m high. Gradients range from 4° to 23°. The NE–SW trending MTR corresponds to the major physiographic high in the study area and is formed by several coalescent seamounts. Gradients of the MTR range from 5° to 11° and the seamounts' summits can reach 190 m water depth (Josephine Seamount. Gago Coutingo is at 1320 m and Jo Sister is at 963 m). On either side of Discovery Gap, the seafloor has slightly different depths. The deepest of the two is to the north, at 5765 m. The south side is 80 m shallower at 5683 m. However, a direct passage between the two sides is prevented by shallower sills. The shallowest is the south sill at 4595 m water depth, followed by the NW sill (4579 m), the central sill (4950 m), and the NE sill (4783 m) in Discovery Gap (Figs. 2 and 4). Each domain is associated with a range of echo-types (Fig. 5).

Discovery Gap is roughly 150 km long orientated NE–SW, with a maximum width of 60 km. Its narrowest point is roughly 9 km wide. Separated by the central sill are two depressions: the central (CD) and southern depression (SD), respectively located at 5308 m and 5399 m water depth, with average gradients of ≤1°. The central depression also slopes with a gradient of 2.5° to the NE (5050–5280 m). The saddle point of the central sill is captured by the multibeam. Therefore, we suggest that there may be some connection between the two depressions to the NW along this sill.

5.2. Water masses

There are 5 water masses present in the study area, which are present to varying degrees both to the south and to the north of Discovery Gap (Fig. 6). The warmest and saltiest of these waters, in the upper 50–100 m, has a temperature of 16–22 °C and a salinity of over 36 PSU. Below this layer, the ENACW occupy a layer down to about 500 m, where the salinity minimum (about 35.6 PSU) is located (Fig. 6). This water is characterized by an almost linear relationship between temperature and salinity and has an average potential temperature of $\theta \approx 11$ °C and salinity of about 35.75 PSU. ENACW is underlain by MOW, which is

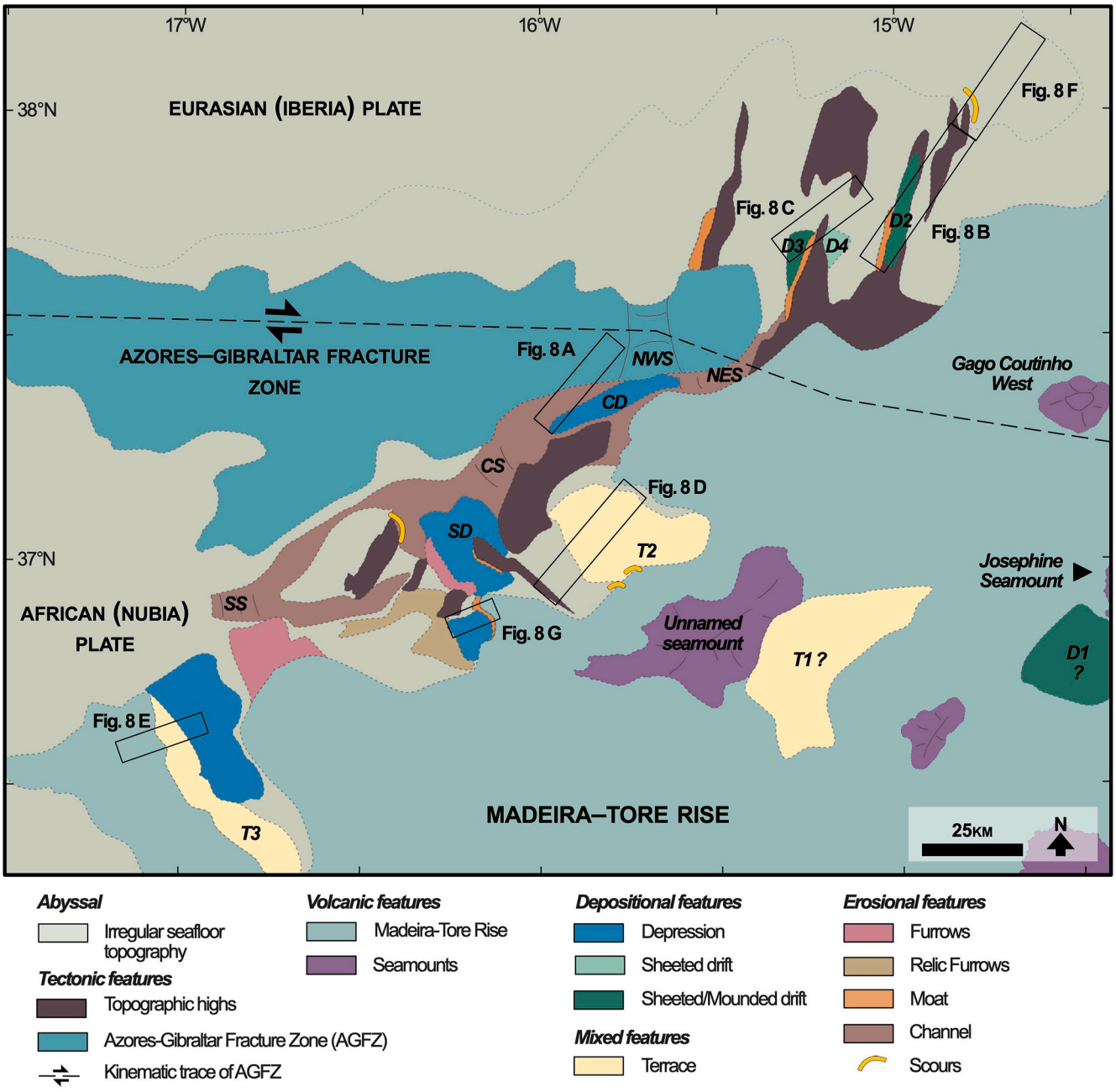

Fig. 4. A morpho-sedimentary features in Discovery Gap. Abbreviations: D: drift; T: terrace; SS: South Sill; CS: Central Sill; NWS: Northwest Sill; NES: Northeast Sill; SD: South depression; CD: Central depression.

responsible for a salinity maximum of 36–36.4 PSU within the intermediate waters in the 700–1500 m depth range. The most noticeable feature of the intermediate waters is an increase in the variability of salinity values and the greater proportion of fresher waters to the north, which indicates the appearance of SAIW in this layer (Figs. 6 and 7).

At depths of 1500–4500 m quite a sharp change in water parameters occurs and the temperature and salinity interrelation again acquires a linear character, denoting NADW. In this water, temperature values decrease from 7 to 2 °C, and salinity changes in the range of 34.9–35.63 PSU. Below 4500 m, minor changes in the physical parameters of the water signal the AABW boundary. The distributions of temperature and salinity become more homogeneous here. Potential temperature values less than 2 °C are registered only in the Madeira abyssal plain and Discovery Gap, a distinctive feature of the gap bottom layer is the significant variability of temperature and salinity values as compared to the abyssal plains located to the south and north of the study area (Fig. 7).

Measurements performed in 2019 showed that vertical variability in the main hydro-physical parameters occurred down to depths of about 4400–4500 m. Below this, the potential temperature and salinity were practically unchanged (salinity about 34.904 PSU, potential temperature about 2.005 °C). We verified that the hydro-physical characteristics of the water mass below 4500 m water depth meet the criteria used to identify the upper boundary of the modified AABW in the eastern Atlantic (Fig. S2).

Measurements obtained for Discovery Gap in previous years (Saunders, 1987; Tarakanov et al., 2013; Boyer et al., 2018) showed that the bottom layer salinity ranged from 34.888 to 34.908 PSU, and the average potential temperature was 2.035 ± 0.026 °C. Our measurements showed similar results at four stations (ANS43001, ANS43002, ANS43004 and ANS43002; Table 2). However, at station ANS43006,

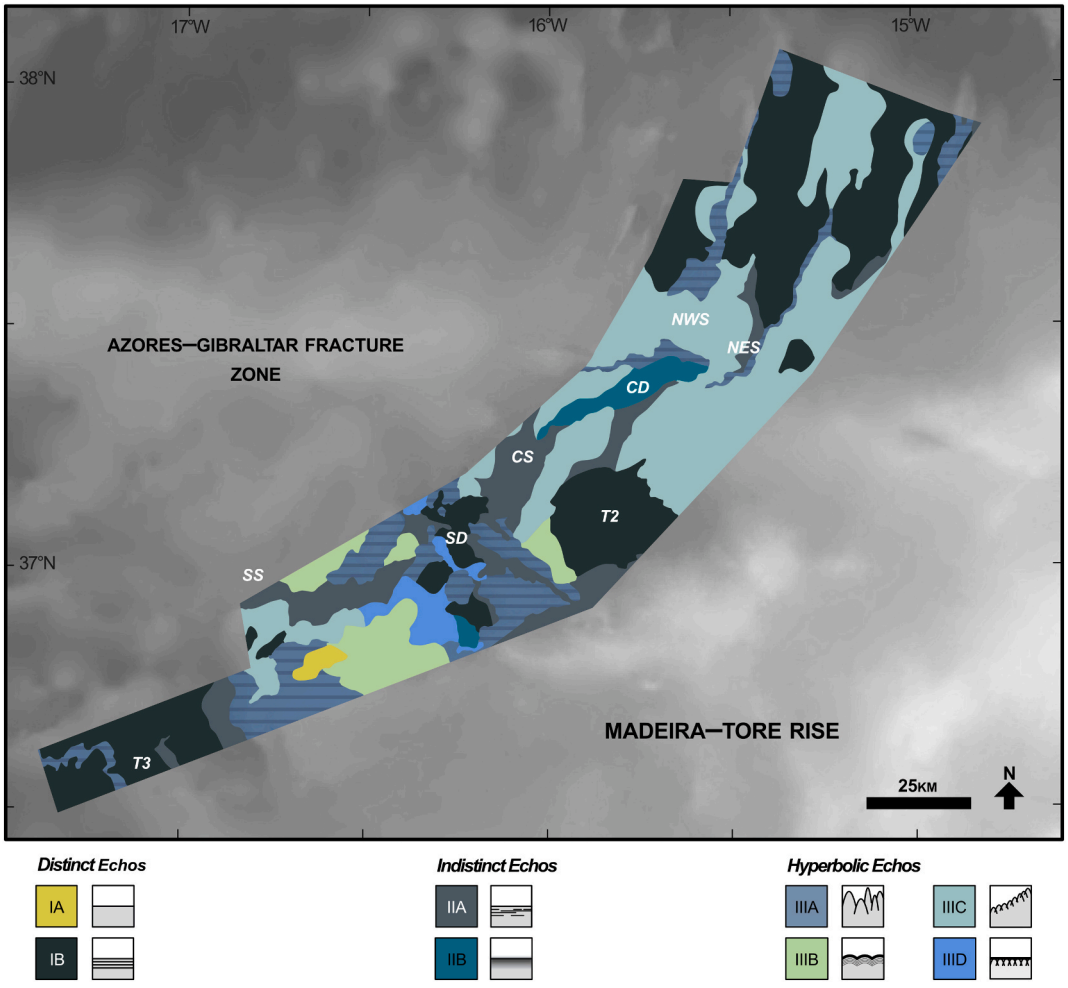

Fig. 5. A map of echo-types in Discovery Gap. Abbreviations as in Fig. 4.

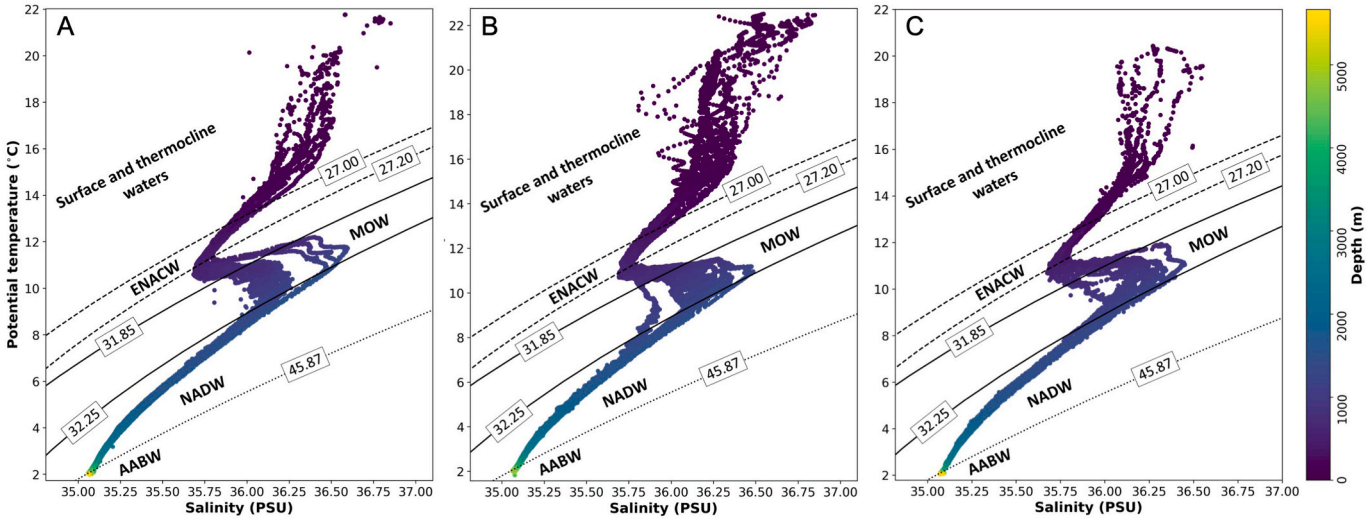

Fig. 6. The figure presents θ-S diagrams for the Madeira abyssal plain (A), Discovery Gap (B), and the Iberian abyssal plain (C). Dashed lines indicate isopycnal corresponding to σ_0, solid lines correspond to isopycnal σ_1. Isopycnal σ_4 is shown by a dotted line. Note the greater potential temperature range along the y-axis in Discovery Gap compared to the abyssal plains.

located in the southern depression in Discovery Gap, a potential temperature value of less than 2 °C was recorded for the first time (Table 2). At this station, the upper boundary of water with a potential temperature of less than 2 °C was found at a depth of 4738 m, and the minimum measured value (1.993 °C) was observed near the bottom in a layer over 200 m thick with 34.9025 PSU salinity.

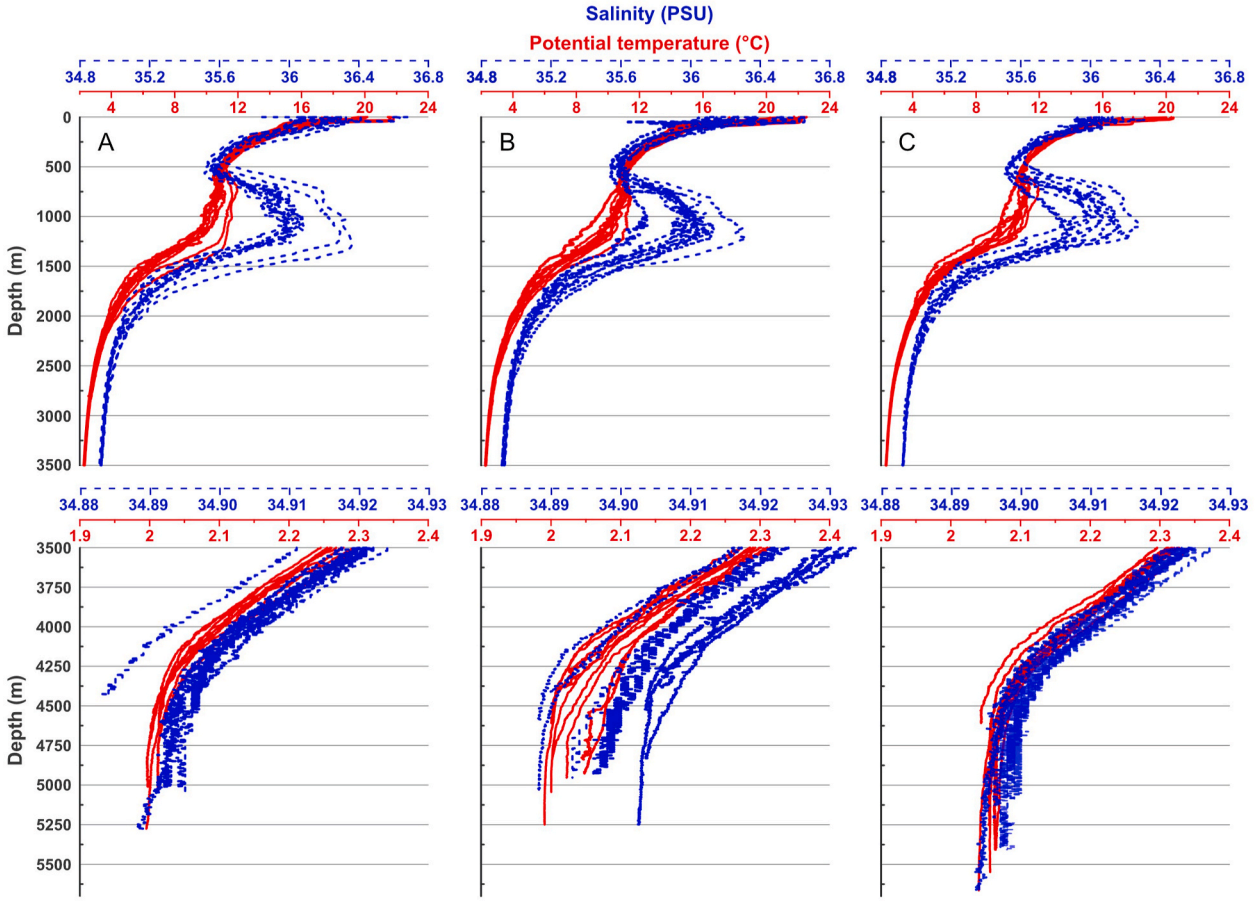

Fig. 7. Vertical distribution of temperature (solid red lines) and salinity (dashed blue lines) in the Madeira abyssal plain (A), the Discovery Gap (B), and the Iberian abyssal plain (C). The profiles are presented at different scales of temperature and salinity for depth ranges of 0–3500 and 3500–5700 m. (For interpretation of the references to colour in this figure legend, the reader is referred to the Web version of this article.)

Table 2
Stations with near-bottom potential temperature in Discovery Gap.

Station	Date	Latitude, °N	Longitude, °W	Maximum sample depth, m	Distance to the bottom, m	Potential temperature, °C
ANS43001	October 03, 2019	37°18.30'	15°42.51'	4584	25	2.003
ANS43002	October 04, 2019	37°06.73'	15°46.70'	4737	23	2.004
ANS43004	October 05, 2019	37°40.75'	15°19.69'	4928	27	2.003
ANS43005	October 06, 2019	37°24.97'	15°51.27'	4430	29	2.020
ANS43006	October 07, 2019	37°01.56'	16°14.45'	5275	26	1.993

The coldest water recorded beyond the north sills of Discovery Gap is 2.0037 °C at 4835 m water depth, which is colder than previously recorded, but still warmer than water within the gap.

5.3. *Morphological features of the Discovery Gap area*

Based on seafloor expression and echo characteristics, the morphological characteristics of the Discovery Gap area can be divided into five groups (Fig. 4): a) tectonic/structural b) volcanic, c) erosional, d) depositional, and e) mixed depositional and erosional features.

a) Tectonic/structural features

Tectonic relief bounding the western wall of Discovery Gap corresponds to a WNW–ESE asymmetrical ridge (where the north side has a gradient of ~8° and the south side ~2°), 260 km long, ~50 km wide and belongs to the eastern segments of the Gloria Fault. The WNW–ESE ridge related to the AGFZ is characterised by both echo-types IIIA and IIIC (Fig. 5).

b) Volcanic features

Additional relief comes from the MTR, which is also characterised by echo-types IIIA and IIIC, including an unnamed seamount to the east of Discovery Gap, on the lower flank of the MTR. It is oriented NE–SW and, with its water depth of 2050 m and length of 77 km, provides a natural boundary between the MTR and Discovery Gap. Within the gap narrow NE–SW striking ridges run parallel to the unnamed seamount with lengths up to 30 km and widths up to 9 km. To the north of the gap the ridges are orientated NNE–SSW and reach 55 km in length with widths of 2–10 km (Fig. 4). One additional ridge striking NW–SE appears to be a 31.7 km long and ~3 km wide protrusion of the MTR into the gap. These ridges are characterised by hyperbolic echo-types IIIA and IIIC resulting from the steep sides (gradients reaching 28°) (Fig. 5).

c) Erosional features

Along the NE sides of the topographic highs, crescent shaped scours occur, some 500 m wide, 2–4 km long, and 50 m deep. These scours can occasionally be found on the south side of highs (Fig. 4) Scours are generally represented by indistinct echo facies IIA (Fig. 5).

Erosional contouritic channels and moats are narrow (500–800 m) and often follow the base of a topographic rise for 4–8 km (and 40 km along Josephine Seamount). Erosional moats and channels are associated with indistinct, high-amplitude reflections, and moats may by associated with adjacent sediment drifts (Fig. 4). Downslope channels lead from the AGFZ and MTR into the gap and the depressions. The echo type characterising these downslope channels is the indistinct facies IIA (Fig. 5). They are typically quite narrow (1.5 km and may open up to over 6 km) and long (~18.3 km), covering gradients of 1.2–8.4°; but they are not related to any lobate or fan-like geometries at the end of the channel. Other features tied to erosional processes are the absence of sediment cover over rough seafloor and large furrows about 10–20 m wide (Fig. 8a). Furrows cannot be well distinguished from rough topography in the bathymetric data due to their small dimensions and the limited resolution (50 m) of the bathymetric data but the amplitudes of theses furrows is ~10–20 m. Relic furrows are furrows which are bounded on top by a reflection in seismic profiles. They are most common on the NE flank of the MTR.

d) Depositional features

A range of features can be associated with deposition in Discovery Gap, most notably sediment drifts forming along erosional scours and moats (Figs. 4 and 8). An area where mounded separated drifts occur is on the Madeira–Tore Rise, just below Josephine Seamount (Fig. 4), with a crest at 1400 m (D1) water depth (Fig. 9). This drift shows a change from high amplitude reflections near the adjacent moat to a weak/transparent unit downslope (Fig. 9). A second mounded drift (D2) forms to the northeast, over a topographic rise, with a crest at ~4680 m (Fig. 4). This drift is elongated in the N–S direction and bounded by two topographic rises on both sides, with a moat to the southwest (Fig. 8b).

A mounded/sheeted drift (D3) occurs beyond the exit sills of Discovery Gap at 4840–4880 m water depth (Fig. 4). It is associated with a moat (~10 m deep) along the base of a NW–SE trending topographic high, and a sheeted drift (4845–4870 m) (D4) on the opposing flank of the same high (Figs. 4 and 8c). The southern depression is infilled by what may be a sheeted drift, where the thickness is mostly uniform but decreases towards the erosional moat on the north side of the depression.

Other sedimentary features include large sediment waves and an extensive sediment blanket over areas with gradients <1° (Fig. 8d), where they appear to follow irregularities in the basement. These sediment waves are a relatively minor depositional feature within Discovery Gap, having a small wave height (10 m) but long wavelengths (10 km), being represented by echo types IB and IIIB in acoustic profiles (Fig. 5).

e) Mixed depositional erosional features

Terraces are large, sub-horizontal areas located in shallower areas of the gap (Figs. 4 and 8). Three main terraces were identified by echo-type IB (Fig. 5). The largest and shallowest one (T1) is found on the Madeira–Tore Rise, bounded by the unnamed seamount, with an area of 1032 km^2 at 3320 m water depth (Fig. 4). A thick sediment accumulation overlies this terrace, with some low-amplitude, wave-like features against the unnamed seamount (Fig. 9). A second terrace (T2) of 585 km^2 at 4720 m water depth occurs in the centre of the gap and has a thick sediment deposit (290 m thick from the V2707 profile) with sediment waves rising up to the Madeira–Tore Rise (Figs. 4 and 8). A third terrace (T3) is located to the south of Discovery Gap (Fig. 4) at 4852 m water depth, having an area of 184 km^2. It is associated with a

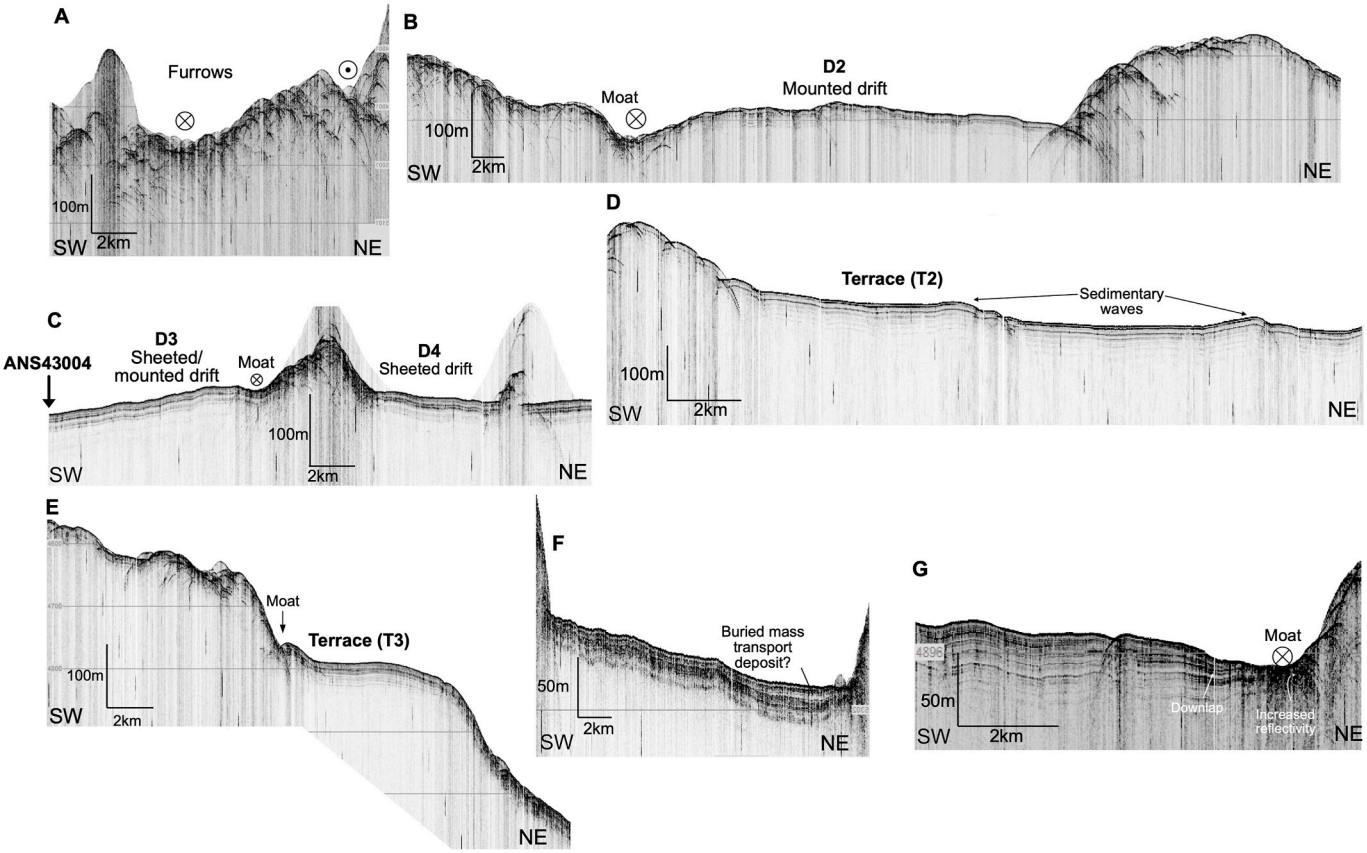

Fig. 8. Morpho-sedimentary features observed in acoustic profiles in Discovery Gap. Positions indicated in Fig. 4.

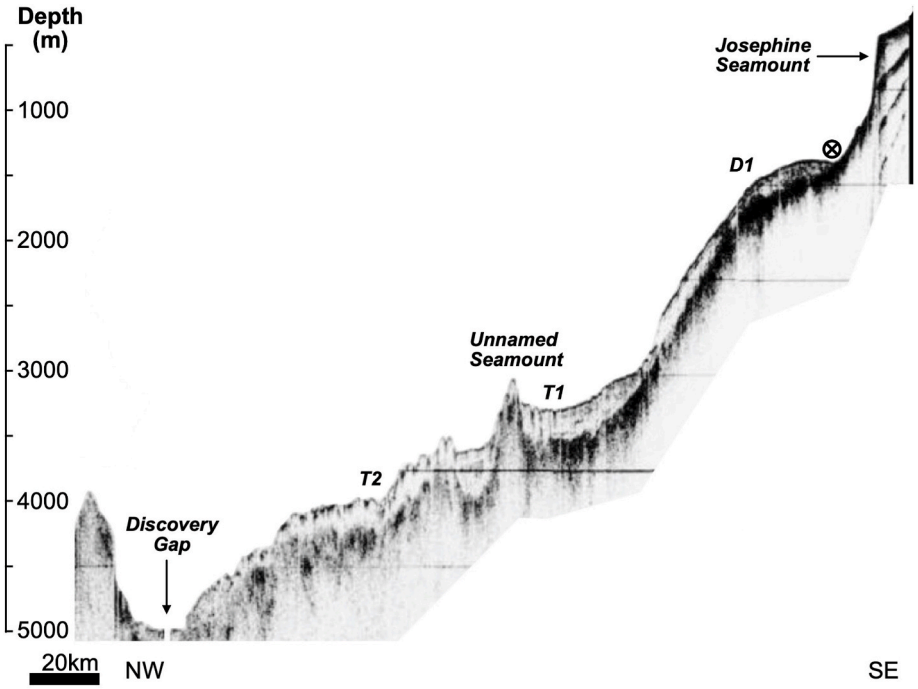

Fig. 9. Seismic line V2707 collected from Discovery Gap. In the figure, a drift builds out on the left side of Josephine Seamount towards Discovery Gap on the left.

mounded deposit which has a moat against the adjacent slope (Fig. 8e).

5.4. Seismic units

Three seismic units (U1–U3) could be identified along the studied seismic lines crossing the sheet-shaped deposit on terrace T2 (Fig. 10 and Table 3). Seismic Unit U1 is ~4.6 m thick and shows a basal boundary that represents an erosional surface (green in Fig. 10) that truncates the reflections from U2, especially near moats and against topographic highs (Fig. 8g) Its top boundary is characterised by very high amplitude seafloor reflections (pink in Fig. 10). This unit has a high acoustic response throughout Discovery Gap, yet it is more transparent in some areas than in others. Reflection terminations in areas with low slope gradients, such as terraces and depressions, show downlap near topographic highs and moats (Fig. 8g).

Seismic unit U2 is about 10.6 m thick and has an erosive basal boundary characterised by a high amplitude reflection (blue in Fig. 10). This unit has moderately high-amplitude, semi-continuous parallel reflections that form sheeted and mounded drifts. It also contains a transparent buried deposit outside the gap in the north (Fig. 8f).

The deepest unit, U3, is at least 41 m thick and contains three internal subunits (a to c in Fig. 10) which are 9.8 to 13.7 m thick, that alternate between well-stratified and transparent. Its basal boundary cannot be determined because of the low penetration of the seismic system used. The unit's reflections have low-amplitude and are discontinuous throughout the gap. There are slightly higher amplitudes in the reflections from subunit 3c as compared to subunits 3a and 3b (Fig. 10), but reflections are generally very weak in all subunits in the depressions, and U3 is transparent elsewhere in the gap (Fig. 8).

5.5. Sedimentary features from seafloor pictures

Four oriented seafloor photos from the flank of the unnamed seamount show muddy sediment ripples, small manganese nodules, irregular sediment cover and largely calm seafloor (Fig. 11). Small-scale obstacle scours with faint current lineations are observed adjacent to the tranquil seafloor and are covered or infilled by muddy sediment (Fig. 11c). Biogenic traces are present but not abundant on the seafloor.

The muddy sediment ripples are formed by an east-directed current flowing perpendicular to the mostly N–S orientated crests. Between the

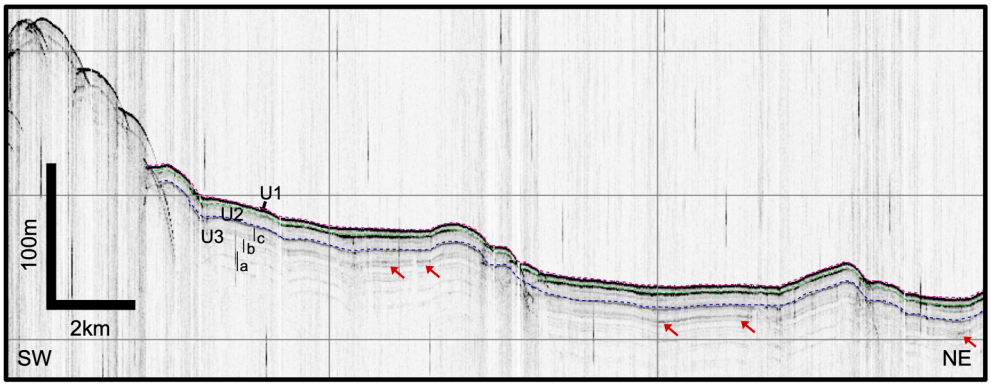

Fig. 10. Seismic units from the central terrace (T2). The red arrows mark deposits with higher amplitude in U3c. Profile location in Fig. 2. (For interpretation of the references to colour in this figure legend, the reader is referred to the Web version of this article.)

Table 3
Seismic units U1 to U3 in Discovery Gap. They are very similar in character and generally quite well distributed throughout the gap, especially on flatter topography.

Seismic Unit	Boundaries	Reflection terminations	Reflection configurations	Shape	Distribution
1	High amplitudes surface reflection	Onlap; downlap	Transparent	Thin sheet	Generally, on terraces
2	Bounded by high amplitude reflections	Truncation and onlap of reflections occurs near moats and at the base of topographic highs	Moderately high amplitude, semi-continuous, parallel reflections	Sheet, mounded, sediment blanket	Terraces, South depression, low gradient topographic highs
3	Base not seen	No onlap, downlap or truncation seen	Massive at the base to well stratified subunits interbedded with transparent subunits. Low amplitude semi-continuous reflections	Sheet	Terraces, South depression (poor)

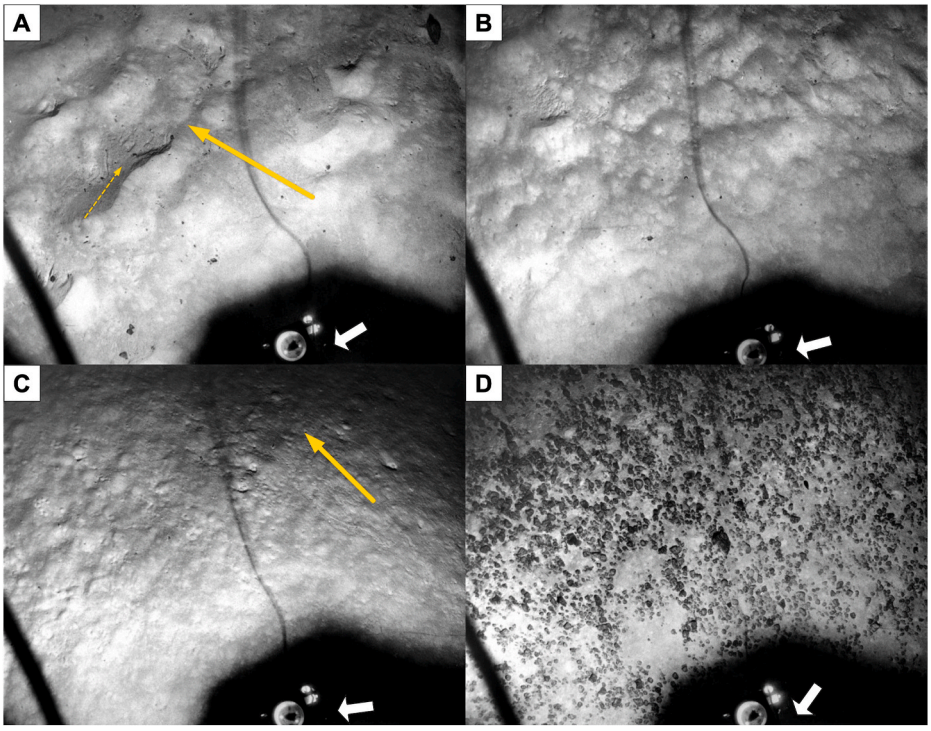

Fig. 11. Seafloor photos taken at the base of the unnamed seamount. They have been reoriented (white arrow points north) with the help of the photographed compass. The current direction (yellow arrow) is inferred from the photographed bedform. A: Muddy ripples with debris and groove marks. The thin dashed line indicates the direction in which debris is being displaced by local turbulence, inferred from the groove marks. B: Irregular seafloor that has been covered by muddy sediment. C: Calm seafloor with faint current lineation and no thick sediment cover. D: Small, irregular manganese nodules with partial sediment cover in the lower right of the photo and no sediment cover in the top left half of the photo. (For interpretation of the references to colour in this figure legend, the reader is referred to the Web version of this article.)

muddy ripples there are groove marks with small, gravel-sized manganese nodules (Fig. 11a). The grooves run parallel to the crests of the ripples, which are partially covered by a muddy sediment layer (Fig. 11). Small manganese nodules are also observed on the flank of the unnamed seamount. Some the manganese nodules have a partial sediment cover, while others slightly further up the slope have no sediment cover (Fig. 11d) where the current is localised.

The resolution of the bathymetric data (50 m horizontal resolution) means that these features cannot be seen on bathymetric data; their appearance in seafloor photos may, however, indicate a greater distribution of such sedimentary features in Discovery Gap.

5.6. Sedimentary facies

The sediments were classified into five sedimentary facies (F1–F5).

5.6.1. Facies 1 (F1) description

Sedimentary facies 1 (F1) is a light-coloured, massive, poorly-sorted, foraminifera-rich, sandy-silty-clay–sand. In CT it has low–moderate radio-density increasing down core. In core ANS43006, this facies is characterised by silty-clay (Fig. 12). Bed thicknesses vary from 11 to 58 cm (Fig. 12) with mostly gradational boundaries. This facies has symmetric and coarsely skewed (Fig. 13 and14), both meso- and leptokurtic, bimodal and unimodal distribution (Fig. 13); it is associated with high ln (Ca/Fe) and low ln(Ti/Ca), ln(Zr/Sr) and magnetic susceptibility (Fig. 12). Organic matter is abundant, taking the form of ~1 cm soft black clumps and sometimes thin laminations or, rarely, subunits.

Biogenic traces have a low radio density infill, as burrow infill is, in most of the cases, similar to the host sediment. A mottled background can be not discarded, but scarce colour differentiation makes a clear characterization difficult. *Planolites* is abundant in this facies, as is *Thalassinoides*. *Chondrites* also occurs regularly across all the cores. *Zoophycos* traces are only occasionally identified and *Palaeophycus* are very rare (Fig. 14). This trace fossil assemblage can be assigned to the *Zoophycos* ichnofacies, typical for distal, low energy environments (Uchman and Wetzel, 2011; Wetzel and Uchman, 2012).

The microfacies of F1 is a wackestone, which becomes a mudstone downcore ANS43006 due to extensive dissolution of foraminifera tests (Fig. 15a). Packed areas in the microfacies relating to bioturbation are not uncommon. Foraminifera display very high rates of dissolution, but nonetheless, bioclastic fragments are still abundant and the matrix can become quite coarse as a result (Fig. 15a). Some foraminifera tests contain a silty infill that does not resemble the surrounding matrix, similar to observations made in ancient contourite successions in Cyprus described by Hüneke et al. (2021). Opaque coating and pyrite can be observed on some foraminifera or forming separate clusters in the matrix (Fig. 15a). Additionally, small sub-angular grains of quartz and faecal pellets occur in certain sections and a slight alignment of grains

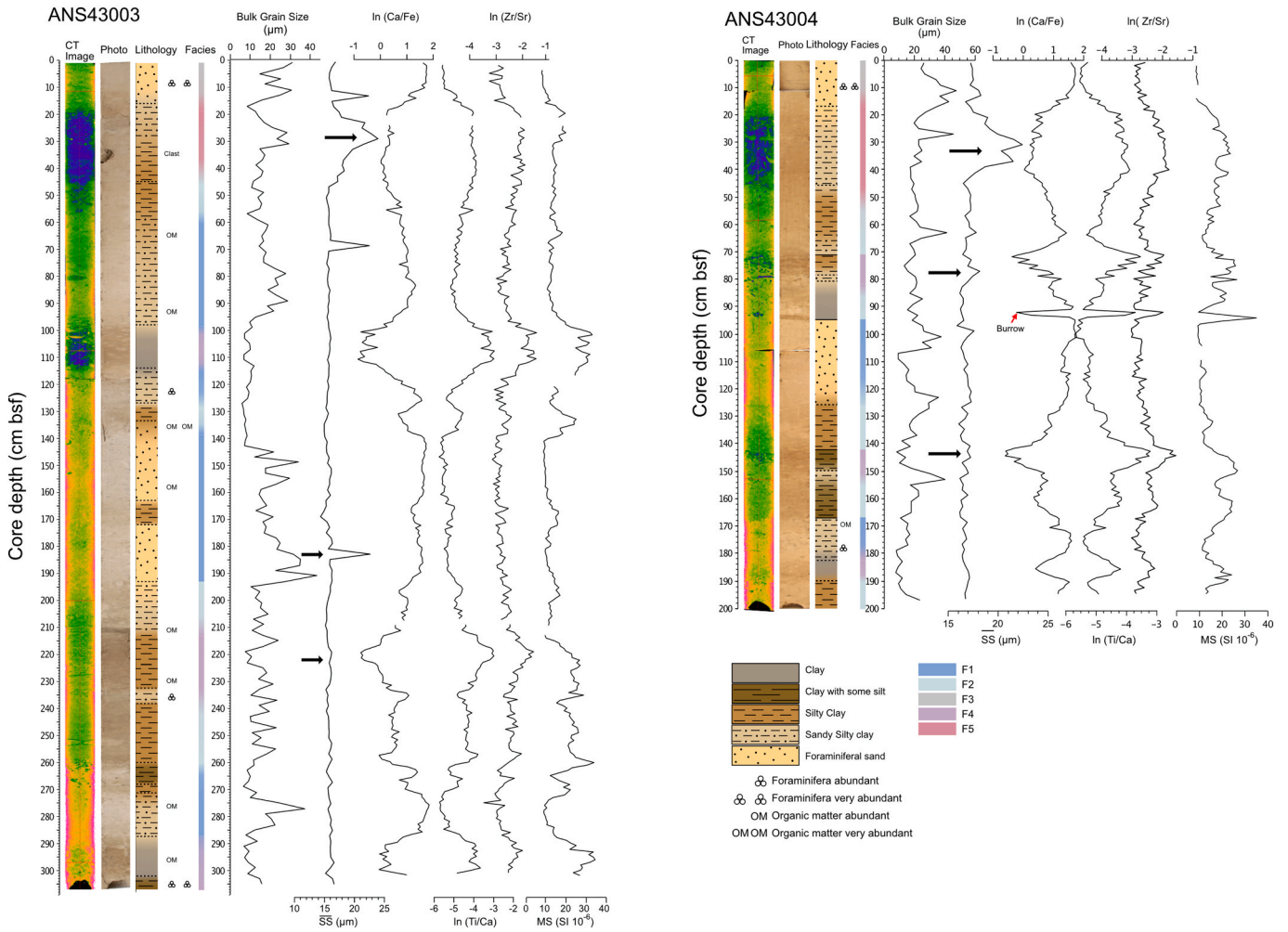

Fig. 12. Sedimentary logs for the sediments collected by cores in Discovery Gap. Their key properties in CT, visual, grain size, sortable silt and XRF are shown.

does occur but is not widely observed.

5.6.2. F1 interpretation

The elevated Ca/Fe ratios and light colour indicate a high carbonate content (Rothwell et al., 2006) while the low sortable silts ($\overline{S}\overline{S}$) and symmetrical–coarse skewness suggests deposition of sediment from suspension but influenced by very weak (<10 cms^{-1}) bottom currents (Brackenridge et al., 2018), which sweep the abyssal floor during normal ocean circulation but do not actively rework the sediment. In thin-section, the infill of some foraminifera tests in wackestones supports the presence of these weak local abyssal currents —insufficient to rework the deposit, but intermittently strong enough to locally displace grains and prevent deposition leading to thin, irregularly spaced organic matter laminations (Hernández-Molina et al., 2011; Hüneke et al., 2021). The meso- to leptokurtic distribution indicates a lack of variety in the sediment supply (Brackenridge et al., 2018). The dominant record of *Planolites* and *Thalassinoides* and abundant organic matter in this facies indicates increased productivity in surface waters and concentration of organic matter mainly in the first centimetres below the seafloor (Müller and Suess, 1979). Therefore, we propose that this is a high-carbonate pelagite with a vertical sediment supply that is not undergoing active reworking by bottom currents. The low to moderate radio density throughout this facies is also characteristic of pelagites (Mena et al., 2015) and the continuous and abundant bioturbation reveals constant sedimentation and low accumulation rates (Wetzel, 1991; Rodríguez-Tovar and Dorador, 2014; Rodríguez-Tovar et al., 2015a, b).

5.6.3. Facies 2 (F2) description

Sedimentary facies 2 (F2) is characterised by dark beds of silty-clay, clay with some silt, and clay. The beds are light to medium brown and organic matter is very abundant in places. XRF shows reduced ln(Ca/Fe), but elevated ln(Ti/Ca) and ln(Zr/Sr) compared to F1 (Fig. 12). Beds vary in thickness from 12 to 46 cm, with mostly gradational boundaries. This facies is poorly sorted, having a meso- to leptokurtic, bimodal and unimodal distribution (Figs. 13 and 14). Trace fossil assemblage consists of *Planolites*, *Thalassinoides*, *Zoophycos*, and *Chondrites*; the two former occur with infilling material lighter than the host sediment (Fig. 14).

The microfacies in F2 is a wackestone–coarse-Globironid-wackestone with some limited sub-horizontal alignment of larger grains. Lenticular packed areas also occur, and are associated with burrows. Intact foraminifera tests are plentiful and are usually unfilled (Fig. 15b). Fractured tests can be infilled with surrounding matrix, mud, silt, or have a pyritized rim (Fig. 15b).

5.6.4. F2 interpretation

The poor sorting, symmetrical to fine skew, and lepto–mesokurtic distribution is common in hemipelagite deposits under normal sedimentation conditions (Brackenridge et al., 2018). The darker colour, when compared to F1, and increase in terrigenous markers in XRF further support higher sediment supply and a hemipelagic origin. However, the high % of $CaCO_3$ (>30%) in this facies points to a pelagic sediment. Therefore, this is another pelagite (low carbonate) but with lower $CaCO_3$ and increased terrestrial input.

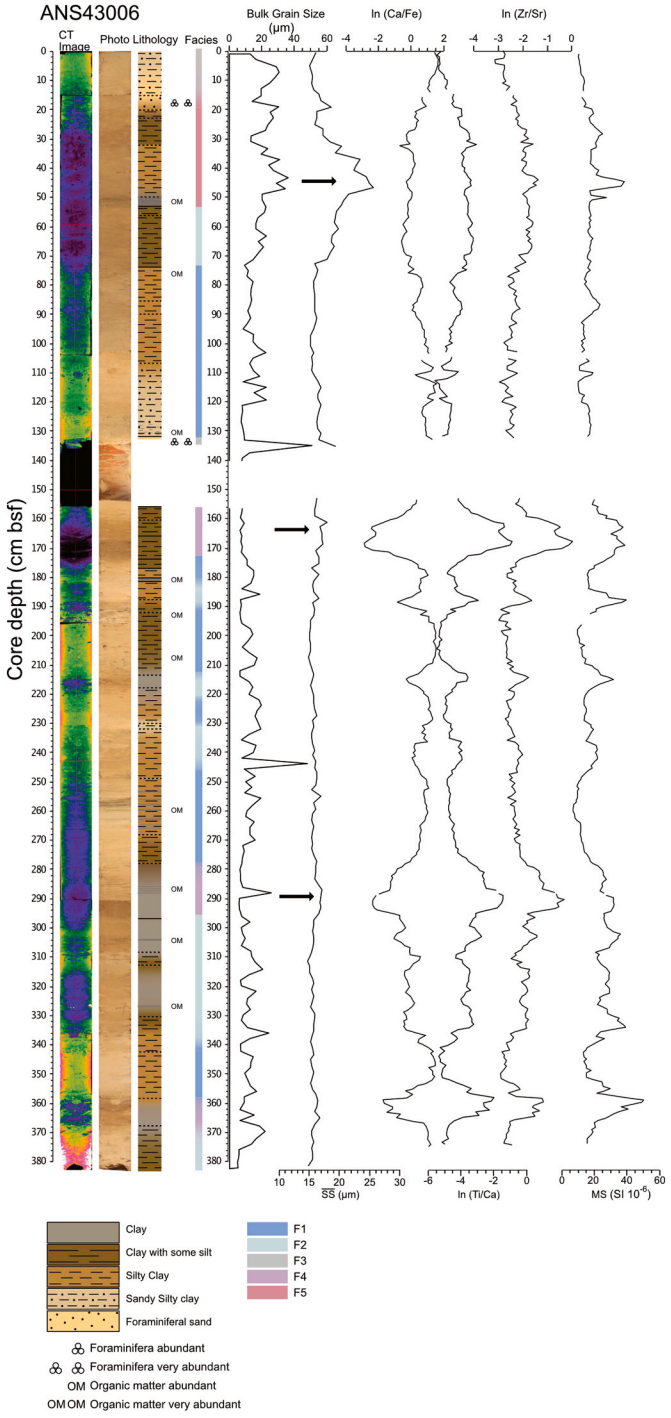

Fig. 12. (*continued*).

The lack of foreign infill of partial foraminifera tests suggests no transport by bottom currents (Hüneke et al., 2021). Lighter infilling material of *Planolites* and *Thalassinoides* compared to the dark host sediment indicates bioturbation from the overlying material. Increased presence of *Chondrites* and *Zoophycos* with respect to facies F1 can be linked to increasing organic matter and reduced oxygen levels at the seafloor (Wetzel, 1991; Rodríguez-Tovar and Dorador, 2014; Rodríguez-Tovar et al., 2015a,b), associated with a stagnant bottom water lacking the ventilation that is tied to bottom currents. Organic matter in F2 may have to do with the poor ventilation of bottom waters or an increased organic influx. The conditions during F2 deposition are less favourable for high carbonate accumulation than during F1 deposition.

5.6.5. *Facies 3 (F3) description*

Sedimentary facies 3 (F3) consists of massive poorly-sorted, structureless foraminifera sand-silt. It is found at: a) the top of all the cores in ~28–30 cm deposits (Fig. 12), where the bulk grain size is fine skewed, with a leptokurtic bimodal distribution (Fig. 13), and the bulk grain size is slightly elevated (Fig. 12); and b) as 2 cm deposits in the centre of ANS43006 (Fig. 12), where the core has separated, and the facies is very poorly sorted, showing a very fine-skewed, platykurtic, bimodal distribution (72.02 and 4.85 μm) (Fig. 13). There is very little mud: 6% compared to 13–22% elsewhere in the core.

Bioturbation is not abundant in F3 but some individual traces of *Planolites* and *Thalassinoides* were identified in CT since they are infilled

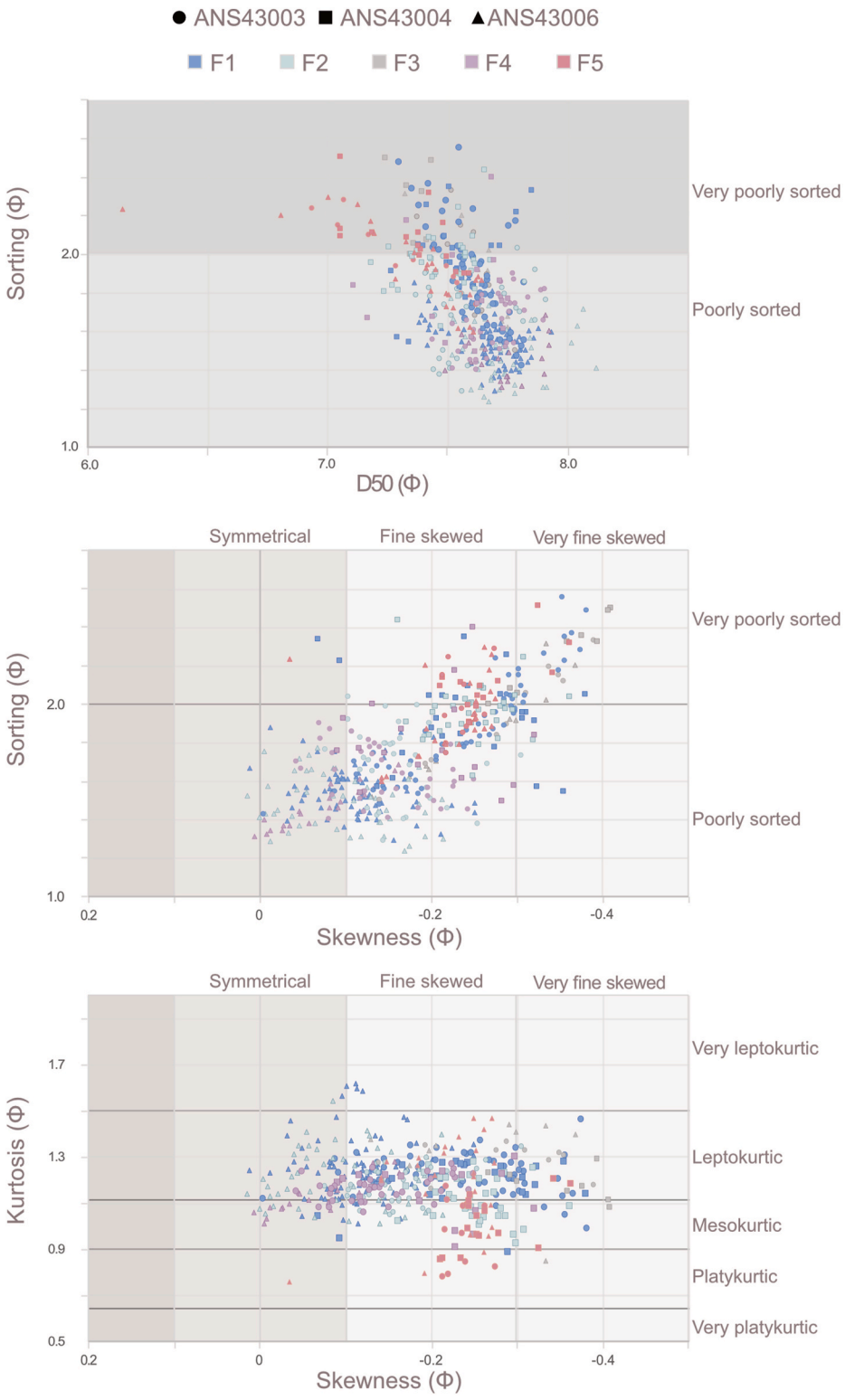

Fig. 13. Grain size parameters for the collected cores. Bottom current influence can be distinguished by the sorting versus the D50 grain size (A), the sorting versus the skewness (B) and the kurtosis versus the skewness (C) following Brackenridge et al. (2018) and de Castro et al. (2021).

by lower radio density sediment —compared to the surrounding sediment, which has a moderate radio density (Fig. 14). In XRF, this facies is characterised by high ln(Ca/Fe), but low ln(Ti/Ca) and ln(Zr/Sr) (Fig. 12).

The microfacies associated with F3 is a wackestone with packed areas owing to bioturbation. The grains are supported by a micritic matrix, though in some areas the matrix becomes sparse (Fig. 15c). Foraminifera tests show some dissolution and chambers are often infilled with matrix sediment. Some diagonal laminations may be present but, because they were destroyed by bioturbation, they are difficult to interpret as proper primary structures (Fig. 15c). Quartz, feldspathoids, and opaque grains make a minor contribution in this facies.

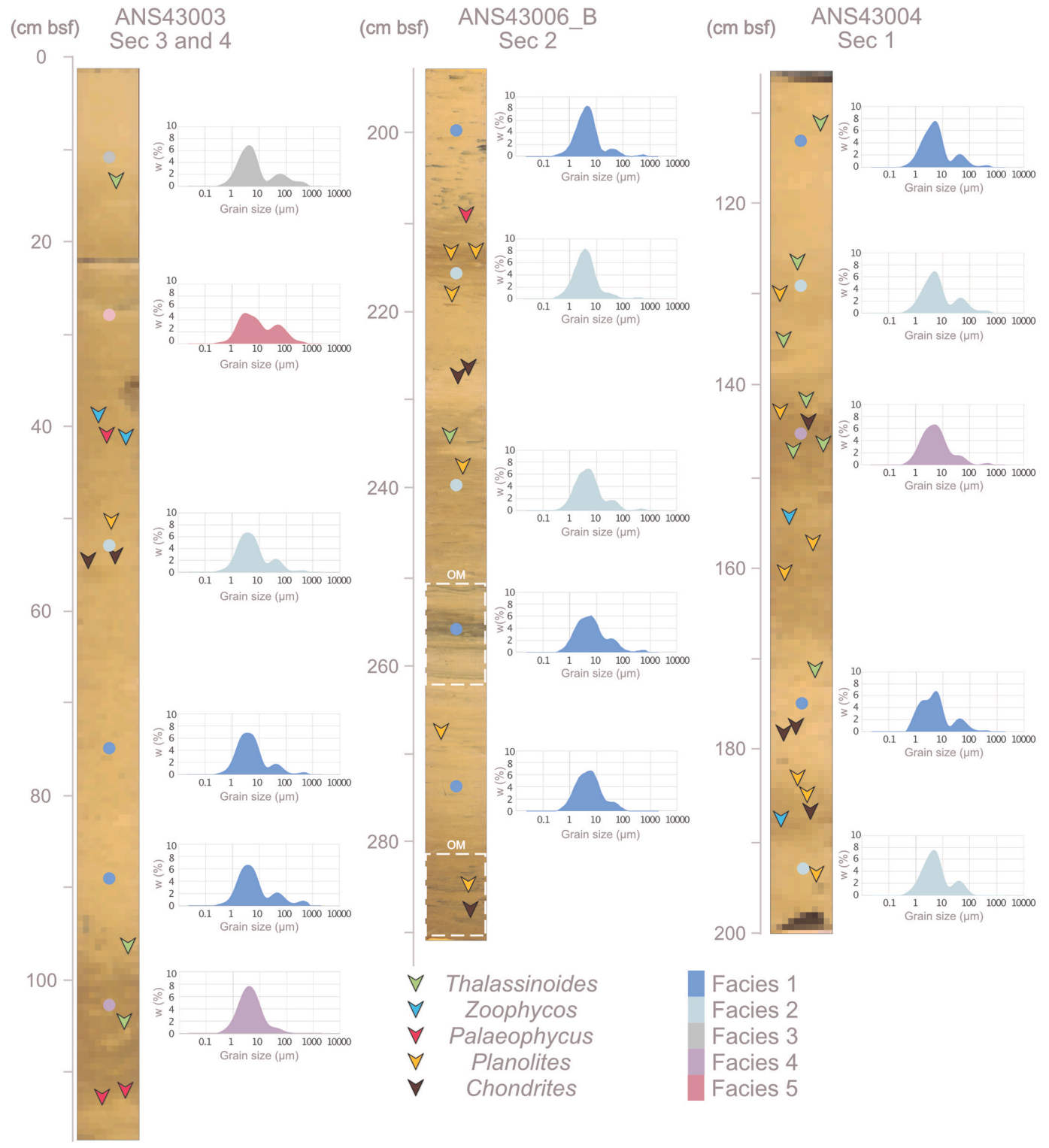

Fig. 14. Identified traces fossils and representative grain size distributions, of all the sedimentary facies along the studied cores.

5.6.6. F3 interpretation

The very high carbonate component increased, bulk grain size, and fine-very fine skew is interpreted as a reworked pelagite. The bimodal distribution, coarse tail, and very-poor sorting are taken as indicators of increased reworking of pelagic sediment while it is being deposited but they could also indicate an increase in the number of foraminifera tests which constitute the fine sand grain size fraction, hence, creating a coarse tailed grain size distribution.

Where the skew shifts to fine, and the kurtosis becomes platykurtic in the centre of ANS43006, we can propose that there is greater winnowing by bottom currents during this time (Brackenridge et al., 2018), possibly indicative of a localised intensification of current in the southern depression, since the same unit correlates laterally to normal pelagites in the other cores.

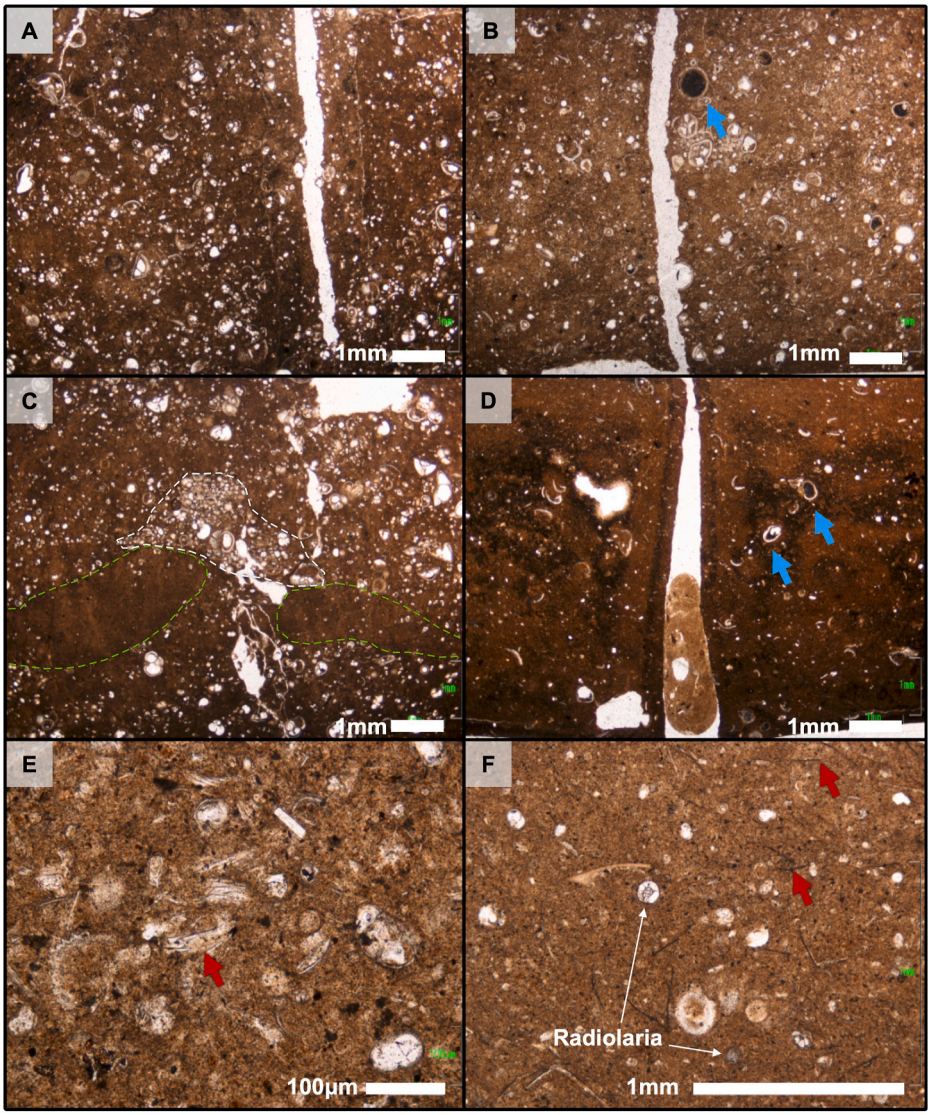

Fig. 15. Microfacies from thin sections conducted on each identified sedimentary facies. A — F1; B – F2; C – F3; D — F4; E and F — both F5. The red arrows point to indeterminate bioclast fragments and the blue arrows point out allochthonous infill of foraminifera tests. In Fig. 15c, the packed areas are outlined in white and the wackestone areas in green, both corresponding to organism burrow infill. (For interpretation of the references to colour in this figure legend, the reader is referred to the Web version of this article.)

5.6.7. Facies 4 (F4) description

Sedimentary facies 4 (F4) is similar to F2 but generally finer, ranging from clay to silty-clay in all the cores. Its bulk sediment character is often poorly-sorted, unimodal, meso- to lepto–mesokurtic and symmetrically–coarsely skewed (Figs. 13 and 14). The radiodensity is typically low and traces are often observed. F4 forms quite thin units up to 22 cm, but more often ~10 cm, with gradational and sharp boundaries. F4 can be distinguished from F2 by its darker colour, the distinctive peaks in terrestrial elements in XRF, and very low ln(Ca/Fe) values (Fig. 12) and percentages of $CaCO_3$. Such changes are tied to peaks in the magnetic susceptibility. F4 is often associated with decreased bulk grain size, yet also has a slight increase above background levels in the sortable silt of the $CaCO_3$-removed fraction (Fig. 12). *Planolites*, *Zoophycos* and *Thalassinoides* are abundant, along with rare *Palaeophycus*. *Chondrites* occurs where there is an overlying unit of F3 (Fig. 14). *Planolites* and *Chondrites* show a lighter infilling than the host sediment.

The microfacies for F4 is a wackestone without packed areas (Fig. 15d). Small, rounded grains of moderately high relief are taken to be fragments of foraminifera tests. Muddy areas are also seen. Foraminifera tests are dissolved and infilled with the matrix sediment. The matrix contains opaque grains and small amounts of pyrite.

In core ANS43006_B, facies F4 is associated with structures that resemble ripples in CT scans (though they could not be identified during logging) which prograde along the core (Fig. S3). Rare biogenic traces typically occur in the muddy layers between ripples (Fig. S3).

5.6.8. F4 interpretation

Although there are peaks in the terrigenous markers in XRF, the dissolution is very high. Therefore, it would be inappropriate to interpret this as an increase in terrigenous supply. Despite the high rate of dissolution, ripples in silty sediments may be generated by relatively high currents from ~15 to 20 cms^{-1} (McCave and Hall, 2006; McCave et al., 2017; Culp et al., 2021), but breaks in the flow have allowed muddy sediment to settle. The presence of ripples in only one core could suggest that this is a turbidite. Deposition of a turbidite can lead to localised intensification of current and create sediment ripples in only one area and this may explain why a thin unit of F3 overlies the rippled F4 in only one core. The $CaCO_3$-free grain size and sortable silt is also low in F4, with only a slight increase in F4, but bulk grain size increases sharply into the overlying F3. However, taking into account the low sedimentation rate in Discovery Gap, this unit of F4 was deposited over the course of MIS 4 and is unlikely to be a single turbiditic current. There is also no peak in the $\%CaCO_3$ across MIS 4 which means that material did not come from above the CCD, becoming buried rapidly in Discovery Gap before it could dissolve.

The disaggregated foraminifera tests likely form from high shear-

stress at the water–sediment interface. This is indicative of reworking of sediment in F4, possibly relating to corrosive AABW. Therefore, this facies is interpreted as reworked hemipelagites. Similarly to F2, light infilling material of *Planolites* and *Thalassinoides* compared to the dark host sediment indicates bioturbation from the overlying material. Frequent appearance of *Chondrites* and *Zoophycos* can reveal increased organic matter and reduced oxygen levels at the seafloor. So bottom currents are not so vigorous as to disrupt benthic communities.

5.6.9. Facies 5 (F5) description

The sedimentary facies 5 (F5) is poorly to very-poorly sorted with a fine–very-fine skew in a bimodal distribution, ranging from lepto-to platykurtic (Figs. 13 and 14). This facies lacks primary structures and is massive or shows slight bi-gradational grading with elevated bulk grain sizes and a peak in the sortable silt fraction (up to 46 and 26 μm, respectively) (Fig. 12). These peaks are not especially noticeable in the XRF element ratios and MS (Fig. 12). In CT, the radio density is very low, and bioturbation is difficult to characterise. *Planolites* and *Thalassinoides* are the most abundant traces with less common *Zoophycos* and rare *Palaeophycus* (Fig. 14).

Facies F5 has a wackestone microfacies, where plagioclase, quartz, muscovite, haematite(?) grains and black opaques are present. Radiolarians are fairly abundant, diatoms are scarce, and foraminifera tend to be dissolved or fractured (Fig. 15e and f). The ln(Si/Ti) does not show any peaks in F5, so it is unlikely to be a terrigenous biproduct.

In ANS43003, this facies also contained a large lithic clast which had minor deformation of surrounding sediment visible only in CT though it is possible the deformation was caused by the gravity corer as it entered the sediment and moved the clast.

5.6.10. F5 interpretation

The facies F5 is interpreted as silty contourites where the prominent peak in $\overline{S}^{-}\overline{S}^{-}$ results from a greater bottom current velocity capable of transporting this fine fraction (McCave and Hall, 2006). Bi-gradational grading and a lack of primary structures resemble contourite facies C3 relating to strengthening and waning of the depositing current (Gonthier et al., 1984). The strongly bimodal distribution and very-poor sorting are indicative of a greater concentrating effect of coarser grains (Brackenridge et al., 2018; de Castro et al., 2020). There is decreased dissolution in this facies, yet there is no large peak in terrigenous or carbonate markers in XRF. This could be because of a local sediment source change (Brackenridge et al., 2018) or because previously deposited sediments are being reworked and coarser foraminifera tests are being carried away. The additional identification of radiolarian and mineral grains in thin section suggests that the sediment supply is more hemipelagic than pelagic during its primary deposition. The lithic clast is assumed to have come from a surrounding topographic high on the MTR.

5.7. Facies associations

The identified sedimentary facies can be found in vertically stacked

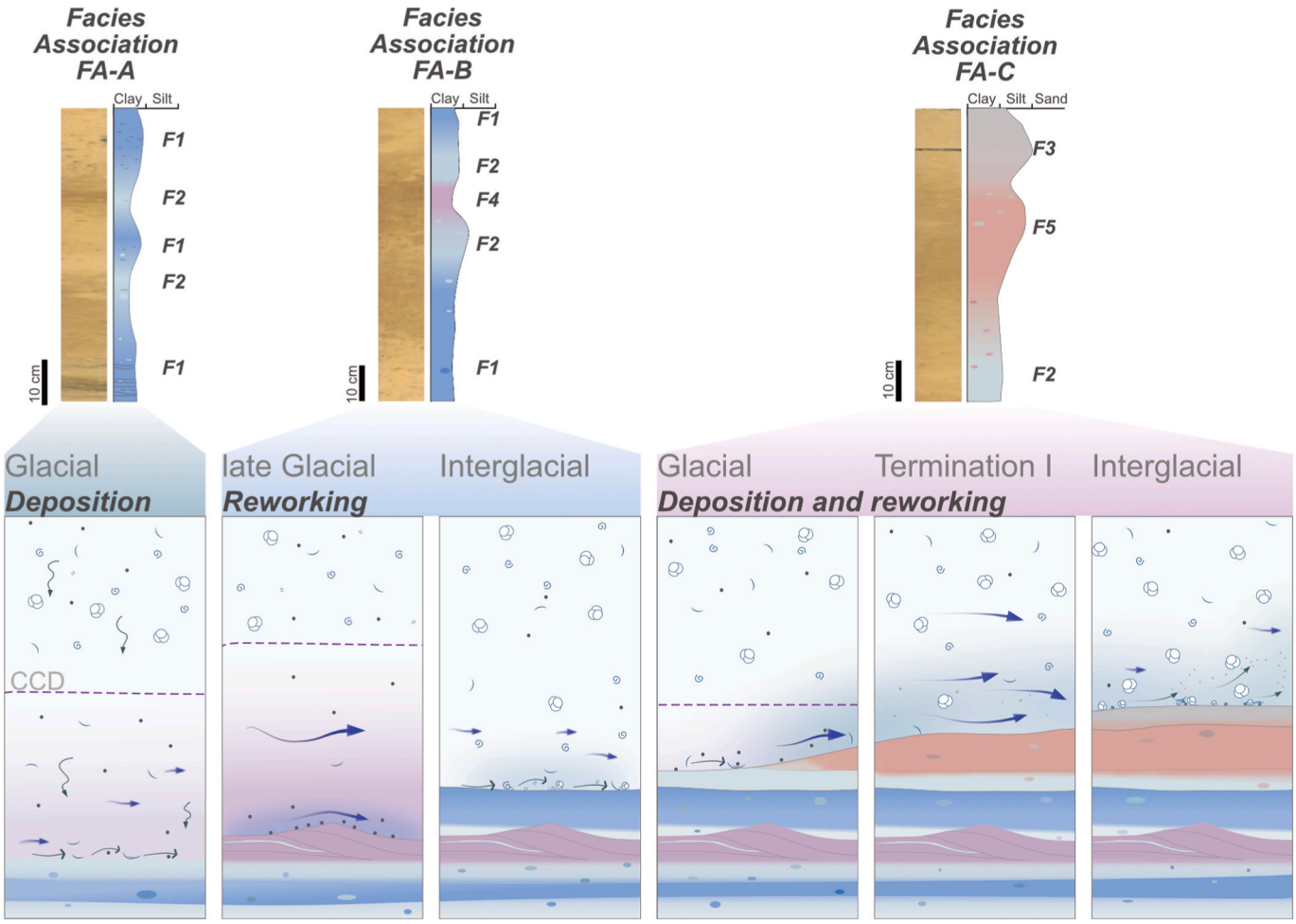

Fig. 16. Facies association (FA) identified in this research (FA-A, FA-B and FA-C) including conceptual sketches for the sedimentary facies association development in Discovery Gap from the Mid-Pleistocene to the Holocene. Their vertical stacking pattern is the result of shifts in depositional processes and conditions in the bottom boundary layer.

facies associations. Three associations (FA-A, FA-B and FA-C) are described below (Fig. 16), but partial sequences relating to both associations are also common.

Facies association A (FA-A) is formed from the two vertically deposited facies F1 and F2 which are interbedded throughout all of the studied cores, usually in the lower half of the core. Sequences of FA-A range in thickness from 18 to over 70 cm with gradational, mottled boundaries between the units (Fig. 16). A significant change is registered between facies F1 and F2 by the increase in the abundance of *Chondrites* and *Zoophycos* (Fig. 14).

Facies association B (FA-B) encompasses the gradation from F1 to F2 to F4 and then back to F2 and F1. The boundaries between these facies are often gradational, although a sharp boundary between F2 and F4 can also be observed (Fig. 12). The thickness of the whole association varies, ranging from 86 to ~150 cm (Fig. 16).

Facies association C (FA-C) comprises the common core-top facies where it is characterised by the sequence of facies F2–F5–F3. The boundary between F3 and F5 is gradational but a drop in grain size along the boundary can be identified (Fig. 12). There are no peaks in XRF which mark this boundary, but sortable silt shows bi-gradational trends across this association (Fig. 12). This association of facies marks some of the coarsest sediment in the collected cores characterised by the highest sortable silt size (Fig. 16).

5.8. Age model

The sediments recovered by the ANS43006_A core in Discovery Gap extend from the present day to 239.5 ka, the Marine Isotope Stage (MIS) 7e (Table 4 and 5). The tie-points correlate the $\delta^{18}O_{Cw}$ isotope signal from ANS43006_A to the global benthic oxygen isotope stack LR04 of Lisiecki and Raymo (2005) and another four tie points were verified with $\delta^{13}C_{Cw}$, $CaCO_3$, and MS curves (Fig. S4, Table 4). A linear interpolation between the applied tie points helped establish the final chronology (Fig. 17). The MIS boundaries were assigned following a clear subdivision of the LR04 stack by Railsback et al. (2015). According to the developed age model for other cores in the Discovery Gap (ANS43006_B, ANS43004, and ANS43003), the collected sediments date to early MIS 7 (Fig. 18).

Interestingly, all the cores capture the same time period despite the varied thickness of units and sedimentation rates (Fig. 18), which may be because below the MIS 7c there are coarser lithologies and/or a hardground which cannot be penetrated. This hypothesis is partially supported by the high acoustic response of the younger seismic unit (U1) (Fig. 10).

Table 4
Thirteen tie points were used to correlate ANS43006_A to the stacked benthic $\delta^{18}O$ isotope curve LR04 (Lisiecki and Raymo, 2005). Four additional points (marked with an asterisk) could also be established with the help of $\delta^{13}C$, $CaCO_3$ and magnetic susceptibility (MS).

Depth (cm)	$\delta^{13}C$	$\delta^{18}O$	Age (ky BP)
1	0.62	2.46	0
20	0.512	2.57	5
40	0.054	4.198	16
50	−0.116	4.276	* 29
90	0.028	3.655	38
140	0.516	3.539	55
173	−0.283	3.878	* 69
190	0.482	2.908	82
220	0.286	2.967	99
240	0.518	2.689	* 122
250	0.634	2.569	126
270	0.208	3.431	* 131
280	−0.099	4.234	135
320	−0.056	3.639	174
340	0.29	3.515	191
360	0.667	2.704	217
	−0.044	2.689	239.5

Table 5
The identified isotopic stratigraphic subdivisions related to the previously defined tie points in core ANS43006_A.

Depth (cm)	*Age (ka)*	Isotopic stratigraphy
0.5	0	MIS 1
19.5	5	MIS 1
39.5	16	MIS 2
59.5	* 29	MIS 2
89.5	38	MIS 3a
139.5	55	MIS 3c
172.5	* 69	MIS 4
189.5	82	MIS 5a
219.5	99	MIS 5c
239.5	* 122	MIS 5e
249.5	126	MIS 5e
269.5	* 131	MIS 5e
279.5	135	MIS 6a
319.5	174	MIS 6d
339.5	191	MIS 7a
359.5	217	MIS 7c
389.5	239.5	MIS 7e

6. Discussion

6.1. Insights into the formation of the Discovery Gap

Except for a few studies focused on the oceanography (e.g., Saunders, 1987; Tarakanov et al., 2013), seismic activity (e.g., Bezzeghoud et al., 2014) and MTR magmatism (e.g., Merle et al., 2006), the deep-ocean floor in the Discovery Gap region is poorly studied. Hence, little is known about its geological evolution and, more specifically, about the formation of Discovery Gap. Accordingly, we present and discuss some hypotheses about Discovery Gap's formation, based on its morphology and its regional setting.

Discovery Gap is bounded by two large features, the eastern segment of the Gloria Fault to the north, and the western seamounts of the MTR to the east. This indicates that the gap developed within the oceanic crust of the African plate. Although the age of this crust is unknown, it should be slightly younger than isochron M0 (121.2–120.6 Ma; Aptian) (Vissers and Meijer, 2012), and hence it can be assigned to the end of the Early Cretaceous or beginning of the Late Cretaceous. The small NE–SW elongated ridges in the Africa plate and the NNE–SSW ridges in the Eurasia plate can be interpreted as abyssal hills and ridges formed in the Cretaceous Mid Atlantic Ridge and, therefore, represent the typical relief of the deep-ocean floor. However, the NE–SW ridges are older than the NNE–SSW trending ridges as supported by the location of magnetic anomalies (Fig. 1). The MTR formed on the Cretaceous oceanic crust through several pulses of intraplate alkaline magmatism from the Late Cretaceous to middle Miocene (e.g., Merle et al., 2006).

Considering the morphological characteristics and geological context of Discovery Gap, we can put together three hypotheses regarding its formation, although alternative hypothesis cannot be ruled out:

i) Discovery Gap's depressions formed as nodal basins during Cretaceous ocean-spreading and their shape remained almost unchanged since then. Nodal basins are common features formed from the interaction between a spreading centre and an oblique transform fault (e.g., Lagabrielle et al., 1992; Okino and Fujioka, 2003). Discovery Gap shows similar morphology when compared to nodal basins (Lagabrielle et al., 1992; Harmon et al., 2018). In the study area there are other depressions trending parallel to the south depression occurring at ~17 °W (Fig. 4). So, Discovery Gap might be a relic feature inherited from past ocean-spreading stages. However, neither fracture zone (ancient transform fault) nor old spreading-ridges are observed in association with these depressions as would be expected in the case of a nodal basin (Fig. 2).

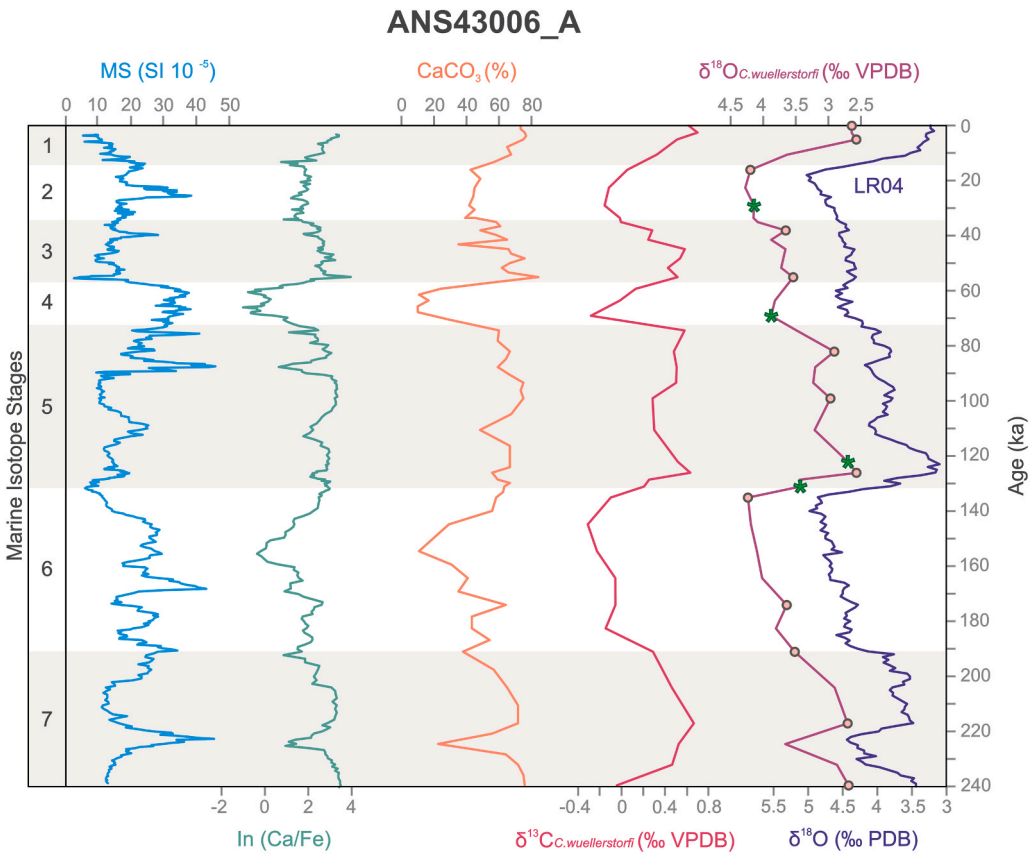

Fig. 17. The replotted age model against age and marine isotope stages (MIS) rather than depth. The green stars and orange circles mark the tiepoints.

ii) As in the previous hypothesis, the Discovery Gap's depressions formed originally as nodal basins in the Cretaceous but were subsequently reshaped by the tectonic activity of the Gloria Fault and magmatism of the MTR. In the first case, the movement along the Gloria Fault produced the WNW–ESE ridge that bounds the northern basin of Discovery Gap. In the second case, magmatic events might extrude along fractures forming the NW–SE ridge that crosses Discovery Gap.

iii) the Discovery Gap's depressions could be the consequence of lithospheric flexure (i.e., subsidence) due to the weight imposed by the nearby MTR. Lithospheric deformation is a common and widely described process around oceanic islands and seamounts (e.g., Watts, 1994; Watts et al., 2006). However, if Discovery Gap formed by this process, it would be expected that other basins were formed around the MTR, but this is not the case (Fig. 4).

Considering all the above, we propose hypothesis ii) as the most probable to explain the formation of Discovery Gap, although further studies need to be conducted and new geophysical data acquired to investigate this hypothesis further.

6.2. Water masses in Discovery Gap

6.2.1. Intermediate water masses

A noteworthy presence of the Mediterranean Outflow Water (MOW) is unsurprising as this water can be traced from the western Atlantic back to the Gulf of Cadiz (van Aken, 2000a).

There is quite a distinct stratification in salinity and density between the MOW and the underlying North Atlantic Deep Water (NADW) which can support the formation of internal waves especially in the vicinity of seamounts (Mosquera Giménez et al., 2019), hence increasing mixing of the water (Polzin, 1997), changing flow around seamounts, and altering sediment dynamics (Pomar et al., 2012).

6.2.2. Deep water masses

The circulation of AABW in the Discovery Gap bottom layer was described in detail in Kapustina and Krechik (2021) and largely depends on the peculiarities of cross-flow over sills and around abyssal hills. At present, cold Antarctic Bottom Water (AABW) is confined by topography and the overlying NADW to the southern depression. It is likely that the depression separates the flow by density and accumulates the densest and coldest bottom water. A similar mechanism was described by Morozov et al. (2012) using examples of AABW overflow in the Romanche and Chain fracture zones (Central Atlantic). This could explain why water with temperatures less than 2.00 °C was not found in the northeastern part of the gap. However, there is also the vertical mixing effect to be considered. Mixing in the bottom layers, in areas of confined topography, is greatest downflow of any sills (Ferron et al., 1998). There are four sills in the gap which must be overcome by the water which helps modify the AABW further. The 80 m discrepancy in depth between the abyssal plains should make it easier for AABW to flow from the Madeira abyssal plain to the Iberian abyssal plain. But our results show that the AGFZ remains the boundary of $\theta < 2$ °C AABW in the Central–NE Atlantic, in agreement with previous work (Saunders, 1987; Tarakanov et al., 2013).

6.3. Morpho-sedimentary features

The relationship between bottom currents, associated oceanographic processes, and the formation of deep-water morphological features has been well studied (e.g., Rebesco et al., 2014). Hydrodynamic processes at water mass interfaces control terrace sedimentary dynamics (Preu et al., 2013; Thiéblemont et al., 2019). The central terrace T2 is located at 4720 m water depth close to the present AABW–NADW mixed

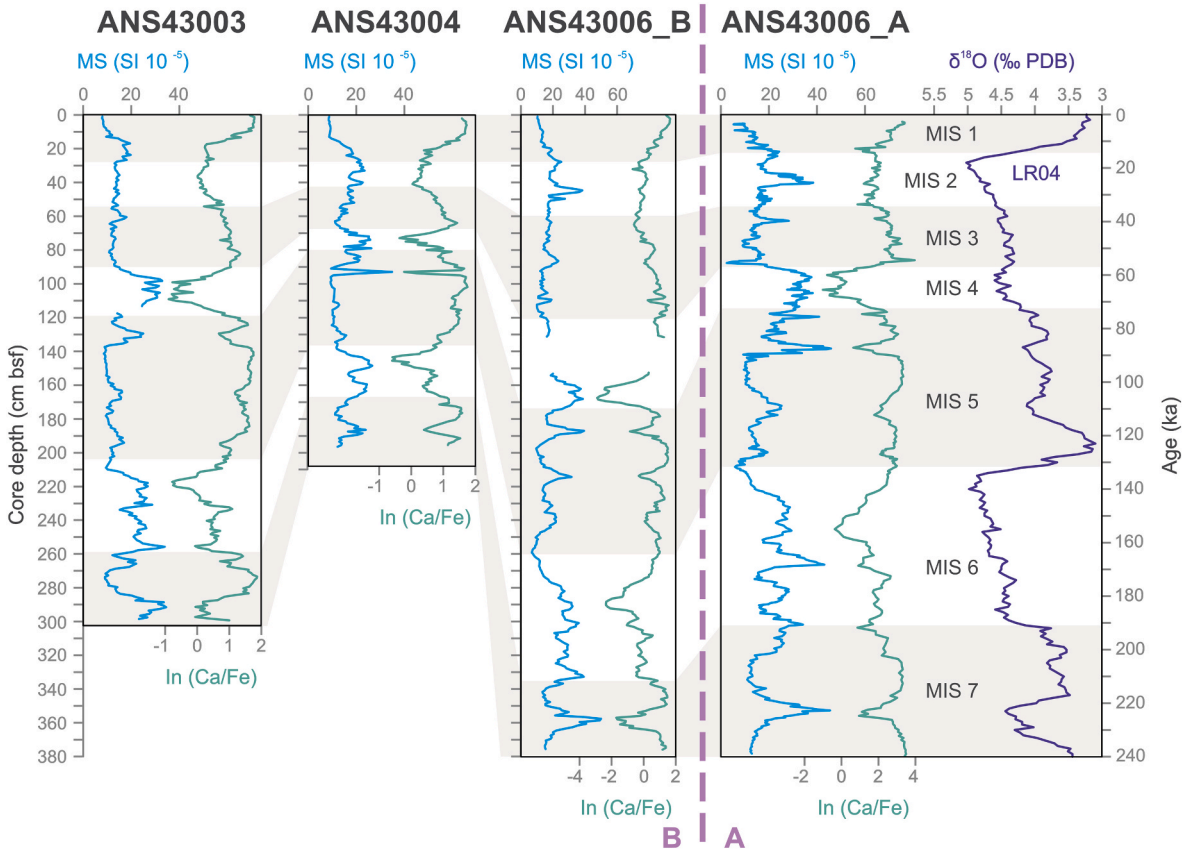

Fig. 18. A correlation of the four Discovery Gap cores based on the age model in Fig. 16 plotted against the LR04 δ18O curve (Lisiecki and Raymo, 2005).

boundary. Past changes in the depth of this water interface shaped the deeper and shallower terraces. The terrace T1 at 3320 m water depth is in agreement with the shallower depths proposed for the AABW and for the AABW–NADW interface in the North Atlantic during glacial times (e.g., Kleiven et al., 2003; Muglia et al., 2018). So, the shallower terrace T1 could be related to the top of the AABW during glacial times, while the central and southern terraces (T2 and T3) could be interglacial features. The sediment supply of the shallower terrace T1 is also governed by the surrounding seamounts. Any slope processes from the MTR are mostly likely being caught on the terrace and blocked by the unnamed seamount. Surplus material reaching Discovery Gap is either very fine (possibly overspill from the MTR) or does not create any distinctive turbiditic fans in Discovery Gap given that extensive turbidites are not recognisable in the collected data.

The shallower drift on the MTR coincides with the MOW–NADW boundary at 1500 m water depth. Plastered drifts with moats are common on gentle slopes where low-velocity currents follow the contours (Faugères et al., 1999; Faugères and Stow, 2008; Rebesco et al., 2014). It is possible that the energy dissipation associated with the collision of meddies with seamounts (Richardson et al., 2000) may be generating these currents along the slope of Josephine Seamount. The MOW is denser and intensified at a greater depth during glacial periods (Schönfeld and Zahn, 2000; Schönfeld et al., 2003). This has been evidenced in the formation of deeper contourites along the Iberian margin (Hernández-Molina et al., 2014a; 2014b, 2016; Mena et al., 2018; Llave et al., 2020). Such an effect could lead to a deeper MOW, greater erosion along the MTR and the flank of the Josephine seamount, and deposition of sediment drifts. The Josephine drift (Figs. 4 and 9) may be a predominantly glacial feature.

Evidence for recent bottom currents includes the distribution of erosional and depositional features (Figs. 4 and 10) and small scale sedimentary features on the seafloor (e.g., Stow et al., 2009; Rebesco et al., 2014). The position of scours and channels relative to topographic highs and adjacent contourite drifts can be used to reconstruct the paleocurrent directions and sediment ripples can provide additional clues as to the bottom current velocity (Faugères et al., 1999; Stow et al., 2009; Collinson and Mountney, 2019). In the gap there are moats and channels which are located predominantly on the southwest side of topographic highs (Fig. 4). Additionally, to the north of the gap, there is a mounded-sheeted drift with a moat on the southwest side of a topographic high and a sheeted drift on the north side (Fig. 4). The spatial distribution of the features suggests a bottom current flowing predominantly from the south to the north, in agreement with direct current measurements (Saunders, 1987; Tarakanov et al., 2013).

However, there are also some scours on the northern side of the highs. The orientation of sediment ripples, groove marks, object scour marks and the localised appearance of these features suggests a local recirculation of current (Heezen and Hollister, 1964) or a counter current originating from the Iberian basin. The former explanation is supported by direct measurements in the gap that show that the water flowing southwards is not much colder than $\theta < 2$ °C (Saunders, 1987; Tarakanov et al., 2013), implying that this reverse current has a significant AABW component. Seafloor photos showing these sedimentary features are apparently quite shallow (2395 m water depth) and formed by a current flowing east along the base of the unnamed seamount, occasionally reaching velocities of 15–30 cms^{-1} (Stow et al., 2009). However, the given depth and the given coordinates of these photos do not coincide with any feature in the gap. Therefore, these features are either much deeper, or on top of the unnamed seamount. Modelling of bottom currents in this area suggests that there may be a current directed to the south in this location (Frey, 2018; Morozov et al., 2022), which coincides with the scours on the north-side of the topographic highs. Hence, there may be some localised shallow recirculation over the unnamed seamount and general recirculation of the bottom waters in

this area.

It seems likely that recirculation is a relatively stable process that occurs throughout the gap. This interpretation is supported by the ripples in the core ANS43006_B and the uneven distribution of the overlying unit, which are likely related to local current variation. This appears to align with observations of recirculated or alternating current in other known gaps (e.g., the Vema Channel and Santos Plateau, the Western Gap, Kane Gap, Wake Island Passage (Hogg et al., 1999; McDonagh et al., 2002; Kawabe et al., 2005; Morozov et al., 2010; Frey, 2018)) and the formation of nearby associated depositional features (e.g., on the Santos Plateau (Borisov et al., 2020)).

6.4. Short-term current variability and sedimentary facies association

Background sedimentation is represented by the facies association FA-A (Fig. 16). The alternation between F1 and F2 is the result of changes in the $CaCO_3$ and terrigenous inputs, largely related to glacial–interglacial changes. Here sediment supply is affected by surface water productivity and carbonate dissolution controls the final sediment accumulation, with dissolution playing the greatest role in late glacial periods when bottom water is especially sluggish (Fig. 16). A shift from background sedimentation is recorded in FA-B and FA-C.

There is a distinctive increase and decrease in terrigenous and heavy mineral markers, ln(Ti/Ca) and ln(Zr/Sr), across FA-B but no increase in bulk grain size (Fig. 12). Such a pattern indicates reworking of carbonate-poor sediment (Fig. 16), or preferential "condensation" of the terrigenous grains by bottom currents (de Castro et al., 2021). This does not match the traditional bigradational contourite sequence in the strict sense of grain size increases (Gonthier et al., 1984). A decrease in the terrigenous component only occurs well into F1 (representing interglacial). Therefore, the weak-current reworking of sediment continues but the sediment supply has become $CaCO_3$ enriched and dissolution has decreased. The most active reworking occurs where F4 contains ripples and is underlain by F1 and overlain by the matrix-poor F3. The limited occurrence of F3 indicates that locally the current has been sufficient to winnow the muddy matrix even as the sediment supply has shifted to carbonate-rich. Localised reworking of sediment by bottom currents, therefore, only occurs in the late glacial–early interglacial period regardless of AABW presence in the early–mid glacial controlling background sedimentation (Fig. 16).

Deposition, rather than just reworking, can be seen in FA-C (Fig. 16). Here, the increase in grain size across the facies is better aligned with the traditional bigradational sequence model for muddy contourites (Gonthier et al., 1984). The maximums of $\overline{SS}$ values in F5 are attributed to the intensification of the AABW current during Termination I (and TII?). The decrease in terrestrial markers and increase in carbonate across F3 at the top of this unit could indicate a transition to winnowing of fines rather than transport (Fig. 16). Occurrence of bottom current deposited sediment at the top of the core is evidence of a more active exchange of bottom water between the Madeira and Iberian abyssal plains in the recent past, at least at Termination I.

The accumulation of carbonates depends on the calcium compensation depth (CCD) (Kennett, 1982). The CCD is controlled to a great degree by the presence of very corrosive AABW, especially during glacial periods (Broecker and Peng, 1982). But there does not appear to be a clear-cut relationship between bottom water presence, bottom current intensification and ice volume/climate change (e.g., Raymo et al., 1990; Lukashina, 2019). Intensification of the current does occur during glacial periods, but its weakening does not occur until the glacial-interglacial transition is over.

Extensive dissolution of the coarse carbonate component can amplify or conceal the variations in the cores. Dissolution was especially extensive in ANS43006 and we propose that the CCD is very close in depth to the southern depression. The most dissolved facies, Facies 4, corresponds well with increased dissolution in the glacial MIS 6 and 4. It was, perhaps, affected by stronger currents than those we proposed but, due to the elevated CCD, accumulation of thicker units of coarser sediment has been prevented. Under such selective removal of a major sediment component, assumptions about terrestrial input and current velocity should be made with great care.

6.5. Sedimentary model

Based on the morphological, hydrological, acoustic, and sedimentological results a new model for sedimentary processes in Discovery Gap is proposed in which vertically deposited sediment is intermittently and locally reworking by weak bottom currents allowing the formation of fine-grained reworked sediments during episodes of enhanced bottom current activity (Fig. 19). Owing to the distal nature of Discovery Gap, the sediment supplied to the gap is mostly from the surface waters, windblown from the Saharan Desert, or derived from the Josephine Seamount and Madeira–Tore Rise. Eddies in the Azores Current (AzC) are the main transport mechanism for suspended particles in the surface waters of the study area according to modelling by Lima et al. (2020). Such interaction between the surface currents, and Josephine Seamount may lead to a local increase in upwelling which in turn brings nutrients to the surface, increasing the local productivity, contributing to a phenomenon known as the island-mass (or seamount) effect (Doty and Oguri, 1956). Furthermore, internal waves breaking against seamounts have the potential to amplify this nutrient flux by increasing diapycnal mixing (Mosquera Giménez et al., 2019; Tuerena et al., 2019). Surface productivity is considered the primary sediment source for pelagic sediments, which can then be mixed with terrigenous sediments from different sources. For example, it is possible that the Josephine Seamount may contribute sediment resuspended by hydrodynamic processes to Discovery Gap (i.e., internal tides and waves) at the surface–intermediate and intermediate–deep water boundaries (Fig. 19) (Zenk, 2008; Pomar et al., 2012; Thiéblemont et al., 2019). Some sediment may be carried from the Madeira abyssal plain which is supplied by a number of turbidites from different sources (Weaver and Rothwell, 1987; Rothwell et al., 1992; Lebreiro et al., 1998).

Elsewhere in the gap, the circulation of the AABW, NADW at deep depths and the MOW at intermediate depths leads to the formation of contourite drifts (Fig. 19). Connecting the identified bottom current features to the regional water masses, it is likely that many of the erosional and depositional features presented thus far in Discovery Gap are associated with the AABW and its variability through geological time. The associated contourite terraces may form due to hydrodynamic processes at the interfaces between different water masses (Hernández-Molina et al., 2009; Preu et al., 2013; Thiéblemont et al., 2019).

The north-directed bottom current generates channels, moats and drifts along the southwestern sides of topographic ridges (Fig. 4). Accumulation of sediment occurs mainly in areas with minimum energy in bottom currents and low topographic gradients (Camerlenghi et al., 2001; Rebesco et al., 2014), as is the case for depressions and terraces within Discovery Gap and outside the gap where current velocity decreases, as was reported in the Samoan passage by Hollister et al. (1974). Where currents are very weak, they may only be capable of transporting sea-floor sediment if it has first been stirred up by burrowing organisms (Wetzel, 1981; Seibold and Fütterer, 1982). Infrequent downslope movement does appear to contribute a coarser fraction of sediment to Discovery Gap and form very thin beds (Fig. 19). These may be diluted distal turbidites, triggered by seismic activity in the region but the potential mixed nature of the sediment drift southwest of the Josephine Seamount, and its implications for Discovery Gap, cannot be confirmed by the present work. Despite the seismicity in the vicinity of the gap associated with the Azores–Gibraltar Fracture Zone there is no evidence that it had a significant control on sediment deposition here, at least not in the studied Quaternary interval. This may be due to alternative routing from topographic highs, which channel the material into the adjacent abyssal plains rather than into Discovery Gap.

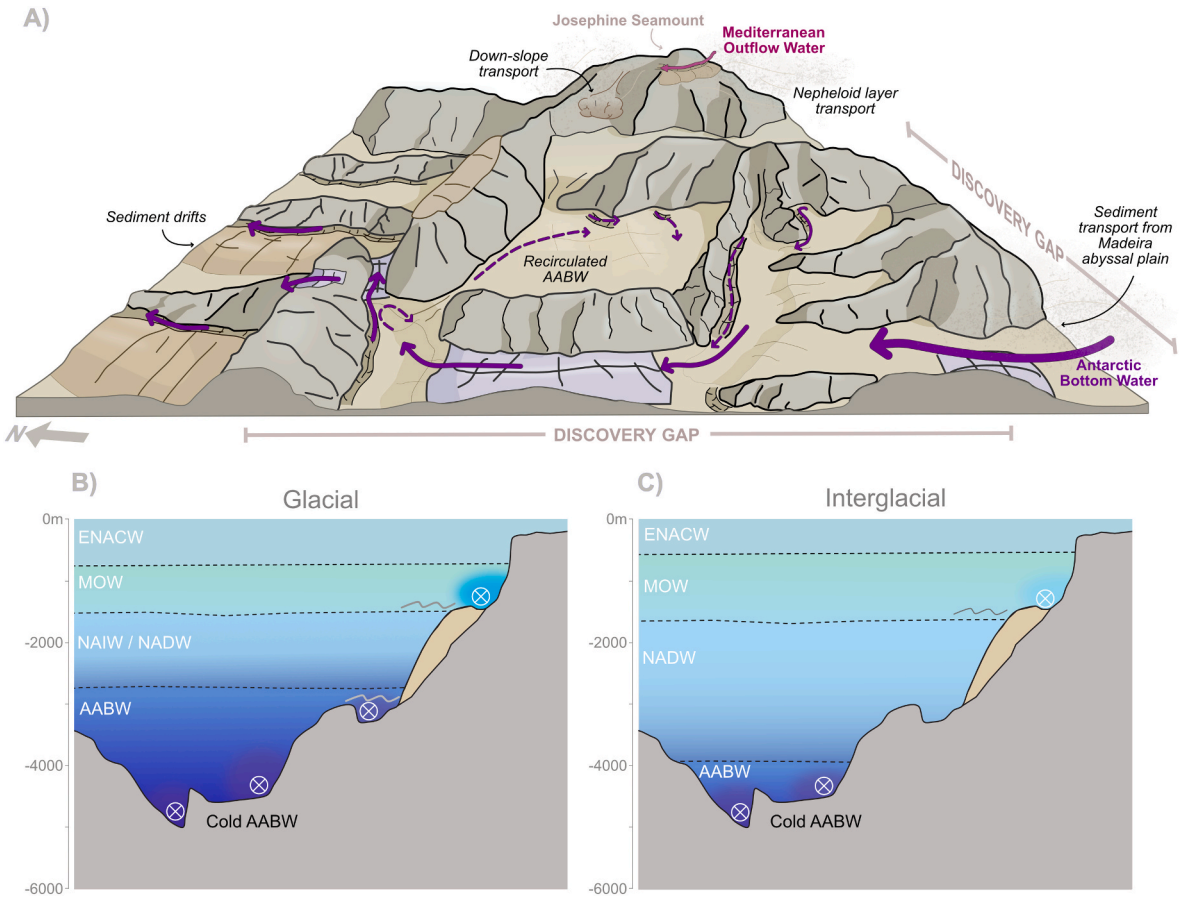

Fig. 19. Sedimentary model of processes in Discovery Gap (A) and the evolution of the water masses during glacial (B) and interglacial (C) stages. The changes in water boundaries in the figure are compiled based on the work of Schönfeld and Zahn (2000); Schönfeld et al. (2003); Lund et al. (2011); Adkins (2013); Ferrari et al. (2014).

6.6. Chronology and interpretation of seismic units

The ages for the identified seismic units are poorly constrained. We are able to estimate the age of the seismic units by extrapolating a sedimentation rate of 1.58 cm ky^{-1} from ANS43003 to the seismic discontinuities (Fig. 10). We hypothesise that the identified boundaries may relate to the Mid-Pleistocene Discontinuity [MPD] and the Late-Quaternary Discontinuity [LDQ] or, alternatively, to a Mid-Pleistocene Transition event and another at ~1.59 Ma associated with drops in sea level (e.g., Llave et al., 2006, 2007; Hernández-Molina et al., 2016). Based on this assumption, the seismic unit U3 is consequently older than the Mid Pleistocene, but it cannot be further constrained. U2 could be Mid Pleistocene in age, and the youngest unit was deposited from the Mid Pleistocene to Holocene.

U1 is interpreted as a dominant pelagic blanket, which does not appear everywhere in the gap, because some areas appear to be experiencing sufficiently vigorous currents in the Late Quaternary and Holocene to prevent deposition of pelagic material. The weak acoustic facies locally develops into the high amplitude surface reflection seen throughout the gap, which could represent coarser recent sediment. U2 is associated with bottom current and down slope deposits. Down slope deposits are identified by heightened reflection amplification or a chaotic/transparent unit among parallel reflections within a profile (e.g., García et al., 2016). This may be due to the deposition of coarser sediment resulting from downslope deposits reaching the gap. But the thickness of these units is very thin suggesting they are very distal mass transport deposits and/or turbidites. U3 is interpreted as an interbedded pelagic and fine grained contourite deposit due to the transparent nature of this deposit and uneven distribution favouring flat areas of topography. Similar seismic facies and sedimentary features have been described in the Theta Gap, a narrow connection (approximately 5 km wide) between the Biscay Abyssal Plain (5100 m water depth) and the Iberian Abyssal Plain (5300 m water depth) where active erosion occurs between the structural highs (incisions of up to 200 m) influenced by turbidites/contour currents that are replaced by the pelagic/hemipelagic deposits caused by the switch-off of turbidity/contour current activity (Fig. 8H and I in Llave et al., 2018).

6.7. Quaternary evolution of the Discovery Gap

Through acoustic and sedimentary analysis, the Quaternary evolution of the gap can be separated into three stages: a) Pre-Quaternary, b) Mid Pleistocene, and c) Mid Pleistocene to Holocene.

a) Pre-Quaternary

Pre-Quaternary evolution cannot be discussed in detail as too many assumptions are required when the dating of seismic units is unconfirmed. If Antarctic Bottom Water (AABW) was circulating before the observed sediment sequences, it seems logical to assume that onset of AABW flow in the gap would correlate to the building of the nearby Madeira Drift (Roque et al., 2015, 2017). Prior to the Quaternary, the Calcium Compensation Depth (CCD) in the Madeira abyssal plain began to deepen in the late Miocene (~8 Ma) (Lebreiro et al., 1998). Consequently, before that time the abyssal plain was permanently under the calcium compensation depth (Lebreiro et al., 1998). So, sediments from this time are likely to be carbonate-poor unless displaced from adjacent seamounts.

b) Mid Pleistocene

The Mid Pleistocene Discontinuity at ~0.72 Ma, from Marine Isotope Stages (MIS) 19 to 17, may be responsible for the formation of the first discontinuity with a high amplitude reflection determined from high-resolution seismic in Discovery Gap. The spatial and temporal distribution of hiatuses and discontinuities can be used to correlate environmental changes (e.g., tectonic uplift and ocean circulation) to changes in the deposition of sediment (e.g., Llave et al., 2001; Hernández-Molina et al., 2014, 2016). Such hiatuses can be created by intensified flow through deep gaps (e.g., Ivanova et al., 2020) or turbidites.

The second discontinuity in the gap could be coeval with the Late Quaternary Discontinuity at 0.6–0.3 Ma, coinciding with Marine Isotopic stages (MIS) 13–11 (Hernández-Molina et al., 2016). In the Madeira abyssal plain, the MIS 13 is represented by a thick white ooze which has been linked to an increase of carbonate ($CaCO_3$) content (Weaver et al., 1992). There is also a lack of any record of the MIS 8 and 2 on the plain (D10323, D10320, 82PCS34) (Weaver and Kuijpers, 1983), which may indicate that enhanced bottom currents prevent the accumulation of sediment on the abyssal plain or there was a shift in the sediment supply. Detailed paleocirculation reconstruction is, however, easier for the younger sediments that were retrieved from Discovery Gap.

c) Mid Pleistocene – Holocene

The cores from Discovery Gap record major glacial–interglacial shifts in the Mid Pleistocene dating back to MIS 7c. Based on the age of the studied cores, the background sedimentation in Discovery Gap is controlled by productivity and dissolution of carbonate. Carbonate dissolution relates to the presence of corrosive AABW (e.g., Gardner, 1975) which is generally considered to be more corrosive in glacials (MIS 6, 4 and 2) than interglacials which is in agreement with our observations in Discovery Gap (Figs. 16 and 18). The corrosiveness of AABW further increases as the glacial period progresses and so that the greatest dissolution occurs at the end of a glacial (Fig. 16) is particularly apparent during the MIS 6. This dissolution leads to a selective reworking and concentration of the terrigenous fraction of a sediment.

Varied presence of AABW during glacial–interglacial times is due to enhanced AABW and weak NADW formation during glacials, contrasting to interglacials which are characterized by strong NADW (Duplessy et al., 1988; Sarnthein et al., 2001). Sea ice formation and the associated brine rejection result in a loss of buoyancy and formation of cold and dense AABW (Gordon, 2001; Talley, 2013). The main reason for the greater volume of AABW in the glacial Atlantic is thought to be a northward migration of the sea ice line and an increase in sea ice production around Antarctica that is accompanied by high negative buoyancy flux (Jansen, 2017). Another possible mechanism for increasing AABW formation is where cooler glacial NADW leads to less melting of Antarctic ice when it reaches the Southern Ocean and produces a saltier AABW (Stocker et al., 1992; Adkins, 2013). These processes lead to increased salinity stratification and shifting of the NADW/AABW boundary in the Atlantic, potentially shallowing to 2000 m during glacials (Lund et al., 2011; Adkins, 2013; Ferrari et al., 2014). This is sufficiently shallow that cold AABW can pass between the Central and NE Atlantic without mixing over the rough topography (Lund et al., 2011; Adkins, 2013). This shallower water would, therefore, be able to erode and form the shallower terrace T1 on the Madeira–Tore Rise (Fig. 19) and carry sediment from the Madeira abyssal plain into the Iberian abyssal plain.

Recent studies have shown that the highest AABW production was during Termination I and, possibly, Termination II (Menviel et al., 2015, 2018; Du et al., 2018, 2020). In our data a peak in $\overline{SS}$ during the Termination I across all of Discovery Gap cores supports enhanced AABW transport rates in the Atlantic during the last deglaciation. Elevated bottom current velocity of AABW across Termination I has also been reported in the Kane Gap (Sivkov et al., 2019). Interestingly, coeval with these transitions between MIS 6–5, 5–4, and 2–1, the largest turbidites have been deposited in the Madeira abyssal plain (Weaver and Kuijpers, 1983).

Along with the changes to the deep waters a deeper, denser water flows out of the Mediterranean in glacial times (Schönfeld and Zahn, 2000; Schönfeld et al., 2003; Sierro et al., 2020). Thus, there is a deepening of the MOW–NADW and ENACW–MOW interfaces in glacial periods (Fig. 19) (Schönfeld and Zahn, 2000; Schönfeld et al., 2003). Vertical instability along these boundaries relating to internal waves and tides (Fig. 19) may be sufficient to create locally enhanced bottom currents that can induce erosion at an intermediate level on adjacent seamounts (Pomar et al., 2012) triggering sediment transport down slope into Discovery Gap, as well as increasing the sediment concentration in the nepheloid layers (Fig. 19) (Puig et al., 2004; Wienberg et al., 2020). Shifts in these interfaces have shaped Discovery Gap through the formation of terraces and sediment drifts even in the shallower parts of the gap (i.e., Josephine drift) (Fig. 19).

7. Conclusions

In this work we have determined the hydrodynamic, morphostructural and sedimentary characteristics of Discovery Gap and adjacent areas, decoded the key recent evolutionary stages and proposed a sedimentary and paleocirculation model for Discovery Gap with implications between the Central and NE Atlantic.

The constriction of sluggish abyssal bottom water by topography reinvigorates the corrosive Antarctic Bottom Water (AABW) enough to erode, rework and deposit sediment. The importance of NE–SW trending highs in controlling the flow of water through Discovery Gap is determined by the presence of erosion at the base of these highs with adjacent sheeted, plastered or mounded contourite drifts. The associations between pelagic, reworked pelagic and fine-grained contourite facies provide evidence for AABW variability and its intermittent influence in Discovery Gap during the Quaternary. Bottom current intensity was greatest during glacial–interglacial transitions, especially at Termination I, coeval to an increase in the sedimentation rate and dissolution of carbonate. Therefore, Quaternary climatic changes are a key controlling factor in deep-marine sedimentation.

This study provides new insights into deep water circulation in the Central–NE Atlantic and how the input of Antarctic water into the NE Atlantic has varied due to climate, amplified by the constriction of the deep marine gateway. Questions remain as to whether other gaps in the NE Atlantic demonstrate similar shifts in the intensity of AABW paleoflow and if these various gaps were equally responsible for deep water exchange during deglacial periods. This study, therefore, highlights the importance of deep marine gaps in aiding the reconstruction of deep water paleocirculation not only in the Central and NE Atlantic but also in other oceanic basins.

Declaration of competing interest

The authors declare that they have no known competing financial interests or personal relationships that could have appeared to influence the work reported in this paper.

Acknowledgements

This project was done within the framework of “The Drifters” Research Group at Royal Holloway University of London (RHUL). The authors thank the captain, crew and onboard scientific team of the 43rd cruise onboard the R/V *Akademik Nikolaj Strakhov*. Research by RT was funded by Projects CGL2015-66835-P and PID2019-104625RB-100 (Secretaría de Estado de I + D + I, Spain), B-RNM-072-UGR18 (FEDER Andalucía) and P18-RT-4074 (Junta de Andalucía). Research by

EL was supported through the CGL2016-80445-R (AEI/FEDER, UE) SCORE projects. The field research, stable isotope interpretation, and the age model construction were carried out within framework of the state assignment of IO RAS (theme No. 0128-2021-0012). Hydrological data processing and core ANS43006_A analysis ($CaCO_3$, MS, and XRF) were supported by the Russian Science Foundation (grant No. 19-17-00246). The SBE 19plus V2 SeaCAT hydrophysical probe (Sea-Bird Electronics, United States) used during the expedition was kindly provided by the Moscow State University.

We thank the editor and the two anonymous reviewers for their comments and suggestions which have helped us to improve the original submitted version of this work. We would also like to thank L. Bashirova for the insightful discussion which has improved the final version of this manuscript.

Appendix A. Supplementary data

Supplementary data to this article can be found online at https://doi.org/10.1016/j.dsr.2021.103681.

References

Adkins, J.F., 2013. The role of deep ocean circulation in setting glacial climates. Paleoceanography 28, 539–561. https://doi.org/10.1002/palo.20046.

Argus, D.F., Gordon, R.G., DeMets, C., Stein, S., 1989. Closure of the Africa-Eurasia-north America plate motion circuit and tectonics of the Gloria Fault. J. Geophys. Res. 94, 5585. https://doi.org/10.1029/JB094iB05p05585.

Bashirova, L.D., Dorokhova, E.V., Sivkov, V.V., Andersen, N., Kuleshova, L.A., Matul, A. G., 2017. Paleocurrents in the Charlie-Gibbs fracture zone during the late quaternary. Oceanology 57, 444–454. https://doi.org/10.1134/S0001437017020035.

Batista, L., Hübscher, C., Terrinha, P., Matias, L., Afilhado, A., Lüdmann, T., 2017. Crustal structure of the Eurasia–Africa plate boundary across the Gloria Fault, North Atlantic ocean. Geophys. J. Int. 209, 713–729. https://doi.org/10.1093/gji/ggx050.

Bezzeghoud, M., Adam, C., Buforn, E., Borges, J.F., Caldeira, B., 2014. Seismicity along the Azores-Gibraltar region and global plate kinematics. J. Seismol. 18, 205–220. https://doi.org/10.1007/s10950-013-9416-x.

Bird, D.E., Hall, S.A., Burke, K., Casey, J.F., Sawyer, D.S., 2007. Early central Atlantic Ocean seafloor spreading history. Geosphere 3, 282. https://doi.org/10.1130/GES00047.1.

Blott, S.J., Pye, K., 2001. GRADISTAT: a grain size distribution and statistics package for the analysis of unconsolidated sediments. Earth Surf. Process. Landforms 26, 1237–1248. https://doi.org/10.1002/esp.261.

Borisov, D., Frey, D., Levchenko, O., 2020. Sediment waves on the Santa Catarina plateau (western south Atlantic). J. South Am. Earth Sci. 102, 102698. https://doi.org/10.1016/j.jsames.2020.102698.

Boyer, T.P., Antonov, J.I., Baranova, O.K., Coleman, C., Garcia, H.E., Grodsky, A., Locarnini, R.A., Mishonov, A.V., Paver, C.R., Reagan, J.R., Seidov, D., Smolyar, I.V., Weathers, K., Zweng, M.M., 2018. World Ocean Database 2018.

Brackenridge, R.E., Stow, D.A.V., Hernández-Molina, F.J., Jones, C., Mena, A., Alejo, I., Ducassou, E., Llave, E., Ercilla, G., Nombela, M.A., Perez-Arlucea, M., Frances, G., 2018. Textural characteristics and facies of sand-rich contourite depositional systems. Sedimentology 65, 2223–2252. https://doi.org/10.1111/sed.12463.

Broecker, W.S., Peng, T.-H., 1982. Tracers in the Sea. Geological Observatory of Columbia University.

Broecker, W.S., Takahashi, T., Li, Y.-H., 1976. Hydrography of the central Atlantic—I. The two-degree discontinuity. Deep Sea Res. Oceanogr. Abstr. 23, 1083–1104. https://doi.org/10.1016/0011-7471(76)90886-X.

Buforn, E., Udías, A., Colombás, M.A., 1988. Seismicity, source mechanisms and tectonics of the Azore-Gibraltar plate boundary. Tectonophysics 152, 89–118.

Camerlenghi, A., Domack, E., Rebesco, M., Gillbert, R., Ishman, S., Leventer, A., Brachfeld, S., Drake, A., 2001. Glacial morphology abd post-glacial contourites in northern prince Gustav channel (NW Weddell Sea, Antarctica). Mar. Geophys. Res. 22, 417–443.

Catuneanu, O., Abreu, V., Bhattacharya, J.P., Blum, M.D., Dalrymple, R.W., Eriksson, P. G., Fielding, C.R., Fisher, W.L., Galloway, W.E., Gibling, M.R., Giles, K.A., Holbrook, J.M., Jordan, R., Kendall, C.G.S.C., Macurda, B., Martinsen, O.J., Miall, A. D., Neal, J.E., Nummedal, D., Pomar, L., Posamentier, H.W., Pratt, B.R., Sarg, J.F., Shanley, K.W., Steel, R.J., Strasser, A., Tucker, M.E., Winker, C., 2009. Towards the standardization of sequence stratigraphy. Earth Sci. Rev. 92, 1–33. https://doi.org/10.1016/j.earscirev.2008.10.003.

Collinson, J.D., Mountney, N., 2019. Sedimentary Structures, fourth ed. Edinburgh.

Connary, S.D., Ewing, M., 1974. Penetration of Antarctic bottom water from the cape basin into the Angola basin. J. Geophys. Res. 79, 463–469. https://doi.org/10.1029/JC079i003p00463.

Culp, J., Parent, A., Abolfazli, E., Strom, K., Romans, B.W., 2021. Advective sorting of silt by currents: a laboratory study. Sedimentology sed 12889. https://doi.org/10.1111/sed.12889.

Damuth, J.E., 1980. Use of high-frequency (3.5–12 kHz) echograms in the study of near-bottom sedimentation processes in the deep-sea: a review. Mar. Geol. 38, 51–75. https://doi.org/10.1016/0025-3227(80)90051-1.

Damuth, J.E., 1978. Echo character of the Norwegian—Greenland sea: relationship to quaternary sedimentation. Mar. Geol. 28, 1–36. https://doi.org/10.1016/0025-3227(78)90094-4.

Damuth, J.E., Hayes, D.E., 1977. Echo character of the East Brazilian continental margin and its relationship to sedimentary processes. Mar. Geol. 24, 73–95. https://doi.org/10.1016/0025-3227(77)90002-0.

de Castro, S., Hernández-Molina, F.J., Rodríguez-Tovar, F.J., Llave, E., Ng, Z.L., Nishida, N., Mena, A., 2020. Contourites and bottom current reworked sands: bed facies model and implications. Mar. Geol. 428, 106267. https://doi.org/10.1016/j.margeo.2020.106267.

de Castro, S., Miramontes, E., Dorador, J., Jouet, G., Cattaneo, A., Rodríguez-Tovar, F.J., Hernández-Molina, F.J., 2021. Siliciclastic and bioclastic contouritic sands: textural and geochemical characterisation. Mar. Petrol. Geol. 128, 105002. https://doi.org/10.1016/j.marpetgeo.2021.105002.

de Lavergne, C., Madec, G., Le Sommer, J., Nurser, A.J.G., Naveira Garabato, A.C., 2016. On the consumption of Antarctic bottom water in the abyssal ocean. J. Phys. Oceanogr. 46, 635–661. https://doi.org/10.1175/JPO-D-14-0201.1.

de Weger, W., Hernández-Molina, F.J., Flecker, R., Sierro, F.J., Chiarella, D., Krijgsman, W., Manar, M.A., 2020. Late Miocene contourite channel system reveals intermittent overflow behavior. Geology 48, 1194–1199. https://doi.org/10.1130/G47944.1.

Dorador, J., Rodríguez-Tovar, F.J., 2018. High-resolution image treatment in ichnological core analysis: initial steps, advances and prospects. Earth Sci. Rev. 177, 226–237. https://doi.org/10.1016/j.earscirev.2017.11.020.

Dorador, J., Rodríguez-Tovar, F.J., 2015. Application of digital image treatment to the characterization and differentiation of deep-sea ichnofacies. Spanish J. Palaeontol. 30, 265. https://doi.org/10.7203/sjp.30.2.17256.

Dorador, J., Rodríguez-Tovar, F.J., 2014. A novel application of digital image treatment by quantitative pixel analysis to trace fossil research in marine cores. Palaios 29, 533–538. https://doi.org/10.2110/palo.2014.044.

Dorador, J., Rodríguez-Tovar, F.J., Mena, A., Francés, G., 2019. Lateral variability of ichnological content in muddy contourites: weak bottom currents affecting organisms' behavior. Sci. Rep. 9, 17713. https://doi.org/10.1038/s41598-019-54246-3.

339 Dorador, J., Rodríguez-Tovar, F.J., Scientists, I.E., 2014a. Digital image treatment applied to ichnological analysis of marine core sediments. Facies 60, 39–44. https://doi.org/10.1007/s10347-013-0383-z.

339 Dorador, J., Rodríguez-Tovar, F.J., Scientists, I.E., 2014b. Quantitative estimation of bioturbation based on digital image analysis. Mar. Geol. 349, 55–60. https://doi.org/10.1016/j.margeo.2014.01.003.

Dorokhova, E.V., Krechik, V.A., Ponomarenko, E.P., Dudkov, I.Y., Shakhovskoy, I.B., Napreenko-Dorokhova, T.V., Ezhov, V.E., Malafeev, G.V., Kuleshova, L.A., Glazkova, T.A., 2021. Intergrated oceanographic research of Discovery gap (Eastern North Atlantic) during the 43rd cruise of the R/V Akademik Nikolaj Strakhov. Oceanology 61, 162–164.

Doty, M.S., Oguri, M., 1956. The island mass effect. ICES J. Mar. Sci. 22, 33–37. https://doi.org/10.1093/icesjms/22.1.33.

Du, J., Haley, B.A., Mix, A.C., 2020. Evolution of the global overturning circulation since the last glacial maximum based on marine authigenic neodymium isotopes. Quat. Sci. Rev. 241, 106396. https://doi.org/10.1016/j.quascirev.2020.106396.

Du, J., Haley, B.A., Mix, A.C., Walczak, M.H., Praetorius, S.K., 2018. Flushing of the deep Pacific Ocean and the deglacial rise of atmospheric CO2 concentrations. Nat. Geosci. 11, 749–755. https://doi.org/10.1038/s41561-018-0205-6.

Dubois-Dauphin, Q., Bonneau, L., Colin, C., Montero-Serrano, J.-C., Montagna, P., Blamart, D., Hebbeln, D., Van Rooij, D., Pons-Branchu, E., Hemsing, F., Wefing, A.-M., Frank, N., 2016. South Atlantic intermediate water advances into the North-east Atlantic with reduced Atlantic meridional overturning circulation during the last glacial period. Geochemistry, Geophys. Geosystems 17, 2336–2353. https://doi.org/10.1002/2016GC006281.

Dudkov, I., Dorokhova, E., 2020. Multibeam bathymetry data of Discovery gap in the Eastern North Atlantic. Data Br 31, 105679. https://doi.org/10.1016/j.dib.2020.105679.

Duplessy, J.C., Shackleton, N.J., Fairbanks, R.G., Labeyrie, L., Oppo, D., Kallel, N., 1988. Deepwater source variations during the last climatic cycle and their impact on the global deepwater circulation. Paleoceanography 3, 343–360. https://doi.org/10.1029/PA003i003p00343.

Embley, R.W., Rabinowitz, P.D., Jacobi, R.D., 1978. Hyperbolic echo zones in the eastern Atlantic and the structure of the southern Madeira Rise. Earth Planet Sci. Lett. 41, 419–433. https://doi.org/10.1016/0012-821X(78)90173-5.

Faugères, J.-C., Mulder, T., 2011. Contour currents and contourite drifts. In: Hüneke, H., Mulder, T. (Eds.), Developments in Sedimentology, 63. Elsevier, pp. 149–214. https://doi.org/10.1016/B978-0-444-53000-4.00003-2.

Faugères, J.-C., Stow, D.A., Imbert, P., Viana, A., 1999. Seismic features diagnostic of contourite drifts. Mar. Geol. 162, 1–38. https://doi.org/10.1016/S0025-3227(99)00068-7.

Faugères, J.-C., Stow, D.A.V., 2008. Chapter 14 contourite drifts. In: Rebesco, M., Camerlenghi, A. (Eds.), Developments in Sedimentology, 60. Elsevier, pp. 257–288. https://doi.org/10.1016/S0070-4571(08)10014-0.

Ferrari, R., Jansen, M.F., Adkins, J.F., Burke, A., Stewart, A.L., Thompson, A.F., 2014. Antarctic sea ice control on ocean circulation in present and glacial climates. Proc. Natl. Acad. Sci. 111, 8753–8758. https://doi.org/10.1073/pnas.1323922111.

Ferron, B., Mercier, H., Speer, K., Gargett, A., Polzin, K., 1998. Mixing in the Romanche fracture zone. J. Phys. Oceanogr. 28, 1929–1945. https://doi.org/10.1175/1520-0485(1998)028<1929:MITRFZ>2.0.CO;2.

Flügel, E., 2004. Microfacies of Carbonate Rocks. Springer Berlin Heidelberg, Berlin, Heidelberg. https://doi.org/10.1007/978-3-662-08726-8.

Folk, R.L., Ward, W.C., 1957. Brazos River bar [Texas]; a study in the significance of grain size parameters. J. Sediment. Res. 27, 3–26. https://doi.org/10.1306/74D70646-2B21-11D7-8648000102C1865D.

Frey, D.I., 2018. Придонные Гравитационные течения в Глубоководных каналах Атлантики [Bottom gravity currents in the deep-water Atlantic channels. Shirshov Institute of Oceanology.

García, M., Hernández-Molina, F.J., Alonso, B., Vázquez, J.T., Ercilla, G., Llave, E., Casas, D., 2016. Erosive sub-circular depressions on the Guadalquivir Bank (Gulf of Cadiz): interaction between bottom current, mass-wasting and tectonic processes. Mar. Geol. 378, 5–19. https://doi.org/10.1016/j.margeo.2015.10.004.

Gardner, J.V., 1975. Late pleistocene carbonate dissolution cycles IN the eastern equatorial atlantic. Dissolution Deep. Carbonates.

GEBCO, 2019. The GEBCO_2019 Grid - a continuous terrain model of the global oceans and land. https://doi.org/10.5285/836f016a-33be-6ddc-e053-6c86abc0788e.

Geldmacher, J., Hoernle, K., Bogaard, P.v. d., Duggen, S., Werner, R., 2005. New 40Ar/39Ar age and geochemical data from seamounts in the Canary and Madeira volcanic provinces: support for the mantle plume hypothesis. Earth Planet Sci. Lett. 237, 85–101. https://doi.org/10.1016/j.epsl.2005.04.037.

Gonthier, E.G., Faugères, J.-C., Stow, D.A.V., 1984. Contourite facies of the faro drift, gulf of Cadiz. Geol. Soc. London, Spec. Publ. 15, 275–292. https://doi.org/10.1144/GSL.SP.1984.015.01.18.

Gordon, A.L., 2001. Bottom water formation. Encycl. Ocean Sci. 334–340. https://doi.org/10.1006/rwos.2001.0006.

Gutscher, M.-A., Dominguez, S., Westbrook, G.K., Le Roy, P., Rosas, F., Duarte, J.C., Terrinha, P., Miranda, J.M., Graindorge, D., Gailler, A., Sallares, V., Bartolome, R., 2012. The Gibraltar subduction: a decade of new geophysical data. Tectonophysics 574 (575), 72–91. https://doi.org/10.1016/j.tecto.2012.08.038.

Harmon, N., Rychert, C., Agius, M., Tharimena, S., Le Bas, T., Kendall, J.M., Constable, S., 2018. Marine geophysical investigation of the Chain fracture zone in the equatorial Atlantic from the PI-LAB experiment. J. Geophys. Res. Solid Earth 123. https://doi.org/10.1029/2018JB015982.

Harvey, J, Arhan, M, 1988. The Water Masses of the Central North Atlantic in 1983–84. J. Phys. Oceanogr. 18 (12), 1855–1875. https://doi.org/10.1175/1520-0485(1988)018<1855:TWMOTC>2.0.CO;2.

Heezen, B.C., Hollister, C., 1964. Deep-sea current evidence from abyssal sediments. Mar. Geol. 1, 141–174. https://doi.org/10.1016/0025-3227(64)90012-X.

Heezen, B.C., Tharp, M., Ewing, M., 1959. The Floors of the Oceans, pp. 1–126. https://doi.org/10.1130/SPE65-p1.

Hensen, C., Duarte, J.C., Vannucchi, P., Mazzini, A., Lever, M.A., Terrinha, P., Géli, L., Henry, P., Villinger, H., Morgan, J., Schmidt, M., Gutscher, M.-A., Bartolome, R., Tomonaga, Y., Polonia, A., Gràcia, E., Tinivella, U., Lupi, M., Çağatay, M.N., Elvert, M., Sakellariou, D., Matias, L., Kipfer, R., Karageorgis, A.P., Ruffine, L., Liebetrau, V., Pierre, C., Schmidt, C., Batista, L., Gasperini, L., Burwicz, E., Neres, M., Nuzzo, M., 2019. Marine transform faults and fracture zones: a joint perspective integrating seismicity, fluid flow and life. Front. Earth Sci. 7 https://doi.org/10.3389/feart.2019.00039.

Hernández-Molina, F.J., Llave, E., Preu, B., Ercilla, G., Fontan, A., Bruno, M., Serra, N., Gomiz, J.J., Brackenridge, R.E., Sierro, F.J., Stow, D.A.V., García, M., Juan, C., Sandoval, N., Arnaiz, A., 2014. Contourite processes associated with the mediterranean outflow water after its exit from the Strait of Gibraltar: global and conceptual implications. Geology 42, 227–230. https://doi.org/10.1130/G35083.1.

Hernández-Molina, F.J., Maldonado, A., Stow, D.A.V., 2008. Chapter 18 abyssal plain contourites. In: Rebesco, M., Camerlenghi, A. (Eds.), Developments in Sedimentology, 60. Elsevier, pp. 345–378. https://doi.org/10.1016/S0070-4571(08)10018-8.

Hernández-Molina, F.J., Paterlini, M., Violante, R., Marshall, P., de Isasi, M., Somoza, L., Rebesco, M., 2009. Contourite depositional system on the Argentine Slope: an exceptional record of the influence of Antarctic water masses. Geology 37, 507–510. https://doi.org/10.1130/G25578A.1.

Hernández-Molina, F.J., Serra, N., Stow, D.A.V., Llave, E., Ercilla, G., Van Rooij, D., 2011. Along-slope oceanographic processes and sedimentary products around the Iberian margin. Geo Mar. Lett. 31, 315–341. https://doi.org/10.1007/s00367-011-0242-2.

Hernández-Molina, F.J., Sierro, F.J., Llave, E., Roque, C., Stow, D.A.V., Williams, T., Lofi, J., Van der Schee, M., Arnáiz, A., Ledesma, S., Rosales, C., Rodríguez-Tovar, F. J., Pardo-Igúzquiza, E., Brackenridge, R.E., 2016. Evolution of the gulf of Cadiz margin and southwest Portugal contourite depositional system: tectonic, sedimentary and paleoceanographic implications from IODP expedition 339. Mar. Geol. 377, 7–39. https://doi.org/10.1016/j.margeo.2015.09.013.

Hernandez-Molina, F.J., Stow, D.A.V., Alvarez-Zarikian, C.A., Acton, G., Bahr, A., Balestra, B., Ducassou, E., Flood, R., Flores, J.-A., Furota, S., Grunert, P., Hodell, D., Jimenez-Espejo, F., Kim, J.K., Krissek, L., Kuroda, J., Li, B., Llave, E., Lofi, J., Lourens, L., Miller, M., Nanayama, F., Nishida, N., Richter, C., Roque, C., Pereira, H., Sanchez Goni, M.F., Sierro, F.J., Singh, A.D., Sloss, C., Takashimizu, Y., Tzanova, A., Voelker, A., Williams, T., Xuan, C., 2014. Onset of mediterranean outflow into the north Atlantic. Science (80- 344, 1244–1250. https://doi.org/10.1126/science.1251306.

Hogg, N.G., Siedler, G., Zenk, W., 1999. Circulation and variability at the southern boundary of the Brazil basin. J. Phys. Oceanogr. 29, 145–157. https://doi.org/10.1175/1520-0485(1999)029<0145:CAVATS>2.0.CO;2.

Hollister, C.D., Johnson, D.A., Lonsdale, P.F., 1974. Current-controlled abyssal sedimentation: Samoan passage, equatorial west Pacific. J. Geol. 82, 275–300. https://doi.org/10.1086/627965.

Hüneke, H., Hernández-Molina, F.J., Rodríguez-Tovar, F.J., Llave, E., Chiarella, D., Mena, A., Stow, D.A.V., 2021. Diagnostic criteria using microfacies for calcareous contourites, turbidites and pelagites in the Eocene–Miocene slope succession, southern Cyprus. Sedimentology 68, 557–592. https://doi.org/10.1111/sed.12792.

Ivanova, E., Borisov, D., Dmitrenko, O., Murdmaa, I., 2020. Hiatuses in the late Pliocene–Pleistocene stratigraphy of the Ioffe calcareous contourite drift, western South Atlantic. Mar. Petrol. Geol. 111, 624–637. https://doi.org/10.1016/j.marpetgeo.2019.08.031.

Jansen, M.F., 2017. Glacial ocean circulation and stratification explained by reduced atmospheric temperature. Proc. Natl. Acad. Sci. 114, 45–50. https://doi.org/10.1073/pnas.1610438113.

Jiménez-Munt, I., Fernàndez, M., Torne, M., Bird, P., 2001. The transition from linear to diffuse plate boundary in the Azores–Gibraltar region: results from a thin-sheet model. Earth Planet Sci. Lett. 192, 175–189. https://doi.org/10.1016/S0012-821X(01)00442-3.

Johnson, D.A., 1984. The Vema Channel: physiography, structure, and sediment—current interactions. Mar. Geol. 58, 1–34. https://doi.org/10.1016/0025-3227(84)90114-2.

Kapustina, M.V., Krechik, V.A., 2021. Propagation of Antarctic bottom water in the Discovery gap (northeast Atlantic) based on measurements from 2019. Oceanology 61, 602–612. https://doi.org/10.1134/S0001437021050052.

Kawabe, M., Yanagimoto, D., Kitagawa, S., Kuroda, Y., 2005. Variations of the deep western boundary current in Wake Island Passage. Deep-Sea Res. Part I Oceanogr. Res. Pap. 52, 1121–1137. https://doi.org/10.1016/j.dsr.2004.12.009.

Kennett, J.P., 1982. Marine Geology, first ed. Prentice-Hall. Inc., New Jersey.

Kleiven, H.F., Jansen, E., Curry, W.B., Hodell, D.A., Venz, K., 2003. Atlantic Ocean thermohaline circulation changes on orbital to suborbital timescales during the mid-Pleistocene. Paleoceanography 18. https://doi.org/10.1029/2001PA000629 n/a-n/a.

Knutz, P.C., 2008. Chapter 24 Palaeoceanographic Significance of Contourite Drifts, pp. 511–535. https://doi.org/10.1016/S0070-4571(08)10024-3.

Lagabrielle, Y., Mamaloukas-Frangoulis, V., Cannat, M., Auzende, J.-M., Honnorez, J., Mevel, C., Bonatti, E., 1992. Vema Fracture Zone (central Atlantic): tectonic and magmatic evolution of the median ridge and the eastern ridge-Transform intersection domain. J. Geophys. Res. 97, 17331. https://doi.org/10.1029/92JB01086.

Laughton, A.S., Whitmarsh, R.B., 1974. The Azores-Gibraltar plate boundary. In: Geodynamics of Iceland and the North Atlantic Area. Springer Netherlands, Dordrecht, pp. 63–81. https://doi.org/10.1007/978-94-010-2271-2_5.

Laughton, A.S., Whitmarsh, R.B., Rusby, J.S.M., Somers, M.L., Revie, J., McCartney, B.S., Nafe, J.E., 1972. A continuous east-west fault on the Azores-Gibraltar ridge. Nature 237, 217–220. https://doi.org/10.1038/237217a0.

Lebreiro, S.M., Weaver, P.P.E., Howe, R.W., 1998. Sedimentation on the Madeira abyssal plain: eocene-pleistocene history of turbidite infill. In: Proceedings of the Ocean Drilling Program, 157 Scientific Results. Ocean Drilling Program. https://doi.org/10.2973/odp.proc.sr.157.128.1998.

Legg, S., Briegleb, B., Chang, Y., Chassignet, E.P., Danabasoglu, G., Ezer, T., Gordon, A.L., Griffies, S., Hallberg, R., Jackson, L., Large, W., Özgökmen, T.M., Peters, H., Price, J., Riemenschneider, U., Wu, W., Xu, X., Yang, J., 2009. Improving oceanic overflow representation in climate models: the gravity current entrainment climate process team. Bull. Am. Meteorol. Soc. 90, 657–670. https://doi.org/10.1175/2008BAMS2667.1.

Lima, M.J., Sala, I., Caldeira, R.M.A., 2020. Physical connectivity between the NE Atlantic seamounts. Front. Mar. Sci. 7 https://doi.org/10.3389/fmars.2020.00238.

Lisiecki, L.E., Raymo, M.E., 2005. A Pliocene-Pleistocene stack of 57 globally distributed benthic δ 18 O records. Paleoceanography 20. https://doi.org/10.1029/2004PA001071 n/a-n/a.

Llave, E., Hernández-Molina, F.J., García, M., Ercilla, G., Roque, C., Juan, C., Mena, A., Preu, B., Van Rooij, D., Rebesco, M., Brackenridge, R., Jané, G., Gómez-Ballesteros, M., Stow, D., 2020. Contourites along the Iberian continental margins: conceptual and economic implications. Geol. Soc. London, Spec. Publ. 476, 403–436. https://doi.org/10.1144/SP476-2017-46.

Llave, E., Hernández-Molina, F.J., Somoza, L., Diaz del Río, V., Stow, D.A.V., Maestro, A., Alveirinho Dias, J.M., 2001. Seismic stacking pattern of the Faro-Albufeira contourite system (Gulf of Cadiz): a Quaternary record of paleoceanographic and tectonic influences. Mar. Geophys. Res. 22, 487–508.

Llave, E., Hernández-Molina, F.J., Somoza, L., Stow, D.A.V., Díaz Del Río, V., 2007. Quaternary evolution of the contourite depositional system in the Gulf of Cadiz. Geol. Soc. London, Spec. Publ. 276, 49–79. https://doi.org/10.1144/GSL.SP.2007.276.01.03.

Llave, E., Jané, G., Maestro, A., López-Martínez, J., Hernández-Molina, F.J., Mink, S., 2018. Geomorphological and sedimentary processes of the glacially influenced northwestern Iberian continental margin and abyssal plains. Geomorphology 312, 60–85. https://doi.org/10.1016/j.geomorph.2018.03.022.

Llave, E., Schönfeld, J., Hernández-Molina, F.J., Mulder, T., Somoza, L., Díaz del Río, V., Sánchez-Almazo, I., 2006. High-resolution stratigraphy of the Mediterranean outflow contourite system in the Gulf of Cadiz during the late Pleistocene: the impact of Heinrich events. Mar. Geol. 227, 241–262. https://doi.org/10.1016/j.margeo.2005.11.015.

Luis, J., Miranda, J.M., Galdeano, A., Patriat, P., Rossignol, J.C., Mendes Victor, L.A., 1994. The Azores triple junction evolution since 10 Ma from an aeromagnetic survey of the Mid-Atlantic Ridge. Earth Planet Sci. Lett. 125, 439–459. https://doi.org/10.1016/0012-821X(94)90231-3.

Lukashina, N.P., 2019. Deep-water circulation in the Hunter Channel (southwest Atlantic) in the late Pleistocene and Holocene based on benthic foraminifera. Oceanology 59, 123–132. https://doi.org/10.1134/S0001437019010132.
Lund, D.C., Adkins, J.F., Ferrari, R., 2011. Abyssal Atlantic circulation during the last glacial maximum: constraining the ratio between transport and vertical mixing. Paleoceanography 26, PA1213. https://doi.org/10.1029/2010PA001938.
Machín, F., Hernández-Guerra, A., Pelegrí, J.L., 2006. Mass fluxes in the canary basin. Prog. Oceanogr. 70, 416–447. https://doi.org/10.1016/j.pocean.2006.03.019.
McCartney, M.S., 1992. Recirculating components to the deep boundary current of the northern North Atlantic. Prog. Oceanogr. 29, 283–383. https://doi.org/10.1016/0079-6611(92)90006-L.
McCartney, M.S., Bennett, S.L., Woodgate-Jones, M.E., 1991. Eastward flow through the mid-Atlantic Ridge at 11°N and its influence on the Abyss of the eastern basin. J. Phys. Oceanogr. 21, 1089–1121. https://doi.org/10.1175/1520-0485(1991)021<1089:EFTTMA>2.0.CO;2.
McCave, I.N., Andrews, J.T., 2019. Distinguishing current effects in sediments delivered to the ocean by ice. I. Principles, methods and examples. Quat. Sci. Rev. 212, 92–107. https://doi.org/10.1016/j.quascirev.2019.03.031.
McCave, I.N., Hall, I.R., 2006. Size sorting in marine muds: processes, pitfalls, and prospects for paleoflow-speed proxies. Geochemistry, Geophys. Geosystems 7. https://doi.org/10.1029/2006GC001284 n/a-n/a.
McCave, I.N., Thornalley, D.J.R., Hall, I.R., 2017. Relation of sortable silt grain-size to deep-sea current speeds: calibration of the 'Mud Current Meter. Deep-Sea Res. Part I Oceanogr. Res. Pap. 127, 1–12. https://doi.org/10.1016/j.dsr.2017.07.003.
McDonagh, E.L., Arhan, M., Heywood, K.J., 2002. On the circulation of bottom water in the region of the Vema Channel. Deep-Sea Res. Part I Oceanogr. Res. Pap. 49, 1119–1139. https://doi.org/10.1016/S0967-0637(02)00016-X.
Mena, A., Francés, G., Pérez-Arlucea, M., Aguiar, P., Barreiro-Vázquez, J.D., Iglesias, A., Barreiro-Lois, A., 2015. A novel sedimentological method based on CT-scanning: use for tomographic characterization of the Galicia Interior Basin. Sediment. Geol. 321, 123–138. https://doi.org/10.1016/j.sedgeo.2015.03.007.
Mena, A., Francés, G., Pérez-Arlucea, M., Hanebuth, T.J.J., Bender, V.B., Nombela, M.A., 2018. Evolution of the Galicia Interior Basin over the last 60 ka: sedimentary processes and palaeoceanographic implications. J. Quat. Sci. 33, 536–549. https://doi.org/10.1002/jqs.3032.
Menviel, L., Mouchet, A., Meissner, K.J., Joos, F., England, M.H., 2015. Impact of oceanic circulation changes on atmospheric δ13CO2. Global Biogeochem. Cycles 29, 1944–1961. https://doi.org/10.1002/2015GB005207.
Menviel, L., Spence, P., Yu, J., Chamberlain, M.A., Matear, R.J., Meissner, K.J., England, M.H., 2018. Southern Hemisphere westerlies as a driver of the early deglacial atmospheric CO2 rise. Nat. Commun. 9, 1–12. https://doi.org/10.1038/s41467-018-04876-4.
Merle, R., Cornen, G., Scharer, U., Girardeau, J., Cotten, J., 2006. Cretaceous alkaline magmatism of Tore-Madeira Rise: petrogenesis and geodynamical aspects related to Madeira hotspot track and NE Atlantic seamounts. J. Volcanol. Geoth. Res. 141, 109–122.
Merle, R., Jourdan, F., Girardeau, J., 2018. Geochronology of the Tore-Madeira Rise seamounts and surrounding areas: a review. Aust. J. Earth Sci. 65, 591–605. https://doi.org/10.1080/08120099.2018.1471005.
Merle, R., Jourdan, F., Marzoli, A., Renne, P.R., Grange, M., Girardeau, J., 2009. Evidence of multi-phase Cretaceous to Quaternary alkaline magmatism on Tore–Madeira Rise and neighbouring seamounts from 40 Ar/39 Ar ages. J. Geol. Soc. London. 166, 879–894. https://doi.org/10.1144/0016-76492008-060.
Miguez-Salas, O., Rodríguez-Tovar, F.J., 2021. Trace fossil analysis of sandy clastic contouritic deposits in the late Miocene Rifian Corridor (Morocco): ichnotaxonomical and palaeoenvironmental insights. J. Afr. Earth Sci. 174, 104054. https://doi.org/10.1016/j.jafrearsci.2020.104054.
Miguez-Salas, O., Rodríguez-Tovar, F.J., 2019. Ichnofacies distribution in the Eocene-Early Miocene Petra Tou Romiou outcrop, Cyprus: sea level dynamics and palaeoenvironmental implications in a contourite environment. Int. J. Earth Sci. 108, 2531–2544. https://doi.org/10.1007/s00531-019-01775-x.
Miguez-Salas, O., Rodríguez-Tovar, F.J., de Weger, W., 2021. The Late Miocene Rifian corridor as a natural laboratory to explore a case of ichnofacies distribution in ancient gateways. Sci. Rep. 11, 4198. https://doi.org/10.1038/s41598-021-83820-x.
Miguez-Salas, O., Rodríguez-Tovar, F.J., De Weger, W., 2020. Macaronichnus and contourite depositional settings: bottom currents and nutrients as coupling factors. Palaeogeogr. Palaeoclimatol. Palaeoecol. 545, 109639. https://doi.org/10.1016/j.palaeo.2020.109639.
Miranda, J.M., Luis, J.F., Lourenço, N., 2018. The Tectonic Evolution of the Azores Based on Magnetic Data, pp. 89–100. https://doi.org/10.1007/978-3-642-32226-6_6.
Mitchum, R.M., Vail, P.R., Sangree, J.B., 1977. Seismic stratigraphy and global changes of sea level, Part 6: stratigraphic interpretation of seismic reflection patterns in depositional sequences. In: Payton, C.E. (Ed.), Seismic Stratgraphy — Applications to Hydrocarbon Exploration, 26. AAPG Mem, pp. 117–133.
Morozov, E.G., Demidov, A.N., Tarakanov, R.Y., Zenk, W., 2010. Abyssal Channels in the Atlantic Ocean. Springer Netherlands, Dordrecht. https://doi.org/10.1007/978-90-481-9358-5.
Morozov, E.G., Tarakanov, R.Y., Frey, D.I., 2022. Bottom Gravity Currents Abd Overflows in Deep Channels of the Atlantic Ocean: Observations, Analysis, and Modeling. Springer Nature Switzerland AG.
Morozov, E.G., Tarakanov, R.Y., Lyapidevskii, V.Y., Makarenko, N.I., 2012. Abyssal cataracts in the Romanche and Chain fracture zones. Dokl. Earth Sci. 446, 1211–1214. https://doi.org/10.1134/S1028334X12100091.
Mosquera Giménez, Á., Vélez-Belchí, P., Rivera, J., Piñeiro, S., Fajar, N., Caínzos, V., Balbín, R., Jiménez Aparicio, J.A., Dominguez-Carrió, C., Blasco-Ferre, J., Carreiro-Silva, M., Morato, T., Puerta, P., Orejas, C., 2019. ocean circulation over North Atlantic underwater features in the path of the mediterranean outflow water: the ormonde and formigas seamounts, and the Gazul mud volcano. Front. Mar. Sci. 6 https://doi.org/10.3389/fmars.2019.00702.
Muglia, J., Skinner, L.C., Schmittner, A., 2018. Weak overturning circulation and high Southern Ocean nutrient utilization maximized glacial ocean carbon. Earth Planet Sci. Lett. 496, 47–56. https://doi.org/10.1016/j.epsl.2018.05.038.
Müller, P.J., Suess, E., 1979. Productivity, sedimentation rate, and sedimentary organic matter in the oceans—I. Organic carbon preservation. Deep Sea Res. Part A. Oceanogr. Res. Pap. 26, 1347–1362. https://doi.org/10.1016/0198-0149(79)90003-7.
Müller, R.D., Roest, W.R., Royer, J.-Y., Gahagan, L.M., Sclater, J.G., 1997. Digital isochrons of the world's ocean floor. J. Geophys. Res. Solid Earth 102, 3211–3214. https://doi.org/10.1029/96JB01781.
Okino, K., Fujioka, K., 2003. The Central Basin Spreading Center in the Philippine Sea: structure of an extinct spreading center and implications for marginal basin formation. J. Geophys. Res. Solid Earth 108. https://doi.org/10.1029/2001JB001095.
Omira, R., Neres, M., Batista, L., 2019. The Gloria transform fault—NE Atlantic: Seismogenic and tsunamigenic potential. In: Transform Plate Boundaries and Fracture Zones. Elsevier, pp. 157–167. https://doi.org/10.1016/B978-0-12-812064-4.00008-6.
Orsi, A.H., Johnson, G.C., Bullister, J.L., 1999. Circulation, mixing, and production of Antarctic bottom water. Prog. Oceanogr. 43, 55–109. https://doi.org/10.1016/S0079-6611(99)00004-X.
Polzin, K.L., 1997. Spatial variability of turbulent mixing in the abyssal ocean. Science (80-.) 276, 93–96. https://doi.org/10.1126/science.276.5309.93.
Pomar, L., Morsilli, M., Hallock, P., Bádenas, B., 2012. Internal waves, an under-explored source of turbulence events in the sedimentary record. Earth Sci. Rev. 111, 56–81. https://doi.org/10.1016/j.earscirev.2011.12.005.
Preu, B., Hernández-Molina, F.J., Violante, R., Piola, A.R., Paterlini, C.M., Schwenk, T., Voigt, I., Krastel, S., Spiess, V., 2013. Morphosedimentary and hydrographic features of the northern Argentine margin: the interplay between erosive, depositional and gravitational processes and its conceptual implications. Deep-Sea Res. Part I Oceanogr. Res. Pap. 75, 157–174. https://doi.org/10.1016/j.dsr.2012.12.013.
Prieto, E., González-Pola, C., Lavín, A., Sánchez, R.F., Ruiz-Villarreal, M., 2013. Seasonality of intermediate waters hydrography west of the Iberian Peninsula from an 8 yr semiannual time series of an oceanographic section. Ocean Sci. 9, 411–429. https://doi.org/10.5194/os-9-411-2013.
Puig, P., Palanques, A., Guillén, J., El Khatab, M., 2004. Role of internal waves in the generation of nepheloid layers on the northwestern Alboran slope: implications for continental margin shaping. J. Geophys. Res. 109, C09011. https://doi.org/10.1029/2004JC002394.
Railsback, L.B., Gibbard, P.L., Head, M.J., Voarintsoa, N.R.G., Toucanne, S., 2015. An optimized scheme of lettered marine isotope substages for the last 1.0 million years, and the climatostrigraphic nature of isotope stages and substages. Quat. Sci. Rev. 111, 94–106. https://doi.org/10.1016/j.quascirev.2015.01.012.
Raymo, M.E., Ruddiman, W.F., Shackleton, N.J., Oppo, D.W., 1990. Evolution of Atlantic-Pacific δ13C gradients over the last 2.5 m.y. Earth Planet Sci. Lett. 97, 353–368. https://doi.org/10.1016/0012-821X(90)90051-X.
Rebesco, M., Camerlenghi, A., 2008. Developments in Sedimentology. Contourites, 60. Elsevier.
Rebesco, M., Hernández-Molina, F.J., Van Rooij, D., Wåhlin, A., 2014. Contourites and associated sediments controlled by deep-water circulation processes: state-of-the-art and future considerations. Mar. Geol. 352, 111–154. https://doi.org/10.1016/j.margeo.2014.03.011.
Richardson, P., Bower, A., Zenk, W., 2000. A census of Meddies tracked by floats. Prog. Oceanogr. 45, 209–250. https://doi.org/10.1016/S0079-6611(99)00053-1.
Rickaby, R.E.M., Elderfield, H., 2005. Evidence from the high-latitude North Atlantic for variations in Antarctic Intermediate water flow during the last deglaciation. Geochemistry, Geophys. Geosystems 6. https://doi.org/10.1029/2004GC000858 n/a-n/a.
Rodríguez-Tovar, F.J., Dorador, J., 2014. Ichnological analysis of Pleistocene sediments from the IODP site U1385 "Shackleton site" on the iberian margin: Approaching paleoenvironmental conditions. Palaeogeogr. Palaeoclimatol. Palaeoecol. 409, 24–32. https://doi.org/10.1016/j.palaeo.2014.04.027.
Rodríguez-Tovar, F.J., Dorador, J., Grunert, P., Hodell, D., 2015a. Deep-sea trace fossil and benthic foraminiferal assemblages across glacial Terminations 1, 2 and 4 at the "Shackleton Site" (IODP Expedition 339, Site U1385). Global Planet. Change 133, 359–370. https://doi.org/10.1016/j.gloplacha.2015.05.003.
Rodríguez-Tovar, F.J., Dorador, J., Martin-Garcia, G.M., Sierro, F.J., Flores, J.A., Hodell, D.A., 2015b. Response of macrobenthic and foraminifer communities to changes in deep-sea environmental conditions from Marine Isotope Stage (MIS) 12 to 11 at the "Shackleton Site. Global Planet. Change 133, 176–187. https://doi.org/10.1016/j.gloplacha.2015.08.012.
Rodríguez-Tovar, F.J., Hernández-Molina, F.J., 2018. Ichnological analysis of contourites: past, present and future. Earth Sci. Rev. 182, 28–41. https://doi.org/10.1016/J.EARSCIREV.2018.05.008.
Rodríguez, Tovar, Francisco, J., Hernández-Molina, F.J., Hüneke, H., Chiarella, D., Llave, E., Mena, A., Miguez-Salas, O., Dorador, J., de Castro, S., Stow, D.A.V., 2019a. Key evidence for distal turbiditic- and bottom-current interactions from tubular turbidite infills. Palaeogeogr. Palaeoclimatol. Palaeoecol. 533, 109233. https://doi.org/10.1016/j.palaeo.2019.109233.
Rodríguez, Tovar, Javier, Francisco, Hernández-Molina, F.J., Hüneke, H., Llave, E., Stow, D., 2019b. Contourite facies model: improving contourite characterization

based on the ichnological analysis. Sediment. Geol. 384, 60–69. https://doi.org/10.1016/j.sedgeo.2019.03.010.
Roque, C., Hernández-Molina, F.J., Madureira, P., Quartau, R., Magalhãs, V., Carrara, G., Santos de Campos, A., Brandão, F., Tomás Vázquez, J., Somoza, L., 2017. Contourite drift off Madeira island (northeast Atlantic) and implications to cenozoic bottom-current circulation. In: 19th EGU General Assembly. Vienna, Austria, p. 16918.
Roque, C., Madureira, P., Santos de Campos, A., Brandão, F., Martins, M.A., Pinto Ribeiro, L., Conceição, P., Dias, F., 2015. Determination of the Base of the Slope region in continental margins dominated by along-slope depositional processes - the case of Madeira Island lower slope (Central Atlantic). In: Resúmenes Sobre El VIII Simposio MIA15 (Iberian Atlantic Margin). Málaga, pp. 497–499.
Roque, D., Parras-Berrocal, I., Bruno, M., Sánchez-Leal, R., Hernández-Molina, F.J., 2019. Seasonal variability of intermediate water masses in the Gulf of Cádiz: implications of the Antarctic and subarctic seesaw. Ocean Sci. 15, 1381–1397. https://doi.org/10.5194/os-15-1381-2019.
Rorden, C., Brett, M., 2000. Stereotaxic display of brain lesions. Behav. Neurol. 12, 191–200. https://doi.org/10.1155/2000/421719.
Rothwell, R.G., Croudace, I.w., 2015. Twenty years of XRF core scanning marine sediments: what do geochemical proxies tell us? In: Croudace, I.W., Rothwell, R.G. (Eds.), Micro-XRF Studies of Sediment Cores. Springer, pp. 25–102. https://doi.org/10.1007/978-94-017-9849-5_2.
Rothwell, R.G., Hoogakker, B., Thomson, J., Croudace, I.W., Frenz, M., 2006. Turbidite emplacement on the southern Balearic Abyssal Plain (western Mediterranean Sea) during Marine Isotope Stages 1–3: an application of ITRAX XRF scanning of sediment cores to lithostratigraphic analysis. Geol. Soc. London, Spec. Publ. 267, 79–98. https://doi.org/10.1144/GSL.SP.2006.267.01.06.
Rothwell, R.G., Pearce, T.J., Weaver, P.P.E., 1992. Late quaternary evolution of the Madeira abyssal plain, canary basin, NE Atlantic. Basin Res. 4, 103–131. https://doi.org/10.1111/j.1365-2117.1992.tb00147.x.
Rothwell, R.G., Rack, F.R., 2006. New techniques in sediment core analysis: an introduction. Geol. Soc. London, Spec. Publ. 267, 1–29. https://doi.org/10.1144/GSL.SP.2006.267.01.01.
Ryan, W.B.F., Carbotte, S.M., Coplan, J.O., O'Hara, S., Melkonian, A., Arko, R., Weissel, R.A., Ferrini, V., Goodwillie, A., Nitsche, F., Bonczkowski, J., Zemsky, R., 2009. Global multi-resolution topography synthesis. Geochemistry, Geophys. Geosystems 10. https://doi.org/10.1029/2008GC002332 n/a-n/a.
Sarnthein, M., Stattegger, K., Dreger, D., Erlenkeuser, H., Grootes, P.M., Haupt Bernd, J., Kiefer, T., Kuhnt, W., Pflaumann, U., Schäfer-Neth, C., Schulz, H., Schulz, M., Seidov, D., Simstich, J., Kreveld Van, S., Vogelsang, E., Völker, A., Weinelt, M., 2001. Fundamental modes and Abrupt changes in North Atlantic circulation and climate over the last 60 ky – concepts, reconstruction and numerical modeling. North. North Atl. -A Chang. Environ. 365–410. https://doi.org/10.1007/978-3-642-56876-3_21.
Saunders, P.M., 1987. Flow through Discovery gap. J. Phys. Oceanogr. 17, 631–643. https://doi.org/10.1175/1520-0485(1987)017<0631:FTDG>2.0.CO.
Schlitzer, R., 2002. Interactive analysis and visualization of geoscience data with Ocean Data View. Comput. Geosci. 28, 1211–1218. https://doi.org/10.1016/S0098-3004(02)00040-7.
Schönfeld, J., Zahn, R., 2000. Late Glacial to Holocene history of the Mediterranean Outflow. Evidence from benthic foraminiferal assemblages and stable isotopes at the Portuguese margin. Palaeogeogr. Palaeoclimatol. Palaeoecol. 159, 85–111. https://doi.org/10.1016/S0031-0182(00)00035-3.
Schönfeld, J., Zahn, R., de Abreu, L., 2003. Surface and deep water response to rapid climate changes at the Western Iberian Margin. Global Planet. Change 36, 237–264. https://doi.org/10.1016/S0921-8181(02)00197-2.
Seibold, E., Fütterer, D., 1982. Sediment dynamics on the Northwest African continental margin. In: Scrutton, R., Talwani, M. (Eds.), The Ocean Floor: Bruse Heezen Commermorative Volume. Wiley, Chichester, pp. 147–163.
Sierro, F.J., Hodell, D.A., Andersen, N., Azibeiro, L.A., Jimenez-Espejo, F.J., Bahr, A., Flores, J.A., Ausin, B., Rogerson, M., Lozano-Luz, R., Lebreiro, S.M., Hernandez-Molina, F.J., 2020. Mediterranean overflow over the last 250 kyr: freshwater forcing from the tropics to the ice sheets. Paleoceanogr. Paleoclimatology 35. https://doi.org/10.1029/2020PA003931.
Sivkov, V.V., Bashirova, L.D., Dorokhova, E.V., Kapustina, M.V., Ponomarenko, E.P., 2019. Study of the contourite drift north of the Kane gap (eastern equatorial Atlantic). Russ. J. Earth Sci. 19, 1–9. https://doi.org/10.2205/2019ES000658.
Srivastava, S., Roest, W., Kovacs, L., Oakey, G., Lévesque, S., Verhoef, J., Macnab, R., 1990. Motion of iberia since the late jurassic: results from detailed aeromagnetic measurements in the newfoundland basin. Tectonophysics 184, 229–260. https://doi.org/10.1016/0040-1951(90)90442-B.
Stevenson, C.J., Talling, P.J., Wynn, R.B., Masson, D.G., Hunt, J.E., Frenz, M., Akhmetzhanhov, A., Cronin, B.T., 2013. The flows that left no trace: very large-volume turbidity currents that bypassed sediment through submarine channels without eroding the sea floor. Mar. Petrol. Geol. 41, 186–205. https://doi.org/10.1016/j.marpetgeo.2012.02.008.
Stocker, T.F., Wright, D.G., Broecker, W.S., 1992. The influence of high-latitude surface forcing on the global thermohaline circulation. Paleoceanography 7, 529–541. https://doi.org/10.1029/92PA01695.
Stow, D.A.V., Hernández-Molina, F.J., Llave, E., Sayago-Gil, M., Díaz del Río, V., Branson, A., 2009. Bedform-velocity matrix: the estimation of bottom current velocity from bedform observations. Geology 37, 327–330. https://doi.org/10.1130/G25259A.1.
Stow, D.A.V., Tabrez, A.R., 1998. Hemipelagites: processes, facies and model. Geol. Soc. London, Spec. Publ. 129, 317–337. https://doi.org/10.1144/GSL.SP.1998.129.01.19.
Talley, L.D., 2013. Closure of the global overturning circulation through the Indian, Pacific, and southern oceans. Oceanography 26, 80–97. https://doi.org/10.5670/oceanog.2013.07.
Tarakanov, R.Y., Morozov, E.G., Gritsenko, A.M., Demidova, T.A., Makarenko, N.I., 2013. Transport of Antarctic bottom water through passages in the east Azores ridge (37° N) in the east Atlantic. Oceanology 53, 432–441. https://doi.org/10.1134/S0001437013040152.
Thiéblemont, A., Hernández-Molina, F.J., Miramontes, E., Raisson, F., Penven, P., 2019. Contourite depositional systems along the Mozambique channel: the interplay between bottom currents and sedimentary processes. Deep-Sea Res. Part I Oceanogr. Res. Pap. 147, 79–99. https://doi.org/10.1016/j.dsr.2019.03.012.
Thornalley, D.J.R., Barker, S., Broecker, W.S., Elderfield, H., McCave, I.N., 2011. The deglacial evolution of North Atlantic deep convection. Science (80-) 331, 202–205. https://doi.org/10.1126/science.1196812.
Tuerena, R.E., Williams, R.G., Mahaffey, C., Vic, C., Green, J.A.M., Naveira-Garabato, A., Forryan, A., Sharples, J., 2019. Internal tides drive nutrient fluxes into the deep chlorophyll maximum over mid-ocean ridges. Global Biogeochem. Cycles 33, 995–1009. https://doi.org/10.1029/2019GB006214.
Uchman, A., Wetzel, A., 2011. Deep-Sea Ichnology: the Relationships between Depositional Environment and Endobenthic Organisms, pp. 517–556. https://doi.org/10.1016/B978-0-444-53000-4.00008-1.
Udías, A., López Arroyo, A., Mezcula, J., 1976. Seismotectonic of the Azores—Alboran region. Tectonophysics 31, 259–289.
van Aken, H.M., 2000a. The hydrography of the mid-latitude northeast Atlantic Ocean. Deep-Sea Res. Part I Oceanogr. Res. Pap. 47, 757–788. https://doi.org/10.1016/S0967-0637(99)00092-8.
van Aken, H.M., 2000b. The hydrography of the mid-latitude northeast Atlantic Ocean: I: the deep water masses. Deep-Sea Res. Part I Oceanogr. Res. Pap. 47, 757–788. https://doi.org/10.1016/S0967-0637(99)00092-8.
Vissers, R.L.M., Meijer, P.T., 2012. Iberian plate kinematics and Alpine collision in the Pyrenees. Earth Sci. Rev. 114, 61–83. https://doi.org/10.1016/j.earscirev.2012.05.001.
Warren, B.A., Speer, K.G., 1991. Deep circulation in the eastern south Atlantic Ocean. Deep Sea Res. Part A. Oceanogr. Res. Pap. 38, S281–S322. https://doi.org/10.1016/S0198-0149(12)80014-8.
Watts, A.B., 1994. Crustal structure, gravity anomalies and flexure of the lithosphere in the vicinity of the Canary Islands. Geophys. J. Int. 119, 648–666. https://doi.org/10.1111/j.1365-246X.1994.tb00147.x.
Watts, A.B., Sandwell, D.T., Smith, W.H.F., Wessel, P., 2006. Global gravity, bathymetry, and the distribution of submarine volcanism through space and time. J. Geophys. Res. 111, B08408. https://doi.org/10.1029/2005JB004083.
Weaver, P.P.E., Kuijpers, A., 1983. Climatic control of turbidite deposition on the Madeira abyssal plain. Nature 306, 360–363. https://doi.org/10.1038/306360a0.
Weaver, P.P.E., Rothwell, R.G., 1987. Sedimentation on the Madeira abyssal plain over the last 300 000 years. Geol. Soc. London, Spec. Publ. 31, 71–86. https://doi.org/10.1144/GSL.SP.1987.031.01.07.
Weaver, P.P.E., Rothwell, R.G., Ebbing, J., Gunn, D., Hunter, P.M., 1992. Correlation, frequency of emplacement and source directions of megaturbidites on the Madeira Abyssal Plain. Mar. Geol. 109, 1–20. https://doi.org/10.1016/0025-3227(92)90218-7.
Weltje, G.J., Tjallingii, R., 2008. Calibration of XRF core scanners for quantitative geochemical logging of sediment cores: theory and application. Earth Planet Sci. Lett. 274, 423–438. https://doi.org/10.1016/j.epsl.2008.07.054.
Wetzel, A., 1991. Ecologic interpretation of deep-sea trace fossil communities. Palaeogeogr. Palaeoclimatol. Palaeoecol. 85, 47–69. https://doi.org/10.1016/0031-0182(91)90025-M.
Wetzel, A., 1981. Ökologische und stratigraphische Bedeutung biogener Gefüge in quartären Sedimenten am NW-afrikanischen Kontinentalhang. "Meteor" Forsch 1–47. -Ergeben.
Wetzel, A., Uchman, A., 2012. Hemipelagic and Pelagic Basin Plains, pp. 673–701. https://doi.org/10.1016/B978-0-444-53813-0.00022-8.
Whitmarsh, R.B., 1970. Erosion and sediment transport beneath the sea. Sci. Prog. 58, 1–25.
Wienberg, C., Titschack, J., Frank, N., De Pol-Holz, R., Fietzke, J., Eisele, M., Kremer, A., Hebbeln, D., 2020. Deglacial upslope shift of NE Atlantic intermediate waters controlled slope erosion and cold-water coral mound formation (Porcupine Seabight, Irish margin). Quat. Sci. Rev. 237, 106310. https://doi.org/10.1016/j.quascirev.2020.106310.
Wüst, G., 1936. Schichtung und Zirkulation des Atlantischen Ozeans. In: Defant, A. (Ed.), Wissenschaftliche Ergebnisse, Deutsche Atlantische Expedition Auf Dem Forschungs - Und Vermessungsschiff „Meteor" 1925-1927. Walter de Gruyter & Co, Berlin, p. 411.
Zenk, W., 2008. Abyssal and contour currents. In: Rebesco, M., Camerlenghi, A. (Eds.), Developments in Sedimentology, 60. Elsevier, pp. 37–57.
Zenk, W., Siedler, G., Lenz, B., Hogg, N.G., 1999. Antarctic bottom water flow through the Hunter Channel. J. Phys. Oceanogr. 29, 2785–2801. https://doi.org/10.1175/1520-0485(1999)029<2785:ABWFTT>2.0.CO;2.